REDUCING LOSS IN IMPLANTABLE AND SPACECRAFT ANTENNA SYSTEMS

by

Andrew Michael Chrysler

A dissertation submitted to the faculty of
The University of Utah
in partial fulfillment of the requirements for the degree of

Doctor of Philosophy

Department of Electrical and Computer Engineering

The University of Utah

May 2018

The University of Utah Graduate School

STATEMENT OF DISSERTATION APPROVAL

The dissertation of **Andrew Michael Chrysler**

has been approved by the following supervisory committee members:

Cynthia M. Furse	, Chair	**1/26/2018** Date Approved
David Schurig	, Member	**1/26/2018** Date Approved
Berardi Sensale-Rodriguez	, Member	**1/26/2018** Date Approved
Rainee Simons	, Member	**1/26/2018** Date Approved
Huanan Zhang	, Member	**1/26/2018** Date Approved

and by **Florian Solzbacher** , Chair of

the Department of **Electrical and Computer Engineering**

and by David B. Kieda, Dean of The Graduate School.

ABSTRACT

Antenna design and reduction of losses in antenna systems are critical for modern communications systems. Two categories of antennas suffer from limited power supply and difficult operating environments: implantable antennas and antennas for spacecraft applications. Minimizing and controlling losses in these two antenna types is critical for developing next-generation implantable devices, spacecraft, and satellites.

Research suggests that future tattoo antennas will be made from low-conductivity ink utilizing the natural insulating property of the body's fat and lossy ground plane of muscle. This paper supports tattoo antenna work by: (1) demonstrating the insulating properties of fat and conductivity of muscle with various antenna systems, (2) showing the effect of biological materials on the current distribution of subdermal antennas, and (3) validating the use of lower-conductivity materials in subdermal antenna design including a novel gold nanoparticle material.

Simulations and measurements are used to evaluate current distributions shared between solid, segmented, and meshed strip dipole antennas and surrounding body tissues. Fat insulates the antenna similar to a thin layer of plastic wrap. Muscle acts as a conductive ground plane. Dipole antennas with mesh or gap structures are more strongly coupled to body tissues than solid antennas. A minimum acceptable conductivity benchmark of 10^5 S/m is established for dipole antennas and Radio-Frequency Identification (RFID) antennas.

This work also provides novel information on the design of low-cost, circularly

polarized (CP), Ka-band (26 GHz), millimeter-wave, 50 Ω edge-fed, corners truncated patch antennas on RT/duroid 5880 ($\varepsilon_r = 2.2$, ½ oz. copper cladding). Microstrip feed width, axial ratio (AR) bandwidth, and best AR at 26 GHz are optimized by the use of 10 mil substrate. The effects of corner truncation are further investigated, showing that increasing corner truncation increases AR bandwidth, increases percent offset between best S_{11} and AR frequencies, and worsens the best AR. A truncation of 0.57 mm is a good compromise between these effects with AR bandwidth of 6.17 % (measured) and 1.37 % (simulated). Increasing ratio of substrate thickness to design frequency, $t / \lambda d$, improves AR bandwidth. For $t / \lambda d$ below a certain threshold, a corners truncated patch antenna will not produce CP. A new nearly-square, corners truncated patch antenna is measured and simulated as a method of increasing circular polarization bandwidth (CPBW).

TABLE OF CONTENTS

LIST OF TABLES

Tables

ACKNOWLEDGMENTS

I would like to thank my advisor, Dr. Cynthia Furse, for helping me become an Electrical Engineer and for all her patience as I took many undergraduate classes working to learn new material. She has helped me develop skills as researcher, lecturer, and professional. Additionally, she exposed me to many opportunities that helped advance my Ph.D.

I thank my committee members, David Schurig, Rainee Simons, Berardi Sensale-Rodriguez, and Huanan Zhang, for their helpful contributions throughout all stages of the process.

I want to thank everyone who contributed to the publications in this dissertation. I especially want to thank Rainee Simons and Felix Miranda with whom I worked at the NASA Glenn Research Center and who are co-authors of the work in Chapter 6 and of a conference presentation. I am very grateful for the opportunity to work at NASA and for their support.

I want to thank Youchung Chung of Daegu University in Korea (co-author of Chapter 5 and a conference paper) for his support and for allowing me to work in his lab during summer 2015. Youchung made me feel very welcome as a visitor in Korea and in his laboratory.

I want to thank Huanan Zhang and Franky Curry of the Chemical Engineering Department at the University of Utah. They provided the gold nanoparticle material used

in Chapter 3 and 4 and are co-authors of the work in Chapter 3.

I want to thank all of the undergraduates with whom I worked at the University of Utah, but especially Kaitlin Hall, who was extremely eager and helpful, and is a co-author of Chapters 3, 4, and 5 and a conference publication.

This work was supported by the NSF EAPSI Fellowship and also by a co-op at the NASA Glenn Research Center. Lastly, as Colorado native, I want to acknowledge that Utah does have the greatest snow on earth.

CHAPTER 1

INTRODUCTION

1.1 Background

Antennas have found use in numerous communication applications including two contemporary applications -- use in implantable medical devices and millimeter-wave antennas for use in satellite and spacecraft applications. Both applications require antennas capable of operating under harsh environmental conditions where power supply or battery may be seriously limited. The loss in antennas used in these applications is of great interest. Antennas for implantable devices have significant losses due to attenuation in the human body. Antennas for satellite communications suffer losses mainly from impedance and polarization mismatches. The research contributions in work covers two types of lossy systems: implantable antennas and Ka-band antennas for spacecraft applications.

Today's implantable devices are roughly 4 cm on a side [1]. Antennas for communication signals and power transfer are designed using the MedRadio band (401 - 406 MHz) [2] to operate in and on the metal battery packs for these devices. However, next-generation implantable medical devices (IMDs) will be significantly smaller. The Utah Electrode Array, packaged along with a control system and battery power, for instance, is 4 mm on a side [3]. Thus, due to frequency band constraints and fundamental physical laws, it is not practical to create an antenna that resides exclusively on the surface

of these future IMDs. This dissertation explores the possibility of using a subdermal tattooed antenna instead, enabling the body surface to provide a much larger area for antenna design. Future implantable antenna research is likely to use this tattoo antenna concept and this work is a first-ever evaluation of that concept. It offers three contributions to the implantable antenna field: 1) the natural fat in the body can act as an insulator, and the muscle beneath it can act as a ground plane for tattoo antennas; 2) the dielectric properties of the body tissues will have a strong but predictable effect on the current distribution of these tattoo antennas; and 3) novel, low-conductivity materials offer strong candidates for future implantable antenna designs. Each of these concepts is explored in one or more chapters of this dissertation.

Losses in spacecraft antennas are considered through the use of 50 Ω edge-fed, corners truncated patch antennas. This antenna design has been used many times in the past [4, 5], but the performance of this antenna type in the Ka-band and other millimeter-wave frequencies is not well-studied. A reliable satellite communication link requires antennas with high efficiency and high gain, which are small in size, light weight, and capable of operating with circular polarization (CP) over extended periods of time under the extreme conditions of space without maintenance. This work contributes to the existing literature by offering new insight on the effects of design frequency, substrate dielectric, substrate thickness, and design geometry on antenna loss and performance of millimeter-wave CP patch antennas.

1.2 Contributions

The scientific contributions of this dissertation will help enable next-generation implantable and spacecraft antennas. After this introductory chapter and a background chapter to follow, the dissertation is divided into four additional chapters, each containing aspects of at least one major technical contribution of this dissertation. These contributions are described below.

1.2.1 Contribution 1 (Chapters 3, 4, and 5): Fat as an Insulator, Muscle as a Ground Plane

Although the biological environment introduces a significant amount of loss into implanted antenna systems, the body's fat is demonstrated to be a good insulator and muscle a lossy ground plane. This is significant, because measurement and simulation data show that future tattoo antenna systems can leverage the properties of the human body. Implanting a tattoo antenna into the fat layer of the human body will provide protection against the short-circuiting effects of the skin and muscle. The body has large regions of fat above muscle and by placing a tattoo antenna into the fat layer, the muscle will act as a lossy ground plane for the antenna system. Investigation of the insulating property of fat is shown in the simulation and measurement of dipole antennas in Chapters 3 and 4. The effect of muscle as a ground plane is investigated in simulation in Chapter 5. The work in Chapters 3 and 5 are accepted publications [6, 7] and Chapter 4 has been submitted [8]. Additionally, this information has been presented at professional conferences [9, 10].

1.2.2 Contribution 2 (Chapters 4 and 5): Current Distribution of Antennas in Biological Environments

The study of the current distribution of antennas in biological environments supports future tattoo antenna work that will use tattoo antennas in the fat layer. The body tissues play a strong role in adapting the current distributions of the antenna. Since practical tattoos are not likely to be solid, but rather to have gaps and imperfections, Chapter 4 evaluates the potential effect of these imperfections by comparing solid, mesh, and segmented dipole antennas in biological environments. Chapter 4 observes that the high conductivity of muscle draws current into the body. Any voids in the antennas (e.g., gaps between segments or holes in the mesh) are particularly important, as they generate stronger coupling to the tissues. Also, Chapter 5 investigates the role biological tissues play in changing the impedance of implantable radio-frequency identification (RFID) antennas. This contribution is supported by Chapter 4, which has been submitted for publication [8] and Chapter 5, which has been accepted for publication [7]. The information contained has also been presented professionally [10].

1.2.3 Contribution 3 (Chapters 3 and 5): Applications and Use of Low-Conductivity Material in Biological Antennas

Initial studies of tattoo inks showed that these inks were of insufficient conductivity to create usable antennas. Chapter 3 investigates the antenna properties of a novel conductive gold nanoparticle material that can be manufactured with a range of conductivities. The loss of the antenna as the conductivity is varied is studied and compared to several other materials. It is demonstrated in Chapter 5 that implantable RFID antennas

made from low-conductivity ink achieve similar performance (S_{11}, read range) to those made from solid metal such as aluminum. Additionally, low conductivity, high-loss, inkjet-printed antennas with thickness below skin-depth still offer a potential future material for implantable antennas. Chapter 3 and Chapter 5 have been accepted for publication [6, 7], and the information contained within has been presented professionally [9, 10].

1.2.4 Contribution 4 (Chapter 6): Effect of Corner Truncation, Board Thickness, Board Dielectric, Design Frequency on Edge-Fed, CP Antenna

Spacecraft antennas require both good matching and circular polarization to be effective. Chapter 6 considers the tradeoff between these two effects in the Ka-band, which is very different than previous studies [4, 5] at lower frequencies. A corners truncated patch is used, and it was found that increasing truncation increases axial ratio (AR) bandwidth, increases percent offset between best S_{11} and AR frequencies, and worsens the best AR. Increasing ratio of substrate thickness to design frequency improves AR bandwidth. For certain ratios of substrate thickness to design frequency, a corners truncated patch antenna will not produce CP. These observations provide future antenna designers in the millimeter-wave frequency guidelines for creating simple, low-cost, CP antennas. This contribution is being prepared for submission [11], and the information contained within has been presented professionally [12].

1.3 References

[1] V. S. Mallela, V. Ilankumaran, and N. S. Rao, "Trends in cardiac pacemaker batteries," *Indian Pacing and Electrophysiology Journal,* vol. 4, no. 4, p. 201, 2004.

[2] "Medical Implant Communications Service (MICS) Federal Register. Rules Reg.," vol. 64, ed, Dec. 1999, pp. 69926-69934.

[3] K. S. Guillory and R. A. Normann, "A 100-channel system for real time detection and storage of extracellular spike waveforms," *Journal of Neuroscience Methods,* vol. 91, no. 1, pp. 21-29, 1999.

[4] P. Sharma and K. Gupta, "Analysis and optimized design of single feed circularly polarized microstrip antennas," *IEEE Transactions on Antennas and Propagation,* vol. 31, no. 6, pp. 949-955, 1983.

[5] M. Haneishi and S. Yoshida, "A design method of circularly polarized microstrip antenna by one-point feed," *Electronics and Communications in Japan,* vol. 64-B, no. 4, pp. 46-54, 1981.

[6] A. Chrysler, K. Hall, F. Curry, C. Furse, and H. Zhang, "Effect of conductivity on subdermal antennas ", ed. *Microwave and Optical Technology Letters - Accepted*.

[7] A. Chrysler, C. Furse, K. Hall, and Y. Chung, "Effect of material properties on a subdermal UHF RFID antenna," ed. *IEEE Journal of RFID - Accepted*.

[8] A. Chrysler, K. Hall, and C. Furse, "A comparison of solid, mesh, and segmented strip dipoles in a subdermal environment," ed. *IEEE Journal of Electromagnetics, RF and Microwaves in Medicine and Biology - Submitted*.

[9] A. Chrysler, C. Furse, and Y. Chung, "Biocompatible, implantable UHF RFID antenna made from conductive ink," in *2016 IEEE International Symposium on Antennas and Propagation (APSURSI)*, 2016, pp. 467-468.

[10] K. Hall, A. Chrysler, and C. Furse, "A comparison of solid, mesh, and segmented broad dipoles in biological environments," in *2017 IEEE International Symposium on Antennas and Propagation (APSURSI)*, San Diego, CA, 2017.

[11] A. Chrysler, R. Simons, C. Furse, and F. Miranda, "A Ka-band (26 GHz) single patch element with truncated corners for circular polarization," ed. *IEEE Transaction Antennas and Propagation - In Preparation*.

[12] A. Chrysler, C. Furse, R. N. Simons, and F. A. Miranda, "A Ka-band (26 GHz) circularly polarized 2x2 microstrip patch sub-array with compact feed," *2017 IEEE International Symposium on Antennas and Propagation & USNC/URSI National Radio Science Meeting*, San Diego, CA, 2017, pp. 1447-1448.

.

CHAPTER 2

REVIEW OF IMPLANTABLE AND SPACECRAFT ANTENNAS

2.1 Implantable Antennas

Implantable medical devices touch virtually every major function in the human body. Cardiac pacemakers and defibrillators [1], neural recording and stimulation devices [2], and cochlear [3] and retinal [4] implants are just a few of the many implantable medical devices available today. Wireless telemetry for these devices is necessary to monitor battery level and device health, upload reprogramming for device function, and download data for patient monitoring. The design of antennas for use in biological environments has progressed over the decades driven by advances in design techniques from a variety of antenna types. Government regulations have also played a role in the direction these designs have taken.

The first uses for implantable antennas were needles used to produce microwave hyperthermia as a therapeutic medical treatment [5]. These early hyperthermia treatments advanced engineering knowledge of electromagnetic field interactions with biological tissues. Much of this knowledge and experience was drawn upon years later for wireless transfer of power or information. As the number, type, and purpose of implantable medical devices grew, the desire for wireless data transfer links for these devices increased, leading

to the popularity of simple inductive coils during the 1990s [6, 7]. However, limited data transfer speeds and the difficulty of aligning inductive coils led to the next creative advancements. In [8], a helical antenna similar to those developed by Kraus [9] was modified for vaginal implantation in order to monitor internal body temperature. The work in [8] increased interest in implantable antennas by using the 433 MHz Industrial, Scientific, and Medical (ISM) band for high-speed data transfer . This interest continued to evolve, and in the early 2000s, circumferential monopole antennas begin to appear in literature and patents [10, 11]. Building upon the monopole and helical antennas seen in wireless mobile communication designs, the implantable antenna design community tried variations of these antennas, and eventually adapted them into spiral microstrip patch antennas as the style of choice in the mid-2000s [12, 13].

Today, antenna designers are being challenged as the size of implantable medical devices is shrinking due to advances in manufacturing and reduction in component size. Antennas are inevitably one of the largest if not the largest component of the telemetry communication system and are generally mounted on or in the implanted battery pack, usually in a body cavity. This limited real estate significantly constrains the performance of implantable antennas. Typical battery packs for cardiac devices are under 4 cm long [14] and new devices for neural recording and stimulation are under 4 mm x 4 mm in size [2]. Half-wave antennas in the MedRadio band (402-405MHz) [15] are 36 cm in air and near 6cm in the body. Reducing 6 cm antennas to fit onto 4 mm x 4 mm devices will result in unacceptable antenna performance and demands a new paradigm. One possible solution to this problem is the tattoo antenna. The tattoo antenna consists of a pick-up feed implanted and insulated in the fat layer that is coupled to an implantable device feed. The tattoo

antenna would have minimal size constraint and reradiate signals transmitted from the implanted device.

2.1.1 Frequency Band Standards

Frequency regulations have influenced the design of implantable medical antennas by standardizing the bands in which they can be designed. Industrial, Scientific, and Medical (ISM) bands (433, 915, 2450 MHz) have been available since 1947 in both the United States and Europe for applications that are used external to the body or used only for short periods of time (hyperthermia treatment, pain control, cardiac ablation, etc.) [16]. Higher frequencies have the advantage of smaller antenna sizes, but the disadvantage of lower depths of penetration within the tissue of the body. Currently, the ISM bands are used to transmit wake/sleep signals or power (via rectennas [17]) to implanted devices [18].

The three ISM bands would be suitable for medical implants, but are crowded with other devices that could potentially interfere with them. Therefore, in 1999, the Federal Communication Commission (FCC) established the Medical Implant Communication Service (MICS) band in the United States, allocating the 402 – 405 MHz frequency range for implanted and on-body communications devices [19]. In 2009, this was expanded into the Medical Device Radiocommunications Service (MedRadio), which added 1 MHz to each side of the MICS band for a total frequency range of 401 – 406 MHz [20].

2.1.2 Power Deposition Standards

Regulatory standards have long played important roles in the development of modern industry and implantable antennas are no exception. Government regulation of

electromagnetic fields in the body gained standardization after a 1992 lawsuit claiming that cell phones were linked to brain tumors [21]. In late 1996 the Federal Communications Commission (FCC) adopted the ANSI/IEEE C95.1-1991 Specific Absorption Rate (SAR) guideline of 1.6 W/kg averaged over 1 g of biological tissue [22].

Advances in computer simulation and research led to the International Commission on Non-Ionizing Radiation Protection (ICNIRP) releasing a new guideline in 1998 relaxing SAR limits to a maximum of 2 W/kg averaged over any 10g or tissue. The latest ANSI/IEEE guideline, C95.1-2005 [23], closely aligns the maximum SAR with the ICNIRP guideline allowing a 2 W/kg limit.

Despite the IEEE revision in 2006, the FCC continues to use the more restrictive 1.6 W/kg limit established in 1996 [22]. It is likely that the FCC limits will continue to be updated as computer simulation models advance and RF exposure safety is further studied [24]. The SAR limit is a major design constraint and any revision made by the FCC is sure to affect implantable antenna design.

2.1.3 Advances in Antenna Design

Microstrip antennas were first developed in the 1950s by DesChamps [25] and saw renewed popularity and increased interest in the mid-1990s with the publication of Pozar and Schuabert's IEEE book, Microstrip Antennas [26]. The use of microstrip antennas in implantable medical communication is closely related to the nature, location, and constraints of implantable devices.

Additional research, improvements, and understanding of the microstrip antenna continued to occur throughout the 1980s with the development of the size-reducing Planar

Inverted F Antenna (PIFA), examination of the non-ideal ground planes, and investigation into protective dielectric coatings.

The most important development of microstrip antennas was the planar inverted F antenna (PIFA). The PIFA was originally presented in 1982 at a Japanese-language only conference [27], and was not published in English until 1987 [28]. Much like the monopole antenna, the PIFA allows a near 50% reduction in volume while maintaining a set resonant frequency. This dramatic reduction in size is accomplished by directly shorting the patch antenna to the lower ground plane. By using this shorting technique, image theory suggests that the antenna will perform as if there were actually two separate patch antennas with equal but opposite current distributions. This doubles the effective size of the antenna.

In another important development of the microstrip antenna, researchers also investigated the effect of placing a patch antenna over a ground plane so small that it no longer appears to be electrically ideal or infinitely large. Research on small ground planes for microstrip antennas provided the early framework necessary for creating implantable microstrip antennas that use small ground planes, such as the metallic battery pack of a pacemaker [29].

Also of great importance to microstrip antennas is the shape of the radiating element. One of the most popular shapes for a radiating element is a spiral pattern. This spiral design originated from the desire to make large bandwidth, frequency independent antennas with radiation characteristics that are solely defined in terms of angles. Thus, spiral antennas [30] were presented in 1959 by J.D. Dyson who was strongly influenced by Rumsey's 1957 presentation on frequency independent antennas [31]. Later, as microstrip antenna use increased, Nakano introduced equiangular spiral antennas backed by reflectors [32, 33] in

the late 1980s, which led to Wu's 1991 paper on spiral microstrip antennas [34].

Since antennas are often required to operate in unfriendly environments, research by Bahl showed the effect of covering microstrip antennas in protective dielectric superstrates that would completely envelop the surface of the antenna [35]. Although Bahl's work did not focus on creating biologically compatible antennas, it provided the intellectual framework necessary to cover implantable antennas in biologically compatible superstrates in order to survive long-term implantation in the body. Originally intended just to protect the antenna, the superstrate serves a key purpose in implantable designs. It reduces the effect of shorting and near-field losses caused by the conductive body tissues. The work in this dissertation builds on this concept by utilizing the minimally-conductive fat layer as electrical insulation for a subdermal tattoo-type implantable antenna, as described in Chapters 3, 4, and 5 [36-38].

Other antenna designs contributing to implantable antennas are mesh antennas and segmented antennas. Segmented antennas use capacitive coupling to pass the current from one segment to another. This is similar to capacitive coupling used for microstrip filter designs [50]. The wider the spacing between segments, the greater the capacitance. We can also expect that more current will couple to and pass through the tissues for wider spacing. In this dissertation, we have evaluated the effect of gaps in the antenna, and how the current divides and passes through both the conductive material of the antenna and the conductive material of the body as described in Chapter 4 [37].

Meshed antennas have been used for space applications [51], wearables [52], and transparent antenna applications [53]. Meshed antennas tend to act like solid antennas of the same shape if the spacing of the mesh elements is less than $\lambda/30$ [52, 53] (in our

application the elements are spaced by less than λ/100 in the tissue). When less dense meshing is used, a minor center frequency shift and reduction in realized gain and bandwidth occurs [52]. Meshes can be made from either solid (wire) material, or ink-jet printed [54]. Previous studies of mesh antennas have been in air or on a nonconducting surface such as glass. This dissertation also considers subdermal mesh antennas implanted in the body, where the conductive material of the body acts as part of the antenna, filling in the space between the grid of the mesh. This is described in Chapter 4 [37].

2.1.4 Implantable Antenna Design

With the foundations of bioelectromagnetics research in place, the early 2000s provided the opportunity to combine this knowledge into design and measurement of the first microstrip implantable antennas designed to be used with a cardiac pacemaker.

Presented at the 2002 IEEE AP-S conference, Soontornpipit and Furse investigated the effect of antenna shape, superstrate type and shape, effect of shorting pins on resonant frequency, and the effect of the small titanium ground plane provided by the cardiac pacemaker [39]. This work was instrumental in establishing the superiority of spiral shape over the serpentine shape with respect to return loss. In addition, this paper provided a critical analysis of the effect of substrates and superstrates on in body performance of implantable antennas. This work [40], along with another paper on implantable spiral microstrip antennas by Rahmat-Samii et al. [13] was published in an IEEE special issue in 2004.

After these two works were published, a variety of new papers were published that continued the development of the implantable antenna. These papers continued research

on topics such as novel antenna type [41], parametric miniaturization of antennas [42], and the effect of the antenna shape on SAR [43].

Since the implantable patch antenna is typically characterized by high Q and narrow bandwidth, researchers have investigated ways of improving bandwidth and creating multiband antennas. Wideband antennas allow for increased data transfer rates and reduce negative performance effects due to implant location and variations in body type. Multiband antenna designs utilize specific bandwidths for different applications. Since conservation of implantable device battery is of high importance, many researchers design implantable antennas that utilize both the MICS band and the 2.4 GHz ISM band [17, 44, 45]. By utilizing both frequency bands, the implantable device may be kept in a power-conserving 'sleep' mode until receiving a 'wake-up' signal in the ISM frequency. Once the device is awake, data transmission may occur without interference in the MICS band.

Early research on microstrip antennas showed that adding microstrip patch layers increased the bandwidth [46]. Many of the broadband antenna designs in the literature consist of patches stacked in two or three layers [47, 48]. In addition to creating wideband microstrip antennas through the stacking technique, a few designs show that broadband or multiband antennas may be created through single layer designs such as Π shapes [49] or split ring resonators [18]. Single layer broadband antennas are created by placing two or more elements that resonate at different frequencies onto a single patch layer.

In addition to the previously mentioned techniques, one antenna in the literature was able to show operation in three bands such that the device could receive power from an outside source through a rectenna operating in the 433 MHz ISM band [22].

2.1.5 Tattoo Antennas

One of the major contributions of this dissertation is the development of tattoo antennas, seen in Chapters 3, 4, and 5 [36-38]. Tattoo antennas are antennas imbedded in the fat layer of the body, which may aid or replace other implantable antenna systems such as those previously discussed. Tattoo antennas have design challenges similar to implantable antennas, as the conductive tissues in the body short-circuit the antennas, carrying the current away from the antenna in ways that are difficult to control.

Development of tattoo antennas has been aided by epidermal antennas on the skin surface. Epidermal antennas have been developed for human monitoring [50-52], strain sensors for wheelchair control [53], body temperature monitoring [54], and more. These antennas take advantage of a plastic sticker between the antenna and the skin, and the lower conductivity of the skin, to reduce the short-circuiting effect seen with antennas that are implanted in contact with conductive tissues [4, 13, 35, 40, 55, 56].

Tattoo antennas are made up of conductive material in the fat layer under the skin. Implantable antennas need some type of electrical insulation to prevent or reduce the shorting effect of the conductive body tissues. Epidermal antennas use a plastic sticker that separates them from the body surface [7, 11, 23]. Implantable microstrip antennas use silicone or other insulating superstrates for the same purpose [28-33]. Tattoo antennas can take advantage of the fat, which is a moderate insulator to reduce the short-circuiting effect of antennas imbedded in more conductive tissue, much like the plastic sticker does for epidermal antennas [51]. The muscle, which is a moderate conductor, provides a lossy ground plane for the antenna, as it also does for epidermal antennas. Tattoo antennas could be made from biocompatible versions of paints [36-39], conductive adhesives [40],

polymers [41, 42], inks [43], and fluidic conductors [44] in a variety of shapes and designs [28-33]. Current work in polymer engineering is underway to develop an injectable nanocomposite hydrogel that is initially a fluid but turns to a solid at body temperature [19-22]. The materials used in this dissertation (Chapters 3 and 5) are good proxies for this up-and-coming new material.

Tattoo antennas could be used in several ways. First, they could be directly connected to subdermal biosensors such as those for blood glucose monitoring [57] or lactate concentration [58]. Also, they could potentially be used as re-radiators for implantable devices, utilizing the larger surface area of the body to create antennas much larger than can be supported on smaller, next-generation implants.

2.1.6 Tattoo RFID Antennas

As personalized healthcare and miniaturized sensors enable monitoring and data acquisition of biological signals at the skin surface, passive RFID technology provides a battery-free telemetry option that links healthcare to the internet of things [1]. Some high-frequency (HF) RFID (13.56 MHz) work in this area includes glucose monitoring [2], orthopedic implant identification [3], and aortic pressure sensors [4]. Passive ultrahigh frequency (UHF) (865-956MHz) RFID has recently been considered for implantable communication applications due to its longer read distances. The worldwide UHF RFID band spans from 865 to 928 MHz with the US center frequency at 915MHz and Korean at 920MHz. UHF RFID antennas are also low-cost, convenient in size, battery free, and able to be seamlessly integrated into real-time healthcare monitoring applications [5].

Epidermal RFID tags placed on the skin surface are part of a trend of wearable

electronics [6]. These are called tattoo tags [7], and are used as temperature sensors [8], strain sensors [9], and more. This is similar to the design of RFID antennas for placement on metal objects [15-17]. RFID tags have also been used extensively inside the body, particularly providing identification for pets and livestock, using very small coil antennas with limited range.

The human body is highly lossy with high dielectric and conductive layers such as skin and muscle. These layers tend to create impedance mismatch in the RFID tag. For this reason, tattoo RFID antennas often use matching structures such as an embedded T-match feed [7, 23, 24]. Impedance matching implantable RFID antennas requires a strong understanding of the electromagnetic environment, similar to other types of implantable antennas. Additionally, future implantable RFID antennas may be placed directly in to the fat layer of the body without plastic coating in order to reduce short-circuiting, similar to the operation of the tattoo antenna. The insulating effect of fat in the human body is discussed in Chapters 3 and 4 [36, 37] and an implantable RFID antenna is discussed in Chapter 5 [38].

2.1.7 Conductive Inks

Both tattoo antennas and RFID tattoo tags seek to use flexible, conductive inks and pastes to create radiating structures. Conductive ink offers potential for rapid fabrication and conformal antenna structures. The materials used for these antennas include inks and paints that could conceivably be injected under the skin. Current work in polymer engineering is underway to develop an injectable nanocomposite hydrogel that is initially a fluid but turns to a solid at body temperature [19-22]. The materials used in this paper are

good proxies for this up-and-coming new material.

RFID antennas have been manufactured at economies of scale using conductive ink, where the reduced conductivity of the ink produces mild reduction of antenna performance [7, 10-13]. When antennas are placed on the surface of the body, the body (particularly the highly conductive muscle) acts like a lossy ground plane and requires careful tuning of the antenna [14].

Although some commercial tattoo inks for body art are conductive [59], the tattoo itself may not be, as the different cellular components uptake the ink nanoparticles, placing insulating cell walls between the conductive particles [60]. Electrical uses of tattoo-type applications include sensor-development [61, 62] and permanent electrical contacts tattooed on the skin [63]. Epidermal 'tattoos' used for electronic applications are also made from patches placed on top of the skin [51].

Other subdermal antennas could be made from biocompatible versions of paints [64-67], conductive adhesives [68], polymers [69, 70], inks [71], and fluidic conductors [72]. The overall conductivity of the antenna is controlled by the conductivity of the material (fluid, ink, etc.), as well as how it interacts with the body.

In Chapter 5 [38], very conductive (up to 2.22×10^7 S/m) Novacentrix printed ink is used for an implantable RFID antenna [71], but the skin depth exceeds the fabricated antenna thickness in the UHF RFID band, leading to skin effect losses. Other inks used in Chapters 3 and 5 are less conductive such as PELCO or ELCOAT (10^5 S/m) [73, 74] but thick enough that skin depth losses are negligible. Various inks provide insight into constraints that injected tattoo antennas will face in surrounding fat/skin (relatively low loss, acting as a sub- and superstrate) and muscle (relatively high conductivity, acting as a

lossy ground plane) [25-27]. Chapter 3 also investigates the use of a novel gold nanoparticle material [36], which acts similar to conductive ink.

2.2 Spacecraft Antennas

A reliable satellite communication link requires antennas with high efficiency and high gain, which are small in size, light weight, and capable of operating with circular polarization (CP) over extended periods of time under the extreme conditions of space without maintenance. Circular polarization is important, because it eliminates the need for precise alignment between the transmitting and receiving apertures, compensates for electromagnetic effects of the ionosphere, and is more resistant to signal degradation due to atmospheric conditions [75].

2.2.1 Millimeter-wave Antennas

Because of the larger available bandwidth for satellite communications at millimeter-wave frequencies, the commercial SATCOM industry and the U.S. Government organizations have expressed tremendous interest in Ka-band links. Consequently, the design of high-efficiency antenna arrays for such applications have been reported by several investigators. As examples, these include horn arrays [76-78], reflectarrays [79-82], slotted waveguide arrays [83, 84], and microstrip arrays [85-89]. Among these designs, the microstrip arrays are attractive due to their inherent simplicity and ease of manufacture, despite their narrow bandwidth. The primary objective of this work is focused on the design of a Ka-band (26 GHz) microstrip patch antenna with corners truncated for CP. The patch is excited by an in-plane single microstrip line coupled to any one of the radiating edges.

Such a feeding arrangement enables the realization of a simple power divider network for a four element sub-array, which forms the basic building block of a larger N × N planar array.

In addition to spacecraft applications, future 5G cellular networks will rely on greater used of millimeter-wave frequency bands [90]. Also, mobile networks tend to experience loss in urban areas, which can be compensated for by using CP antennas [91]. Thus, the desire for low-cost, millimeter-wave antennas is an area of great research interest for the future.

2.2.2 Circularly Polarized Microstrip Antennas

Although patch antennas were first introduced in the early 1950s [92], their popularity increased dramatically in the 1970s [93] and by the early 1980s, many CP designs had been demonstrated [94-96]. Of the early CP designs, the corners truncated patch antenna first reported in [97, 98] has achieved lasting popularity due to simple design equations and easy fabrication.

Truncated corner CP theory was validated by experiments performed at S-band (3.175 GHz) and X-band (9.57 GHz) frequencies. In [97], the S-band CP patch antenna was fabricated on a 1/8" polystyrene ($\varepsilon_r = 2.52$) substrate and excited by a probe feed. In [98], the X-band CP antenna was designed using perturbation theory for best AR, and it was demonstrated that the AR bandwidth increases with thickness of the dielectric substrate. The corners truncated patch antenna operates by generating two orthogonal linearly polarized modes (at slightly different frequencies due to the truncated and untruncated corners) that resolve as CP [93, 97].

The AR bandwidth (frequency range below AR < 3 dB) and the return loss bandwidth (S_{11} frequency range below -10dB) determine the usable frequency range for a CP antenna. The usable region where the AR bandwidth and return loss bandwidth overlap is considered to be the CP bandwidth (CPBW). Patch antennas tend to have narrow return loss bandwidth [99] and truncated corners CP patch antennas tend to have narrow CPBW since the best AR frequency is offset from the return loss bandwidth due to resonant frequencies of the diagonal orthogonal modes.

In most single patch works, such as [97] and [98], the narrow CPBW effect is noted but not further investigated. Other higher frequency works on array design in the Ka-band tend to disregard the narrow CPBW of a single patch in favor of optimizing the CP performance of the complete patch array [85, 88, 89]. Other works that consider the narrow CPBW are low frequency (4 GHz), use air dielectric ($\varepsilon_r = 1$), and favor increasing CPBW through broadbanding techniques such as U-slots or L-probe feeds [100, 101]. Increasing CPBW using the U-slot and L-probe methods introduces manufacturing complexity and may be difficult, cost-intensive, or both at millimeter wave frequencies where patch dimensions are much smaller. Additionally, the probe method of feeding a patch from the back is more difficult to manufacture and becomes more difficult to realize at millimeter-wave frequencies.

The work in Chapter 6 addresses three previously unconsidered design effects of single patch elements: (1) the CPBW of single edge-fed corners truncated patch antennas at millimeter wave frequencies (2) CPBW as a function of higher dielectrics (such as those commonly available from Rogers Corporation) (3) Increasing CPBW through a combination of corner truncation and broadband effect of nearly-square patch antennas.

2.3 References

[1] A. J. Johansson, "Simulation and verification of pacemaker antennas," in *Engineering in Medicine and Biology Society, 2003. Proceedings of the 25th Annual International Conference of the IEEE*, 2003, vol. 4, pp. 3279-3281: IEEE.

[2] K. Guillory and R. Normann, "A 100-channel system for real time detection and storage of extracellular spike waveforms," *Journal of Neuroscience Methods,* vol. 91, no. 1, pp. 21-29, 1999.

[3] T. Buchegger, G. Ossberger, E. Hochmair, U. Folger, A. Reisenzahn, and A. Springer, "An ultra low power transcutaneous impulse radio link for cochlea implants," in *Ultra Wideband Systems, 2004. Joint with Conference on Ultrawideband Systems and Technologies. Joint UWBST & IWUWBS. 2004 International Workshop on*, 2004, pp. 356-360: IEEE.

[4] K. Gosalia, G. Lazzi, and M. Humayun, "Investigation of a microwave data telemetry link for a retinal prosthesis," *IEEE Transactions on Microwave Theory and Techniques,* vol. 52, no. 8, pp. 1925-1933, 2004.

[5] L. Taylor, "Microwave antenna implanted in the human brain," *IEEE Antennas and Propagation Society Newsletter,* vol. 22, no. 5, pp. 10-11, 1980.

[6] Z. Tang, B. Smith, J. H. Schild, and P. H. Peckham, "Data transmission from an implantable biotelemeter by load-shift keying using circuit configuration modulator," *IEEE Transactions on Biomedical Engineering,* vol. 42, no. 5, pp. 524-528, 1995.

[7] P. Vaillancourt, A. Djemouai, J. Harvey, and M. Sawan, "EM radiation behavior upon biological tissues in a radio-frequency power transfer link for a cortical visual implant," in *Engineering in Medicine and Biology Society, 1997. Proceedings of the 19th Annual International Conference of the IEEE*, 1997, vol. 6, pp. 2499-2502: IEEE.

[8] W. G. Scanlon, N. E. Evans, and Z. M. McCreesh, "RF performance of a 418-MHz radio telemeter packaged for human vaginal placement," *IEEE Transactions on Biomedical Engineering,* vol. 44, no. 5, pp. 427-430, 1997.

[9] J. D. Kraus, "The helical antenna," *Proceedings of the IRE,* vol. 37, no. 3, pp. 263-272, 1949.

[10] M. D. Amundson, J. A. Von Arx, W. J. Linder, P. Rawat, and W. R. Mass, "Circumferential antenna for an implantable medical device," ed: Google Patents, 2002.

[11] A. J. Johansson, "Wireless communication with medical implants: Antennas and propagation," 2004. Ph.D. dissertation, Lund University, 2004.

[12] P. Soontornpipit, C. M. Furse, and Y. Chung, "Design of implantable microstrip antenna for communication with medical implants," *IEEE Transactions on Microwave Theory and Techniques,* vol. 52, no. 8, pp. 1944-1951, 2004.

[13] J. Kim and Y. Rahmat-Samii, "Implanted antennas inside a human body: Simulations, designs, and characterizations," *IEEE Transactions on Microwave Theory and Techniques,* vol. 52, no. 8, pp. 1934-1943, 2004.

[14] V. S. Mallela, V. Ilankumaran, and N. S. Rao, "Trends in cardiac pacemaker batteries," *Indian Pacing and Electrophysiology Journal,* vol. 4, no. 4, p. 201, 2004.

[15] "Medical Implant Communications Service (MICS) Federal Register. Rules Reg.," vol. 64, ed, Dec. 1999, pp. 69926-69934.

[16] "Documents of the International Radio Conference," *Proceedings of the International Radio Conference*, Atlantic City, 1947.

[17] F.-J. Huang, C.-M. Lee, C.-L. Chang, L.-K. Chen, T.-C. Yo, and C.-H. Luo, "Rectenna application of miniaturized implantable antenna design for triple-band biotelemetry communication," *IEEE Transactions on Antennas and Propagation,* vol. 59, no. 7, pp. 2646-2653, 2011.

[18] C. Sánchez-Fernández, O. Quevedo-Teruel, J. Requena-Carrion, L. Inclan-Sanchez, and E. Rajo-Iglesias, "Dual-band microstrip patch antenna based on short-circuited ring and spiral resonators for implantable medical devices," *IET Microwaves, Antennas & Propagation,* vol. 4, no. 8, pp. 1048-1055, 2010.

[19] F. R. a. Regulations, "MICS Band Plan," ed, 2003.

[20] ITU. *Establishment of Medical Device Radiotelecommunications Band*. [Online] Available:https://www.itu.int/dms_pub/itus/oth/ 02/01/S020100002B4813PDFE.pdf

[21] J. E. Moulder, L. S. Erdreich, R. S. Malyapa, J. Merritt, W. F. Pickard, and Vijayalaxmi, "Cell phones and cancer: What is the evidence for a connection?," *Radiation Research,* vol. 151, no. 5, pp. 513-531, 1999.

[22] Institute of Electrical and Electronic Engineers (IEEE), *Standard for Safety Levels with Respect to Human Exposure to Radiofrequency Electromagnetic Fields, 3 kHz to 300 GHz*, 1995, 2006.

[23] "IEEE Standard for Safety Levels With Respect to Human Exposure to Radio Frequency Electromagnetic Fields, 3 kHz to 300 GHz," ed: *IEEE Std* C95.1-2005, 2006, pp. 1-238.

[24] J. C. Lin, "Safety risks from cell phones needs review [health matters]," *IEEE Microwave Magazine,* vol. 14, no. 4, pp. 42-46, 2013.

[25] G. A. Deschamps and W. Sichak, "Microstrip microwave antennas," in *3rd USAF Symposium on Antennas*, 1953, pp. 103-105.

[26] D. M. Pozar and D. H. Schaubert, *Microstrip antennas: The analysis and design of microstrip antennas and arrays*. John Wiley & Sons, 1995.

[27] K. Kobayashi, S. Nishiki, T. Taga, and A. Sasaki, "Detachable mobile radio units for the 800 MHz land mobile radio system," in *Vehicular Technology Conference, 1984. 34th IEEE*, 1984, vol. 34, pp. 6-11: IEEE.

[28] T. Taga and K. Tsunekawa, "Performance analysis of a built-in planar inverted F antenna for 800 MHz band portable radio units," *IEEE Journal on Selected Areas in Communications,* vol. 5, no. 5, pp. 921-929, 1987.

[29] J. Huang, "The finite ground plane effect on the microstrip antenna radiation patterns," *IEEE Transactions on Antennas and Propagation,* vol. 31, no. 4, pp. 649-653, 1983.

[30] J. Dyson, "The equiangular spiral antenna," *IRE Transactions on Antennas and Propagation,* vol. 7, no. 2, pp. 181-187, 1959.

[31] V. Rumsey, "Frequency independent antennas," in *1958 IRE International Convention Record*, 1966, vol. 5, pp. 114-118: IEEE.

[32] H. Nakano, K. Nogami, S. Arai, H. Mimaki, and J. Yamauchi, "A spiral antenna backed by a conducting plane reflector," *IEEE Transactions on Antennas and Propagation,* vol. 34, no. 6, pp. 791-796, 1986.

[33] H. Nakano, S. R. Kerner, and N. G. Alexopoulos, "The moment method solution for printed wire antennas of arbitrary configuration," *IEEE Transactions on Antennas and Propagation,* vol. 36, no. 12, pp. 1667-1674, 1988.

[34] S.-C. Wu and N. Alexopoulos, "Spectral domain analysis of a square microstrip spiral antenna," in *Antennas and Propagation Society International Symposium, 1991. AP-S. Digest*, 1991, pp. 970-973: IEEE.

[35] I. Bahl, P. Bhartia, and S. Stuchly, "Design of microstrip antennas covered with a dielectric layer," *IEEE Transactions on Antennas and Propagation,* vol. 30, no. 2, pp. 314-318, 1982.

[36] A. Chrysler, K. Hall, F. Curry, C. Furse, and H. Zhang, "Effect of Conductivity on Subdermal Antennas ", ed. *Microwaveand Optical Technology Letters - Accepted*.

[37] A. Chrysler, K. Hall, and C. Furse, "A comparison of solid, mesh, and segmented strip dipoles in a subdermal environment," ed. *IEEE Journal of Electromagnetics RF and Microwaves in Medicine and Biology - Submitted*.

[38] A. Chrysler, C. Furse, K. Hall, and Y. Chung, "Effect of material properties on a subdermal UHF RFID antenna," ed. *IEEE Journal of RFID - Accepted*.

[39] C. Furse, R. Mohan, A. Jakayar, S. Karidehal, B. McCleod, and S. Going, "A biocompatible antenna for communication with implantable medical devices," in *IEEE International Symposium on Antennas and Propagation*, 2002.

[40] P. Soontornpipit, C. M. Furse, and Y. C. Chung, "Design of implantable microstrip antenna for communication with medical implants," *IEEE Transactions on Microwave Theory and Techniques,* vol. 52, no. 8, pp. 1944-1951, 2004.

[41] P. Soontornpipit, C. M. Furse, and Y. C. Chung, "Miniaturized biocompatible microstrip antenna using genetic algorithm," *IEEE Transactions on Antennas and Propagation,* vol. 53, no. 6, pp. 1939-1945, 2005.

[42] A. Kiourti, M. Tsakalakis, and K. S. Nikita, "Parametric study and design of implantable PIFAs for wireless biotelemetry," *Proceedings of the 2nd International Conference on Wireless Mobile Communications*, Kos Island, Greece, 2011, pp. 96-102.

[43] J. Kim and Y. Rahmat-Samii, "SAR reduction of implanted planar inverted F antennas with non-uniform width radiator," in *Antennas and Propagation Society International Symposium 2006, IEEE*, 2006, pp. 1091-1094: IEEE.

[44] T. Karacolak, A. Z. Hood, and E. Topsakal, "Design of a dual-band implantable antenna and development of skin mimicking gels for continuous glucose monitoring," *IEEE Transactions on Microwave Theory and Techniques,* vol. 56, no. 4, pp. 1001-1008, 2008.

[45] C. J. Sanchez-Fernandez, O. Quevedo-Teruel, J. Requena-Carrion, L. Inclan-Sanchez, and E. Rajo-Iglesias, "Dual-band microstrip patch antenna based on short-circuited ring and spiral resonators for implantable medical devices," *IET Microwaves, Antennas & Propagation,* vol. 4, no. 8, pp. 1048-1055, 2010.

[46] A. Sabban, "A new broadband stacked two-layer microstrip antenna," in *Antennas and Propagation Society International Symposium, 1983*, 1983, vol. 21, pp. 63-66: IEEE.

[47] A. Kiourti and K. S. Nikita, "Miniature scalp-implantable antennas for telemetry in the MICS and ISM bands: Design, safety considerations and link budget analysis," *IEEE Transactions on Antennas and Propagation,* vol. 60, no. 8, pp. 3568-3575, 2012.

[48] C. m. Lee, T. C. Yo, C. H. Luo, C. H. Tu, and Y. Z. Juang, "Compact broadband stacked implantable antenna for biotelemetry with medical devices," *Electronics Letters,* vol. 43, no. 12, pp. 660-662, 2007.

[49] C. M. Lee, T. C. Yo, F. J. Huang, and C. H. Luo, "Bandwidth enhancement of planar inverted- F antenna for implantable biotelemetry," *Microwave and Optical Technology Letters,* vol. 51, no. 3, pp. 749-752, 2009.

[50] G. Marrocco, "RFID Antennas for the UHF Remote Monitoring of Human Subjects," *IEEE Transactions on Antennas and Propagation,* vol. 55, no. 6, pp. 1862-1870, 2007.

[51] M. A. Ziai and J. C. Batchelor, "Temporary on-skin passive UHF RFID transfer tag," *IEEE Transactions on Antennas and Propagation,* vol. 59, no. 10, pp. 3565-3571, 2011.

[52] A. Chrysler, C. Furse, and Y. Chung, "Biocompatible, implantable UHF RFID antenna made from conductive ink," in *2016 IEEE International Symposium on Antennas and Propagation (APSURSI)*, 2016, pp. 467-468.

[53] O. O. Rakibet, C. V. Rumens, J. C. Batchelor, and S. J. Holder, "Epidermal passive RFID strain sensor for assisted technologies," *IEEE Antennas and Wireless Propagation Letters,* vol. 13, pp. 814-817, 2014.

[54] S. Milici, S. Amendola, A. Bianco, and G. Marrocco, "Epidermal RFID passive sensor for body temperature measurements," in *2014 IEEE RFID Technology and Applications Conference (RFID-TA)*, 2014, pp. 140-144.

[55] C. Furse, H. Lai, C. Estes, A. Mahadik, and A. Duncan, "An implantable antenna for communication with implantable medical devices," in *IEEE Antennas and Propagation/URSI International Symposium*, 1999.

[56] T. Karacolak, R. Cooper, and E. Topsakal, "Electrical properties of rat skin and design of implantable antennas for medical wireless telemetry," *IEEE Transactions on Antennas and Propagation,* vol. 57, no. 9, pp. 2806-2812, 2009.

[57] F. Palmisano, D. Centonze, A. Guerrieri, and P. G. Zambonin, "An interference-free biosensor based on glucose oxidase electrochemically immobilized in a non-conducting poly (pyrrole) film for continuous subcutaneous monitoring of glucose through microdialysis sampling," *Biosensors and Bioelectronics,* vol. 8, no. 9-10, pp. 393-399, 1993.

[58] A. Poscia, D. Messeri, D. Moscone, F. Ricci, and F. Valgimigli, "A novel continuous subcutaneous lactate monitoring system," *Biosensors and bioelectronics,* vol. 20, no. 11, pp. 2244-2250, 2005.

[59] R. Vasold, E. Engel, B. König, M. Landthaler, and W. Bäumler, "Health risks of tattoo colors," *Analytical and Bioanalytical Chemistry,* vol. 391, no. 1, pp. 9-13, 2008.

[60] E. C. Cho, Q. Zhang, and Y. Xia, "The effect of sedimentation and diffusion on cellular uptake of gold nanoparticles," (in eng), *Nat Nanotechnol,* Research Support, N.I.H., Extramural Research Support, Non-U.S. Gov't Research Support, U.S. Gov't, Non-P.H.S. vol. 6, no. 6, pp. 385-91, Apr 24 2011.

[61] S. Chinnayelka and M. McShane, "Competitive binding assays in microcapsules as" smart tattoo" biosensors," in *Sensors, 2005 IEEE*, 2005, p. 4: IEEE.

[62] O. Couture *et al.*, "Ultrasound-inducible fluorescent particles for internal tattooing," in *Ultrasonics Symposium (IUS), 2009 IEEE International*, 2009, pp. 85-88: IEEE.

[63] S. A. Hoenig, P. L. Gildenberg, and K. K. Murthy, "Generation of pernanent, dry, electrical contacts by tattooing carbon into skin tissue," *IEEE Transactions on Biomedical Engineering,* no. 4, pp. 380-382, 1978.

[64] A. Moscicki, J. Felba, T. Sobierajski, J. Kudzia, A. Arp, and W. Meyer, "Electrically conductive formulations filled nano size silver filler for ink-jet technology," in *Polymers and Adhesives in Microelectronics and Photonics, Polytronic, 2005. Polytronic 2005. 5th International Conference on*, 2005, pp. 40-44: IEEE.

[65] J. Sidén, M. Fein, A. Koptyug, and H.-E. Nilsson, "Printed antennas with variable conductive ink layer thickness," *IET Microwaves, Antennas & Propagation,* vol. 1, no. 2, pp. 401-407, 2007.

[66] B. J. Willis, *Compact form fitting small antennas using three-dimensional rapid prototyping*. The University of Utah, 2012.

[67] K. Hall, A. Chrysler, and C. Furse, "A comparison of solid, mesh, and segmented broad dipoles in biological environments," in *2017 IEEE International Symposium on Antennas and Propagation (APSURSI)*, San Diego, CA, 2017.

[68] M. A. Gaynes, R. H. Lewis, R. F. Saraf, and J. M. Roldan, "Evaluation of contact resistance for isotropic electrically conductive adhesives," *IEEE Transactions on Components, Packaging, and Manufacturing Technology: Part B,* vol. 18, no. 2, pp. 299-304, 1995.

[69] K. Bock, "Polytronics-electronics and systems on flexible substrates," in *VLSI Technology, 2005.(VLSI-TSA-Tech). 2005 IEEE VLSI-TSA International Symposium on*, 2005, pp. 53-56: IEEE.

[70] A. R. Duggal and L. M. Levinson, "A novel high current density switching effect in electrically conductive polymer composite materials," *Journal of Applied Physics,* vol. 82, no. 11, pp. 5532-5539, 1997.

[71] NovaCentrix. *NovaCentrix Web Page*. [Online] Available: https://www.novacentrix.com/

[72] M. D. Dickey, "Emerging applications of liquid metals featuring surface oxides," *ACS Applied Materials & Interfaces,* vol. 6, no. 21, pp. 18369-18379, 2014.

[73] HanaTech. *ELCOAT Ink Purchase Site*. [Online] Available: http://www.hanatechno.com/front/php/product.php?product_no=377&main_cate_no=86&display_group=1

[74] Ted Pella Co. *PELCO 16062 Technical Notes*. [Online] Available: https://www.tedpella.com/technote_html/16062_TN.pdf

[75] B. Y. Toh, R. Cahill, and V. F. Fusco, "Understanding and measuring circular polarization," *IEEE Transactions on Education,* vol. 46, no. 3, pp. 313-318, 2003.

[76] F. Bongard, M. Gimersky, S. Doherty, X. Aubry, and M. Krummen, "3D-printed Ka-band waveguide array antenna for mobile SATCOM applications," in *2017 11th European Conference on Antennas and Propagation (EUCAP)*, 2017, pp. 579-583.

[77] A. I. Dimitriadis, M. Favre, M. Billod, J. P. Ansermet, and E. d. Rijk, "Design and fabrication of a lightweight additive-manufactured Ka-band horn antenna array," in *2016 10th European Conference on Antennas and Propagation (EuCAP)*, 2016, pp. 1-4.

[78] Y. B. Jung and S. O. Park, "Ka-band shaped reflector hybrid antenna illuminated by microstrip-fed horn array," *IEEE Transactions on Antennas and Propagation,* vol. 56, no. 12, pp. 3863-3867, 2008.

[79] J. Huang and R. J. Pogorzelski, "A Ka-band microstrip reflectarray with elements having variable rotation angles," *IEEE Transactions on Antennas and Propagation,* vol. 46, no. 5, pp. 650-656, 1998.

[80] M. M. Tahseen and A. A. Kishk, "Broadband performance of novel closely spaced elements in designing Ka-band circularly polarized reflectarray antennas," *IEEE Antennas and Wireless Propagation Letters,* vol. 16, pp. 1184-1187, 2017.

[81] A. Yu, F. Yang, A. Z. Elsherbeni, and J. Huang, "Design and measurement of a circularly polarized Ka-band reflectarray antenna," in *2009 3rd European Conference on Antennas and Propagation*, 2009, pp. 2769-2773.

[82] R. Deng, F. Yang, S. Xu, and M. Li, "An FSS-backed 20/30-GHz dual-band circularly polarized reflectarray with suppressed mutual coupling and enhanced performance," *IEEE Transactions on Antennas and Propagation,* vol. 65, no. 2, pp. 926-931, 2017.

[83] S. Chatterjee and A. Majumder, "Design of circularly polarized waveguide crossed slotted array antenna at Ka band," in *2015 International Conference on Microwave and Photonics (ICMAP)*, 2015, pp. 1-2.

[84] T. Li, H. Meng, and W. Dou, "Design and implementation of dual-frequency dual-polarization slotted waveguide antenna array for Ka-band application," *IEEE Antennas and Wireless Propagation Letters,* vol. 13, pp. 1317-1320, 2014.

[85] J. Huang, "A Ka-band circularly polarized high-gain microstrip array antenna," *IEEE Transactions on Antennas and Propagation,* vol. 43, no. 1, pp. 113-116, 1995.

[86] A. S. Hussam, F. Mohmmad, W. M. Abdel-Wahab, G. Rafi, and S. Safavi-Naeini, "A 4x4 circularly polarized aperture coupled antenna array for Ka-band satellite communication," in *2015 IEEE International Symposium on Antennas and Propagation; USNC/URSI National Radio Science Meeting*, 2015, pp. 1896-1897.

[87] Nasimuddin, Q. Xianming, and C. Zhi Ning, "A wideband circularly polarized microstrip array antenna at Ka-band," in *2016 10th European Conference on Antennas and Propagation (EuCAP)*, 2016, pp. 1-4.

[88] A. Chen, Y. Zhang, Z. Chen, and S. Cao, "A Ka-band high-gain circularly polarized microstrip antenna array," *IEEE Antennas and Wireless Propagation Letters,* vol. 9, pp. 1115-1118, 2010.

[89] A. Chen, Y. Zhang, Z. Chen, and C. Yang, "Development of a Ka-band wideband circularly polarized 64-element microstrip antenna array with double application of the sequential rotation feeding technique," *IEEE Antennas and Wireless Propagation Letters,* vol. 10, pp. 1270-1273, 2011.

[90] W. Roh *et al.*, "Millimeter-wave beamforming as an enabling technology for 5G cellular communications: Theoretical feasibility and prototype results," *IEEE communications magazine,* vol. 52, no. 2, pp. 106-113, 2014.

[91] K.-L. Wong, "Planar antennas for wireless communications," *Microwave Journal,* vol. 46, no. 10, pp. 144-145, 2003.

[92] G. A. Deschamps and W. Sichak, "Microstrip microwave antennas," *Proceedings of the Third Symposium on USAF Antenna Research*, 1953, pp. 103-105.

[93] K. F. Lee and K. F. Tong, "Microstrip patch antennas—basic characteristics and some recent advances," *Proceedings of the IEEE,* vol. 100, no. 7, pp. 2169-2180, 2012.

[94] S. Long, S. Liang, D. Schaubert, and F. Farrar, "An experimental study of the circular-polarized elliptical printed-circuit antenna," *IEEE Transactions on Antennas and Propagation,* vol. 29, no. 1, pp. 95-99, 1981.

[95] S. Liang, "The elliptical microstrip antenna with circular polarization," *IEEE Transactions on Antennas and Propagation,* vol. 29, no. 1, pp. 90-94, 1981.

[96] H. Weinschel, "A cylindrical array of a circularly polarized microstrip antenna," in *1975 Antennas and Propagation Society International Symposium*, 1975, vol. 13, pp. 177-180.

[97] P. Sharma and K. Gupta, "Analysis and optimized design of single feed circularly polarized microstrip antennas," *IEEE Transactions on Antennas and Propagation,* vol. 31, no. 6, pp. 949-955, 1983.

[98] M. Haneishi and S. Yoshida, "A design method of circularly polarized microstrip antenna by one-point feed," *Electronics and Commun. in Japan,* vol. 64-B, no. 4, pp. 46-54, 1981.

[99] A. A. Oliner, D. R. Jackson, and J. L. Volakis, "Antenna engineering handbook," *McGrawHill, New York,* 2007.

[100] S. S. Yang, K.-F. Lee, A. A. Kishk, and K.-M. Luk, "Design and study of wideband single feed circularly polarized microstrip antennas," *Progress In Electromagnetics Research,* vol. 80, pp. 45-61, 2008.

[101] K. F. Tong and T. P. Wong, "Circularly polarized U-slot antenna," *IEEE Transactions on Antennas and Propagation,* vol. 55, no. 8, pp. 2382-2385, 2007.

CHAPTER 3[1]

EFFECT OF CONDUCTIVITY ON SUBDERMAL ANTENNAS

3.1 Abstract

This paper is an initial exploration of the material effects of subdermal antennas in the fat layer under the skin for the MedRadio band (401-457 MHz) through the Industrial Scientific Medical (ISM) 902-928 MHz. Subdermal strip dipoles were made of materials with conductivities ranging from 5.0×10^3 to 5.8×10^7 S/m, including a biocompatible gold nanoparticle polymer.

3.2 Introduction

Epidermal antennas have been developed for human monitoring [1-3], strain sensors for wheelchair control [4], body temperature monitoring [5], and more. These antennas take advantage of a plastic sticker between the antenna and the skin, and the low conductivity of the skin, to reduce the short-circuiting effect seen with antennas that are implanted in contact with conductive tissues [6-11]. This paper is an initial exploration of subdermal antennas that use the fat layer as insulation instead. This paper focuses on the

---

[1] Content of this chapter is taken from an article titled "Effect of Conductivity on Subdermal Antennas" coauthored by K. Hall, F. Curry, H. Zhang, C. Furse and accepted in *Microwave and Optical Technology Letters*

effect on conductivity of the subdermal antennas and surrounding tissues at frequencies ranging from the MedRadio band (401-457 MHz) through the Industrial Scientific Medical (ISM) 902-928 MHz.

Subdermal antennas could be used in several ways. First, they could be directly connected to subdermal biosensors such as those for blood glucose monitoring [12] or lactate concentration [13]. Also, they could potentially be used as re-radiators for implantable devices, utilizing the larger surface area of the body to create antennas much larger than can be supported on next-generation implants. Subdermal antennas made up of conductive material in the fat layer under the skin can take advantage of the fat, which is a moderate insulator to reduce the short-circuiting effect of antennas imbedded in more conductive tissue, much like the plastic sticker does for epidermal antennas [2]. The muscle, which is a moderate conductor, provides a lossy ground plane for the antenna, as it also does for epidermal antennas.

Subdermal antennas could be made from biocompatible versions of paints [14-17], conductive adhesives [18], polymers [19, 20], inks [21], and fluidic conductors [22]. The overall conductivity of the antenna is controlled by the conductivity of the material (fluid, ink, etc.), as well as how it interacts with the body. Some tattoo inks, for instance, are highly conductive [23], but the tattoo itself may not be, as the different cellular components uptake the ink nanoparticles, placing insulating cell walls between the conductive particles [24]. Electrical uses of tattoo-type applications include sensor-development [25, 26] and permanent electrical contacts tattooed on the skin [27]. Epidermal ‘tattoos’ used for electronic applications are also made from patches placed on top of the skin [2].

This paper is an initial exploration of the material property effects in a subdermal

antenna system. Strip dipoles made up of copper tape, a biocompatible gold nanocomposite, an ink-jet printed conductive ink, and a thicker conductive paint with conductivities ranging from 5.0 x 10^3 to 5.8 x 10^7 S/m were used in this study. Section 3.3 evaluates the effect of the antenna conductivity and thickness/skin depth effects, the insulating effect of the fat/skin, and the lossy ground plane effects of the muscle through both simulation and measurement. Conclusions are summarized in Section 3.4.

3.3 Antenna, Materials, Properties

Strip dipole antennas painted/placed/printed in a skin-fat-muscle model were used in this study. Strip dipoles are thin, flat dipoles with an arm width 20 – 30% of the arm length. Slightly broader band than a thin wire dipole, strip dipoles have higher peak resistance and reactance [28]. In this work, the dipoles are 30 mm long and about 6 mm wide which corresponds to a 2.5 GHz design frequency (in free space) for a Hertzian dipole and about 2 GHz for the strip dipole. In the body, the design frequency is much lower, depending on the configuration, closer to the MedRadio band.

Strip dipoles made of four different materials are considered in this work. Their properties are given in Table 3.1, and the antennas are shown in Figure 3.1. The antenna made from copper tape serves as a benchmark. The antenna made from gold nanoparticle polymer is biocompatible, highly conductive, soft and flexible [29]. By mixing various concentrations of polyurethane and gold nanoparticles, three different gold nanocomposite conductivities were produced (7.9 x 10^5, 1.0 x 10^5, 5.0 x 10^3 S/m).

The other antennas are made from conductive inks, and although they are not specifically biocompatible themselves, they provide good proxies for materials that could

potentially be used for subdermal injection. The NovaCentrix material is a conductive ink that can be inkjet printed with small (250 μm) feature size onto a sheet of thin PET plastic [21]. PELCO product #16062 is a conductive paint from Ted Pella Co. that is easily spread [30]. The thickness of the copper tape and PELCO is significantly greater than the skin depth, the gold nanoparticle polymer is close to the skin depth, and the NovaCentrix material is thinner than the skin depth.

3.3.1 Effect of Antenna Conductivity

To evaluate the effect of reduced conductivity, dipoles with various conductivities were simulated in free space using CST software. The S_{11} of the simulated dipoles are compared to measured results of antennas made from gold nanocomposites in Figure 3.2. The S_{11} minima of three of the materials shown in Figure 3.1 are shown in Figure 3.2 as large black squares, and the performances of all four are summarized in Table 3.2. Figure 3.2 shows that as the conductivity or skin depth is reduced the resonant frequency is lowered, the S_{11} degrades, and the bandwidth is increased. Increased bandwidth for low conductivity dipoles was also seen in [31], and lower conductivity limit of 500 S/m for RFID dipole antennas at 915 MHz was predicted in [32]. Notably, the PELCO antenna (1×10^5 S/m) has a deeper S_{11} than gold nanocomposite (7.9×10^5 S/m), mainly due to its greater thickness. The thinner gold nanocomposite experiences more skin depth effects.

Similar effects are also seen when the dipoles are placed on a block of excised pork (loin) muscle of size 150 mm x 90 mm x 30 mm. For this measurement, the antenna is placed directly on the pork muscle with no insulating layer. A passive, two prong probe constructed from a modified SMA connector jack is used for measurement. The measured

S_{11} and impedance are seen in Figure 3.3 when the antennas are in direct contact with the pork muscle. The trends of lower resonant frequency, increased bandwidth, and degraded S_{11} as conductivity of the antenna decreases are seen in both simulation and measurement, although the exact values are not the same. This is likely due to difference in conductivity and permittivity of *ex vivo* pork when compared to *in vivo* human muscle. Past studies show that excised tissue often decreases in conductivity and permittivity compared to in vivo tissues [33] due mainly to lack of blood flow [34]. Additionally, the excised pork in this study is at a refrigeration temperature, which also changes dielectric properties of biological tissues at microwave frequencies [35, 36].

3.3.2 Insulating Effect of Fat

Implantable antennas detune or short out against conductive materials of the body, so they are normally insulated with silicone or other non-conductive material [6-11]. Epidermal antennas are printed on a thin (~10 μm) plastic sticker, which electrically insulates them from the skin [2]. The objective of subdermal antennas is to use the fat layer as a semi-insulator to reduce the shorting effect of the more conductive muscle below. To evaluate the effect of insulation on the antenna performance, the measurement set ups in Figure 3.4 are used. The results from these measurements are shown in Figure 3.5. The antennas are made from copper, except for (5.), which is gold nanocomposite with a conductivity of 7.9×10^5 S/m. Comparing the antennas insulated with fat and/or plastic wrap (1.,2.,3.) with those in direct contact with muscle (4.,5.) shows the impact of insulating the antenna. Insulated antennas have better S_{11} and higher resonant frequency. Comparing the antenna insulated with fat (1.) to that insulated with both fat and plastic

wrap (2.) shows that fat is doing as good a job insulating the antenna as plastic wrap. This is a significant finding, as it lets us translate information from epidermal antennas printed on plastic stickers to the design of subdermal antennas in the fat.

The thickness of the insulation also matters, which we know from [6-11]. Comparing the antenna insulated with fat (4 mm thick) and plastic wrap (12.5 μm thick) (2.) to insulation with only plastic wrap (3.) shows that the antenna with thicker insulation has higher resonant frequency and better S_{11}.

3.3.3 Ground Effects of Muscle

The muscle has a higher conductivity and dielectric constant than fat and skin, as seen in Table 3.1. Thus, it serves as a lossy ground plane for the antenna, which is electrically very near to it. This proximity effect creates a large input impedance compared to an antenna in free space [37]. This effect from low conductivity ground planes is also seen in ground penetrating radar where the ground significantly perturbs the antenna input impedance [38, 39]. Other work in lossy half spaces indicates that as the ground dielectric and conductivity increases, the resonant frequency shifts downward, the peak resistance is reduced, and the peak reactance increases [40].

Figure 3.6 shows a series of simulations of a copper dipole antenna over a block of muscle (150 mm x 90 mm x 30 mm) with an 8 mm fat layer (as shown in (1.) of Figure 3.4) in which the conductivity and dielectric properties of the body tissues are varied.

In the first simulation, the body tissue properties are the same as those in Table 3.1, and when compared to the same dipole in free space (as in Figure 3.2) the resonance is shifted down to 830 MHz with S_{11} performance below -15 dB. Next, the conductivity and

dielectric properties of the pork are changed to that of perfect electric conductor (PEC). The resonant frequency is further reduced to 740 MHz, and the performance is degraded to unacceptable levels as expected by [41]. When the dielectric properties of fat are converted to vacuum, the resonant frequency is increased above 2 GHz, close to the free space resonant frequency seen in Figure 3.2.

When the fat and muscle are converted to vacuum and PEC respectively, the resonant frequency remains close to 2 GHz, but the antenna performance is the worst seen, which indicates the high dielectric of the fat helps to create electric separation between the antenna and the ground plane as expected from microwave theory [42]. The muscle is acting as a lossy ground plane, but the low conductivity and high dielectric actually improve antenna performance when compared to the PEC ground plane.

3.4 Conclusions

This paper is an initial exploration of the material effects of subdermal antennas made up of conductive material in the fat layer under the skin in the MedRadio band (401-457 MHz) through the Industrial Scientific Medical (ISM) 902-928 MHz. Subdermal strip dipoles were made of copper tape, a biocompatible gold nanoparticle polymer, a NovaCentrix conductive ink that can be inkjet printed and PELCO conductive paint. The conductivities ranged from 5×10^3 to 5.8×10^7 S/m. The thickness of the copper and PELCO is significantly greater than the skin depth, the gold nanoparticle polymer is close to the skin depth at its highest conductivity, and the NovaCentrix material is thinner than the skin depth.

Whether the antennas were in air or in contact with muscle, as the conductivity or

skin depth of the antenna material is reduced the resonant frequency is lowered, the S_{11} degrades, and the bandwidth is increased, similar to results previously reported for other types of antennas in air in [31, 32]. A minimum conductivity of 10^3 S/m could provide sufficient antennas for some applications. Antennas with conductivities of 10^5 S/m and above were similar to those that were 10^7 S/m. Fat was found to sufficiently insulate antennas as well as plastic of other good insulators, such that they have better S_{11} and higher resonant frequency. Thicker insulation (in this case thicker fat) is better than thin, consistent with results seen for other types of implantable antennas [6-11].

These results demonstrate the potential of subdermal antennas, placed in the fat layer below the skin, to be effective radiating elements for implantable biological systems.

Table 3.1 Material properties of the conductive materials and tissues

	Conductivity [S/m]	L [mm]	W [mm]	Dielectric Constant ε_r	Thickness	Skin Depth [2 GHz]	Skin Depth [402 MHz]
Copper Tape	5.8×10^7	30	6.35		70 µm	1.48 µm	3.29 µm
Gold Nanoparticle [109]	7.9×10^5 1.0×10^5 5.0×10^3	30	6		10.0 µm 12.2 µm 13.4 µm	12.7 µm 35.6 µm 159 µm	5.61 µm
NovaCentrix [79]	2.04×10^5 - 2.22×10^7	30	6.35		0.75 – 1 µm	2.39 - 24.9 µm	5.32 - 55.6 µm
PELCO #16062 Ink [82]	1×10^5	30	3		100 µm	35.6 µm	79.4 µm
Skin [113, 122, 123]	0.68			46.7	0.062 µm	13.6 mm	30.4 mm
Fat [113, 122, 123]	0.081			11.6	8.00 mm	39.5 mm	88.2 mm
Muscle [113, 122, 123]	0.82			57.9	Simulation, 200 mm Measurement > 25 mm	12.4 mm	27.7 mm

Table 3.2 Measured results for strip dipole antennas in free space. These are shown as black squares in Figure 3.2.

	Center Frequency [GHz]	Center S_{11} [dB]	Bandwidth [%]
Copper Tape	2.18	-37.9	20.2
Au Nano (7.9×10^5 S/m)	1.91	-23.6	20.9
PELCO Ink #16062	2.14	-20.0	32.3
NovaCentrix	1.98	-14.9	16.7

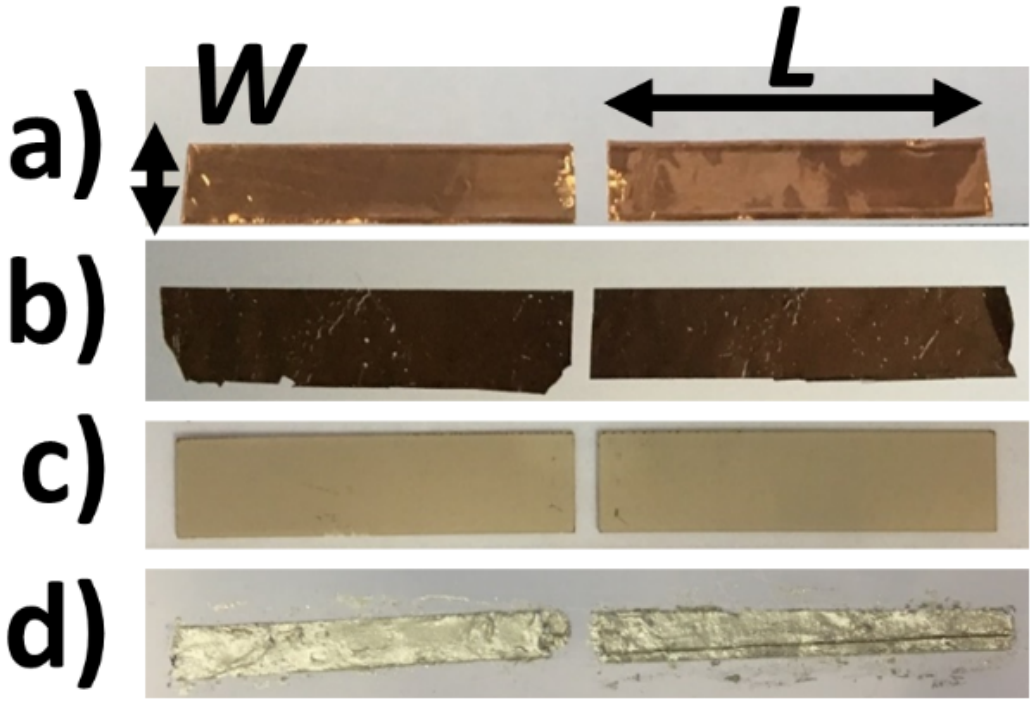

Figure 3.1 Fabricated antennas. From top to bottom: a) Copper tape, b) gold nanocomposite, c) NovaCentrix printed, d) PELCO #16062 ink.

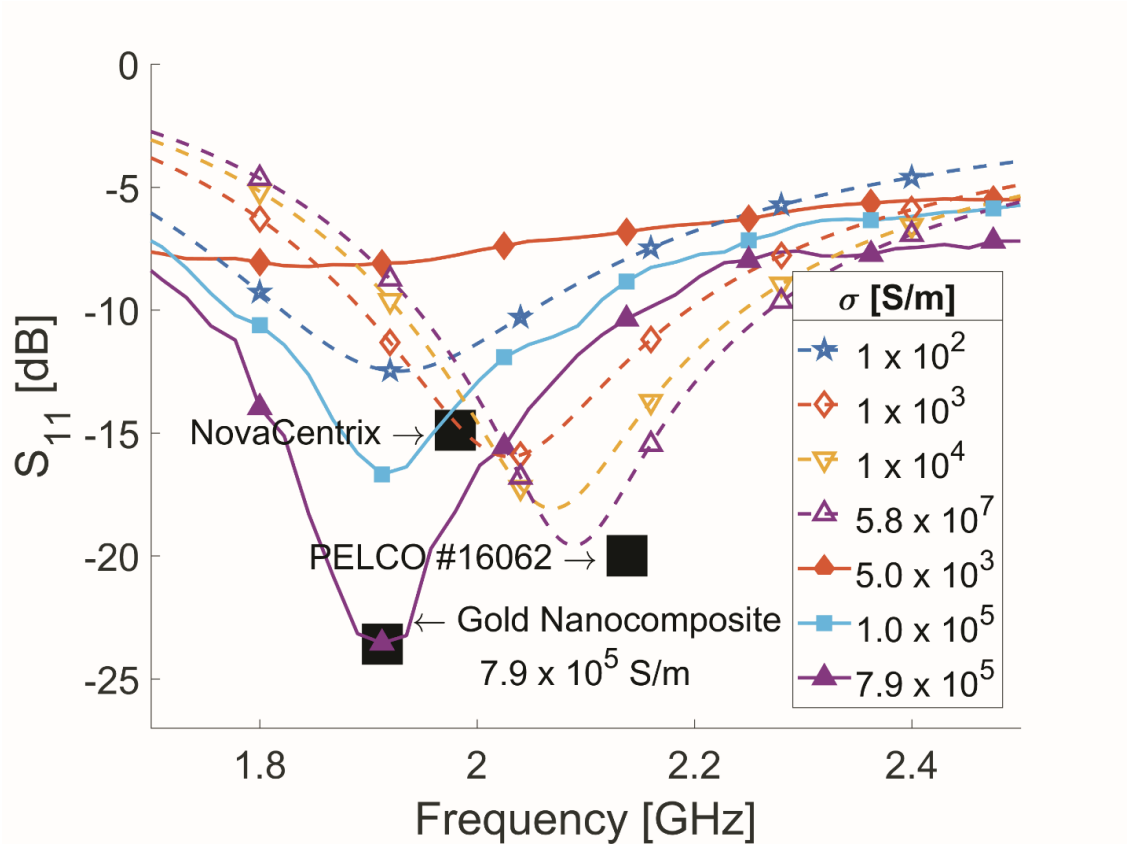

Figure 3.2 Effect of conductivity on the S_{11} of a strip dipole in free space. Dashed lines show simulated results, and solid lines show measurements for the gold nanocomposite material. Squares show the minimum S_{11} for dipoles made from Novacentrix and PELCO inks as well as the most conductive gold nanocomposite. Reducing the conductivity reduces the resonant frequency, degrades the S_{11}, and increases the bandwidth.

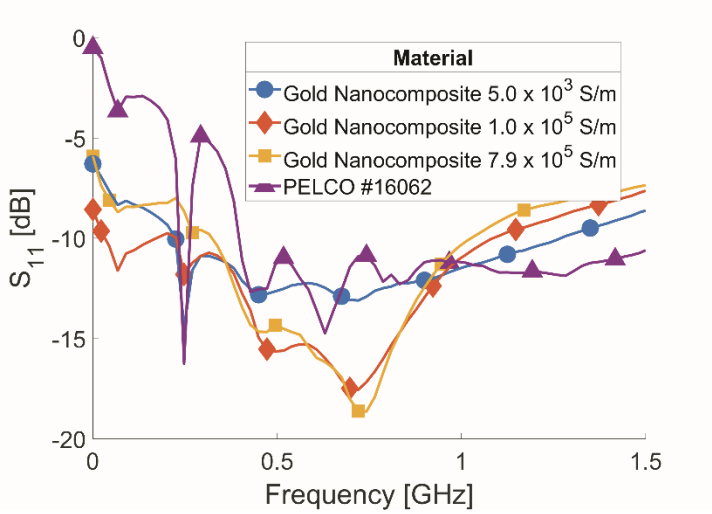

(a)

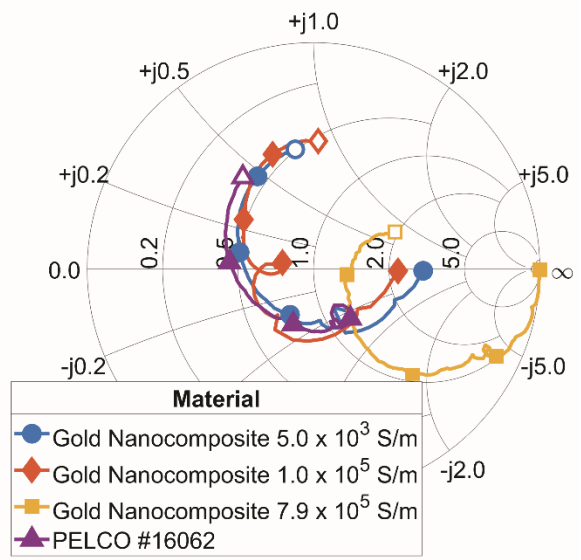

(b)

Figure 3.3 Measured effect of conductivity on the S_{11} of a strip dipole placed on excised (pork) muscle. Reducing the conductivity reduces the resonant frequency, degrades the S_{11}, and increases the bandwidth.

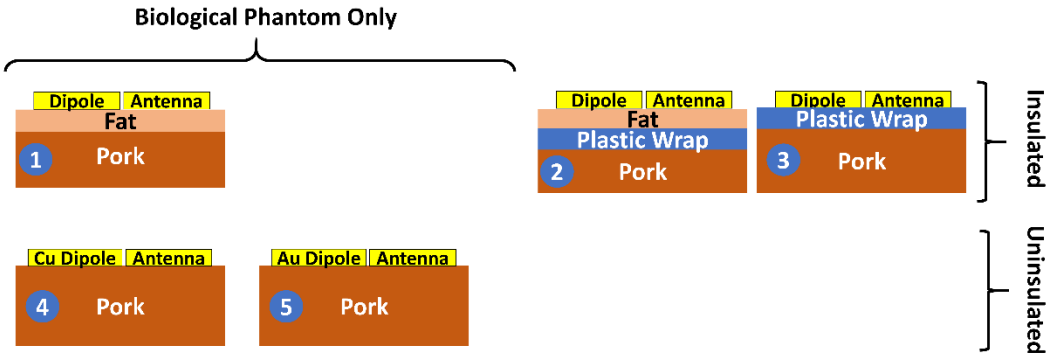

Figure 3.4 Measurement set ups for evaluating the impact of fat as an electrical insulator. The plastic wrap is approximately 12.5 μm thick, and the fat is 4 mm thick.

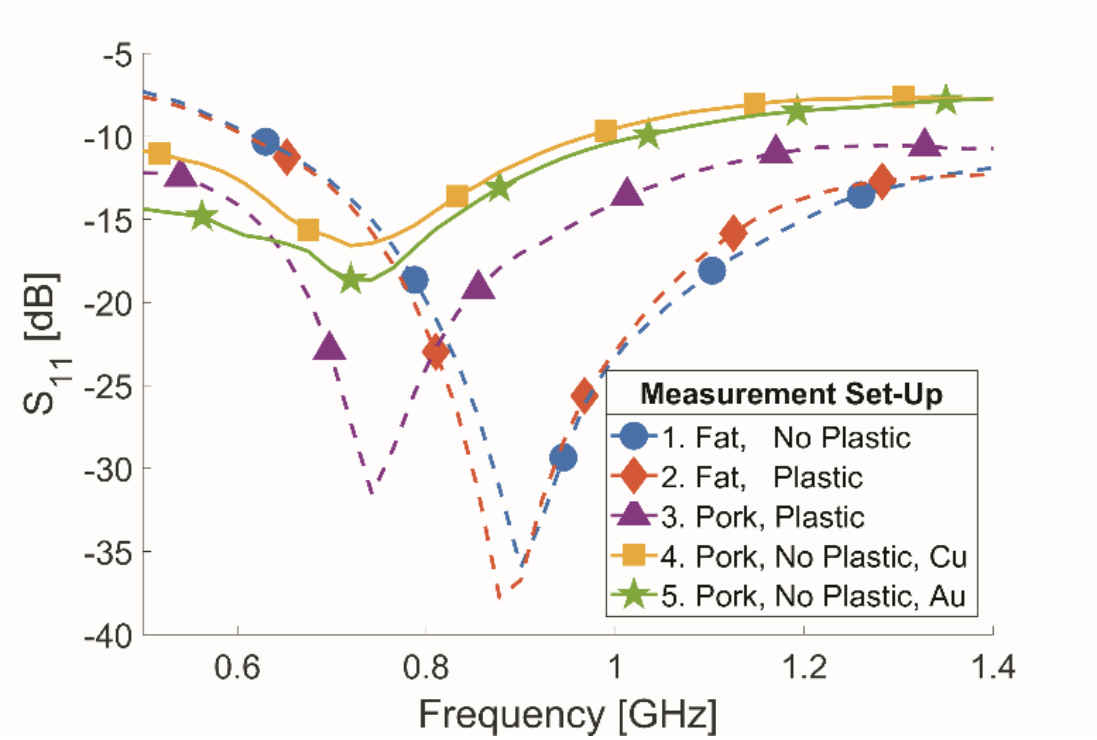

Figure 3.5 Measured S11 for strip dipoles in the configurations in Figure 3.4. The antennas are made from copper, except for (5.), which is gold nanocomposite with a conductivity of 7.9 x 10^5 . Dashed lines are for antennas insulated with plastic wrap and/or fat. Solid lines are for antennas in direct contact with excised pork muscle.

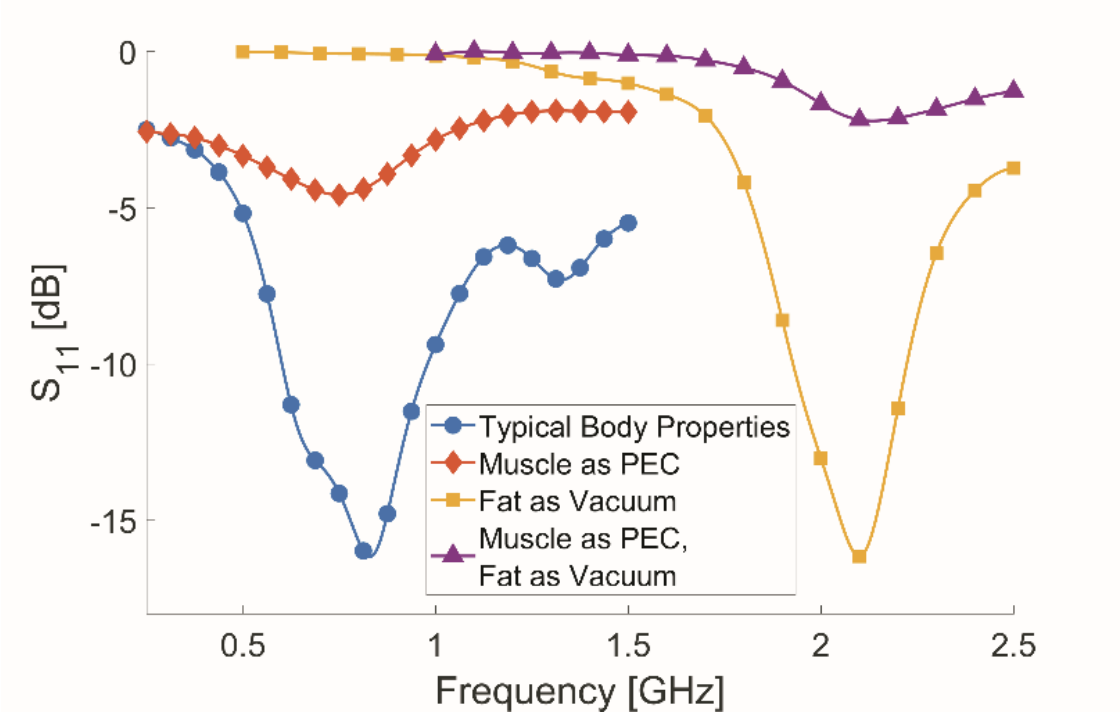

Figure 3.6 Simulated S11 of a copper strip dipole with variations in biological material properties. In the first case, the simulation is depicted by (1.) in Figure 3.4 using the material properties listed in Table 3.1. In the second case the dimensions remain constant, but the pork is replaced by a block of PEC. In the third case, the 8 mm fat layer is replaced with vacuum. In the last case, both the muscle and fat are replaced by PEC and vacuum respectively. The high dielectric fat increases electrical distance from antenna to ground plane. The muscle acts as a ground plane, but the high dielectric and low conductivity do not degrade performance as much as PEC.

3.5 References

[1] G. Marrocco, "RFID antennas for the UHF remote monitoring of human subjects," *IEEE Transactions on Antennas and Propagation,* vol. 55, no. 6, pp. 1862-1870, 2007.

[2] M. A. Ziai and J. C. Batchelor, "Temporary on-skin passive UHF RFID transfer tag," *IEEE Transactions on Antennas and Propagation,* vol. 59, no. 10, pp. 3565-3571, 2011.

[3] A. Chrysler, C. Furse, and Y. Chung, "Biocompatible, implantable UHF RFID antenna made from conductive ink," in *2016 IEEE International Symposium on Antennas and Propagation (APSURSI)*, 2016, pp. 467-468.

[4] O. O. Rakibet, C. V. Rumens, J. C. Batchelor, and S. J. Holder, "Epidermal passive RFID strain sensor for assisted technologies," *IEEE Antennas and Wireless Propagation Letters,* vol. 13, pp. 814-817, 2014.

[5] S. Milici, S. Amendola, A. Bianco, and G. Marrocco, "Epidermal RFID passive sensor for body temperature measurements," in *2014 IEEE RFID Technology and Applications Conference (RFID-TA)*, 2014, pp. 140-144.

[6] C. Furse, H. Lai, C. Estes, A. Mahadik, and A. Duncan, "An implantable antenna for communication with implantable medical devices," in *IEEE Antennas and Propagation/URSI International Symposium*, 1999.

[7] K. Gosalia, G. Lazzi, and M. Humayun, "Investigation of a microwave data telemetry link for a retinal prosthesis," *IEEE Transactions on Microwave Theory and Techniques,* vol. 52, no. 8, pp. 1925-1933, 2004.

[8] J. Kim and Y. Rahmat-Samii, "Implanted antennas inside a human body: Simulations, designs, and characterizations," *IEEE Transactions on Microwave Theory and Techniques,* vol. 52, no. 8, pp. 1934-1943, 2004.

[9] P. Soontornpipit, C. M. Furse, and Y. C. Chung, "Design of implantable microstrip antenna for communication with medical implants," *IEEE Transactions on Microwave Theory and Techniques,* vol. 52, no. 8, pp. 1944-1951, 2004.

[10] I. Bahl, P. Bhartia, and S. Stuchly, "Design of microstrip antennas covered with a dielectric layer," *IEEE Transactions on Antennas and Propagation,* vol. 30, no. 2, pp. 314-318, 1982.

[11] T. Karacolak, R. Cooper, and E. Topsakal, "Electrical properties of rat skin and design of implantable antennas for medical wireless telemetry," *IEEE Transactions on Antennas and Propagation,* vol. 57, no. 9, pp. 2806-2812, 2009.

[12] F. Palmisano, D. Centonze, A. Guerrieri, and P. G. Zambonin, "An interference-free biosensor based on glucose oxidase electrochemically immobilized in a non-conducting poly (pyrrole) film for continuous subcutaneous monitoring of glucose through microdialysis sampling," *Biosensors and Bioelectronics,* vol. 8, no. 9-10, pp. 393-399, 1993.

[13] A. Poscia, D. Messeri, D. Moscone, F. Ricci, and F. Valgimigli, "A novel continuous subcutaneous lactate monitoring system," *Biosensors and Bioelectronics,* vol. 20, no. 11, pp. 2244-2250, 2005.

[14] A. Moscicki, J. Felba, T. Sobierajski, J. Kudzia, A. Arp, and W. Meyer, "Electrically conductive formulations filled nano size silver filler for ink-jet technology," in *Polymers and Adhesives in Microelectronics and Photonics, Polytronic, 2005. Polytronic 2005. 5th International Conference on*, 2005, pp. 40-44: IEEE.

[15] J. Sidén, M. Fein, A. Koptyug, and H.-E. Nilsson, "Printed antennas with variable conductive ink layer thickness," *IET Microwaves, Antennas & Propagation,* vol. 1, no. 2, pp. 401-407, 2007.

[16] B. J. Willis, *Compact form fitting small antennas using three-dimensional rapid prototyping*. The University of Utah, 2012.

[17] K. Hall, A. Chrysler, and C. Furse, "A comparison of solid, mesh, and segmented broad dipoles in biological environments," in *2017 IEEE International Symposium on Antennas and Propagation (APSURSI)*, San Diego, CA, 2017.

[18] M. A. Gaynes, R. H. Lewis, R. F. Saraf, and J. M. Roldan, "Evaluation of contact resistance for isotropic electrically conductive adhesives," *IEEE Transactions on Components, Packaging, and Manufacturing Technology: Part B,* vol. 18, no. 2, pp. 299-304, 1995.

[19] K. Bock, "Polytronics-electronics and systems on flexible substrates," in *VLSI Technology, 2005.(VLSI-TSA-Tech). 2005 IEEE VLSI-TSA International Symposium on*, 2005, pp. 53-56: IEEE.

[20] A. R. Duggal and L. M. Levinson, "A novel high current density switching effect in electrically conductive polymer composite materials," *Journal of Applied Physics,* vol. 82, no. 11, pp. 5532-5539, 1997.

[21] Novacentrix. *NovaCentrix Web Page*. [Online] Available: https://www.novacentrix.com/

[22] M. D. Dickey, "Emerging applications of liquid metals featuring surface oxides," *ACS Applied Materials & Interfaces,* vol. 6, no. 21, pp. 18369-18379, 2014.

[23] R. Vasold, E. Engel, B. König, M. Landthaler, and W. Bäumler, "Health risks of tattoo colors," *Analytical and bioanalytical chemistry,* vol. 391, no. 1, pp. 9-13, 2008.

[24] E. C. Cho, Q. Zhang, and Y. Xia, "The effect of sedimentation and diffusion on cellular uptake of gold nanoparticles," (in eng), *Nat Nanotechnol,* Research Support, N.I.H., Extramural Research Support, Non-U.S. Gov't Research Support, U.S. Gov't, Non-P.H.S. vol. 6, no. 6, pp. 385-91, Apr 24 2011.

[25] S. Chinnayelka and M. McShane, "Competitive binding assays in microcapsules as" smart tattoo" biosensors," in *Sensors, 2005 IEEE*, 2005, p. 4: IEEE.

[26] O. Couture *et al.*, "Ultrasound-inducible fluorescent particles for internal tattooing," in *Ultrasonics Symposium (IUS), 2009 IEEE International*, 2009, pp. 85-88: IEEE.

[27] S. A. Hoenig, P. L. Gildenberg, and K. K. Murthy, "Generation of pernanent, dry, electrical contacts by tattooing carbon into skin tissue," *IEEE Transactions on Biomedical Engineering,* no. 4, pp. 380-382, 1978.

[28] K. Balmain and E. Jordan, *Electromagnetic waves and radiating systems*. Prentice Hall, New Jersey, 1968.

[29] Y. Kim *et al.*, "Stretchable nanoparticle conductors with self-organized conductive pathways," *Nature,* Letter vol. 500, no. 7460, pp. 59-63, 08/01/print 2013.

[30] Ted Pella Co. *PELCO 16062 Technical Notes*. [Online] Available: https://www.tedpella.com/technote_html/16062_TN.pdf

[31] M. Shahpari and D. V. Thiel, "The impact of reduced conductivity on the performance of wire antennas," *IEEE Transactions on Antennas and Propagation,* vol. 63, no. 11, pp. 4686-4692, 2015.

[32] C. D. Rouse, M. R. Kurz, B. R. Petersen, and B. G. Colpitts, "Performance evaluation of conductive-paper dipole antennas," *IEEE Transactions on Antennas and Propagation,* vol. 61, no. 3, pp. 1427-1430, 2013.

[33] R. J. Halter *et al.*, "The correlation of in vivo and ex vivo tissue dielectric properties to validate electromagnetic breast imaging: Initial clinical experience," *Physiological Measurement,* vol. 30, no. 6, pp. S121-S136, 06/02 2009.

[34] S. Gabriel, R. W. Lau, and C. Gabriel, "The dielectric properties of biological tissues: II. Measurements in the frequency range 10 Hz to 20 GHz," *Physics in Medicine and Biology,* vol. 41, no. 11, p. 2251, 1996.

[35] S. Lee Chin and Michael, "Changes in dielectric properties of ex vivo bovine liver at 915 MHz during heating," *Physics in Medicine & Biology,* vol. 46, no. 1, p. 197, 2001.

[36] L. Chin and M. Sherar, "Changes in the dielectric properties of rat prostate ex vivo at 915 Mhz during heating," *International Journal of Hyperthermia,* vol. 20, no. 5, pp. 517-527, 2004/08/01 2004.

[37] R. E. Collins and F. J. Zucker, "Antenna Theory-part 2," *New York: M cGraw-Hill,* p. 20, 1969.

[38] A. A. Lestari, A. G. Yarovoy, and L. P. Ligthart, "Ground influence on the input impedance of transient dipole and bow-tie antennas," *IEEE Transactions on Antennas and Propagation,* vol. 52, no. 8, pp. 1970-1975, 2004.

[39] A. A. Lestari, A. G. Yarovoy, and L. P. Ligthart, "Numerical and experimental analysis of circular-end wire bow-tie antennas over a lossy ground," *IEEE Transactions on Antennas and Propagation,* vol. 52, no. 1, pp. 26-35, 2004.

[40] P. Parhami and R. Mittra, "Wire antennas over a lossy half-space," *IEEE Transactions on Antennas and Propagation,* vol. 28, no. 3, pp. 397-403, 1980.

[41] P. Raumonen, L. Sydanheimo, L. Ukkonen, M. Keskilammi, and M. Kivikoski, "Folded dipole antenna near metal plate," in *IEEE Antennas and Propagation Society International Symposium. Digest. Held in conjunction with: USNC/CNC/URSI North American Radio Sci. Meeting (Cat. No.03CH37450)*, 2003, vol. 1, pp. 848-851 vol.1.

[42] D. M. Pozar, *Microwave engineering*. John Wiley & Sons, 2009.

CHAPTER 4

A COMPARISON OF SOLID, MESH, AND SEGMENTED STRIP DIPOLES IN A SUBDERMAL ENVIRONMENT

4.1 Abstract

The objective of this paper is to evaluate the feasibility of subdermal (tattoo) antennas in the fat layer, which use the low conductivity of the fat to electrically insulate the antenna. Simulations and measurements were used to evaluate the current distributions that are shared between solid, segmented, and meshed strip dipole antennas and surrounding body tissues to give insight into the performance of subdermal antennas. The body tissues play a strong role in adapting the current distributions. The high dielectric materials electrically shorten the antenna, keeping current from reaching its ends. The high conductivity of muscle draws current into the body. Any voids in the antennas (e.g., gaps between segments or holes in the mesh) are particularly important, as they generate stronger coupling to the tissues. The feasibility of using fat as insulation for subdermal antennas is confirmed with measurement and verified in simulation. This paper paves the way for future design work for subdermal antennas that use the fat layer as electrical insulation. This enables biomedical telemetry antennas that are much larger and more flexible in their designs.

4.2 Introduction

Wireless telemetry for implanted medical devices is necessary to monitor battery level, device health, and patient well-being. Antennas used for these applications have unique design challenges, as the conductive tissues in the body short-circuit the antennas, carrying the current away from the antenna in ways that are difficult to control. Electrical insulation is used to prevent or reduce this effect, such as the plastic sticker that separates epidermal antennas from the body surface [1-3] or the silicone or other insulating superstrates on implantable antenna designs [4-9]. This paper is an exploration of subdermal antennas near the Industrial Scientific Medical (ISM) 915 MHz band. We evaluate how they may use the fat layer as electrical insulation, and how the muscle below impacts the current as well. Fat is a relatively low-conductivity tissue compared to muscle and other higher water content tissues. This work will focus on the current distributions, and how the current moves through these tissues.

Subdermal antennas could be made from biocompatible versions of paints [10-13], conductive adhesives [14], polymers [15, 16], inks [17], and fluidic conductors [18] in a variety of shapes and designs [4-9]. Current work in polymer engineering is underway to develop an injectable nanocomposite hydrogel that is initially a fluid but turns to a solid at body temperature [19-22]. The materials used in this paper are good proxies for this up-and-coming new material.

This paper evaluates the subdermal current distributions of simple strip dipoles (shown in Figure 4.1) that are either solid, meshed, or segmented where the current is carried both by the antenna and the surrounding tissues. The simple strip dipole is chosen, not because it is the best implantable antenna design, but because its simplicity allows a

complete consideration of this shared current distribution. Segmented and meshed dipoles are considered, because one of the prospective methods of creating subdermal antennas is to tattoo or inject conductive materials under the skin, which may result in antennas with voids in and around the conductive material. In this case, the current would be carried by both the conductive parts of the antenna and the surrounding conductive body. We consider segmented and meshed antennas to evaluate these potential effects on the current distribution.

This work examines the current distribution shared between the dipole and surrounding tissues, and its impact on antenna performance. Solid strip dipoles are traditional designs made where the material making up the arms of the antennas is solid (doesn't have any holes). Segmented antennas use capacitive coupling to pass the current from one segment to another. This is similar to capacitive coupling used for microstrip filter designs [23]. The wider the spacing between segments, the greater the capacitance. We can also expect that more current will couple to and pass through the tissues for wider spacing.

Meshed antennas have been used for space applications [24], wearables [25], and transparent antenna applications [26]. Meshed antennas tend to act like solid antennas of the same shape if the spacing of the mesh elements is less than $\lambda/30$ [25, 26] (in our application, the elements are spaced by less than $\lambda/100$ in the tissue). When less dense meshing is used, a minor center frequency shift and reduction in realized gain and bandwidth occurs [25]. Meshes can be made from either solid (wire) material, or ink-jet printed [27]. Previous studies of mesh antennas have been in air or on a nonconducting surface such as glass. This paper considers subdermal mesh antennas implanted in the

body, where the conductive material of the body acts as part of the antenna, filling in the space between the grid of the mesh.

Section 4.3 of this paper describes the antennas and their material properties. Section 4.4 describes the simulated current distributions and antenna performance. In Section 4.5, measurements of a subdermal antenna confirm these effects for solid strip dipole antennas, comparing the simulations with perfect electric conductor (PEC) to measurements of antennas made from PELCO conductive paste [28] and a novel gold nanocomposite material [29]. Conclusions are summarized in Section 4.6.

4.3 Antennas, Materials, Properties

Strip dipole antennas in a layered skin-fat-muscle biological model were used in this study. Strip dipoles (shown in Figure 4.1 (a-c)) are thin, flat dipoles with an arm width 20 – 30% of the arm length. Slightly broader band than a thin wire dipole, strip dipoles have higher peak resistance and reactance [30]. In this work, the dipoles are about L = 30 mm long and about W = 6 mm wide, which corresponds to a 2.5 GHz design frequency in free space for a Hertzian dipole and about 2 GHz for the strip dipole. In the body, the design frequency is much lower, depending on the configuration, closer to the 915 MHz ISM band. The segmented antenna was made slightly longer to account for the gaps, and the mesh antenna dimensions were based on the closest dimensions that would match a commercially-available mesh material [31].

The dipoles in Figure 4.1 (a-c) are all simulated in the subdermal body model shown in Figure 4.2 (a). The length of the solid strip dipole is exactly 30 mm, while the segmented (L = 31 mm) and mesh (L = 30.2 mm) dipoles are slightly longer. The widths of the solid

and segmented strip dipoles are 6 mm, while the mesh dipole is slightly wider (8.2 mm) to accommodate the commercial mesh material. The simulated solid and segmented dipole are 100 μm thick. The simulated mesh dipole is 280 μm thick, again because of the commercially available copper mesh material. For these PEC antennas, these thicknesses exceed the skin depth.

The simulated antennas are imbedded in a subdermal model of skin, fat, and muscle shown in Figure 4.2 (a). The properties of the tissues at 915 MHz are given in Table 4.1 [32-34]. The conductive antenna is imbedded in the center of the 8 mm thick fat layer below the skin, which is 1 mm thick. The muscle is 30 mm thick. The fat acts as a semi-insulator, reducing the shorting effect of more conductive tissues such as muscle. Further discussion of the simulated antennas is in Section 4.4.

The fabricated strip dipoles are made from PELCO conductive paste [28] and a novel gold nanocomposite material [29] shown in Figure 4.1 (d and e), respectively. Both antennas are the same length (L = 30 mm), but the PELCO dipole is W = 3 mm and the gold nanoparticle strip dipole is W = 6 mm. These antennas are measured using the sub-fat and pseudo-epidermal body models in Figure 4.2 (b, c). Further discussion of this measurement is found in Section 4.5.

4.4 Subdermal Antenna Current Distributions

The ultimate goal of this work is to be able to tattoo an antenna under the skin, using the subdermal fat layer as electrical insulation, as shown in Figure 4.2 (a). Subdermal antennas could be made from biocompatible versions of paints [10-13], conductive adhesives [14], polymers [15, 16], inks [17], and fluidic conductors [18]. The gold

nanocomposite material shown in Figure 4.1 (e) could potentially be re-engineered to cross link and solidify at body temperature [19-22]. Any of these fluidic materials could be injected under the skin, but holes and gaps would be expected to occur due to variability in the injection method. This work examines the effect of voids and gaps on the current distribution and the performance of the subdermal antennas.

The solid, segmented, and meshed strip dipoles shown in Figure 4.1 (a-c) in the subdermal environment shown in Figure 4.2 (a) were simulated using CST full wave electromagnetic simulations. The antennas were imbedded in the center of the fat layer and excited with a 50 Ω source. CST was used to calculate the current distributions shown in Figure 4.3 and the S_{11} values shown in Figure 4.4. CST uses the magnetic field on the surface of the antenna to calculate the surface current. Each current distribution is taken at the peak resonance (the frequency at which the S_{11} reaches a minima). This is 0.70 GHz, 0.69 GHz, 1.8 GHz for the solid, mesh, and segmented dipole antennas, respectively. A summary of the antenna properties is shown in Table 4.2.

4.4.1 Solid Dipole

The solid strip dipole shown in Figure 4.1 (a) was simulated in the center of the fat layer (subdermal environment) shown in Figure 4.2 (a). The S_{11} as a function of frequency is shown in Figure 4.4. The current distribution at the peak resonance (0.70 GHz) is shown in the top row of Figure 4.3. Several observations can be made from these figures. The peak resonance is controlled by the effective length of the antenna. For this dipole, the current does not travel to the tips of its arms, so the full physical size of the antenna is not used. In air (not shown), the current is also zero at the tips, but the overall short-circuiting

effect from the tissues in the body reduces the tip currents even further. The maximum current density occurs at the edges of the antenna. This makes the edges of the strip the dominant radiating feature of the antenna. Because the strip dipole is relatively wide, it effectively acts like two closely spaced parallel antennas. This concept will be seen again in the mesh antenna. The width of the strip antenna can be thought of as creating multiple paths for the current. On the outer edge of the strip, the current path is slightly longer than in the center. This makes the strip dipole broader band than an ideal Hertzian dipole of the same length. The current distribution transmits further into the body below the antenna than outside the body above the antenna. This is because it is drawn or guided deeper into the body by the conductive muscle tissue.

4.4.2 Mesh Dipole

The second row in Figure 4.3 shows the current distribution of the subdermal mesh dipole seen in Figure 4.1 (c) at its peak resonance (0.69 GHz). The holes in the mesh antenna are less than $\lambda/100$ in tissue, so it acts very much like the solid antenna [25, 26]. The current is again zero at the tip, at approximately the same distance along the arms as for the solid dipole. This gives it essentially the same peak resonance, which can be seen in Figure 4.4. The mesh antenna also radiates dominantly from its edges. Where the solid dipole behaved similar to two parallel antennas, the mesh behaves similar to five parallel wire dipoles excited by the same source. The orthogonal connecting wires (at 1.29 mm intervals) help couple the currents between these wires. The current distribution is strongest along the outer wires, just as it is for the edges of the solid strip dipole. The difference between the current distribution on these outer edges and the center creates a bandwidth

very similar to that of the solid dipole (see Figure 4.4).

The difference between the two antennas is that the gaps in the mesh structure allow the current to couple even more strongly to the tissues for the mesh antenna, making the current concentrate closer to the antenna as seen in the right column of Figure 4.3. A zoomed-in version is shown at the bottom, near the color bar. This leads to more penetration into the tissue than for the solid dipole, and a reduced S_{11}, as shown in Figure 4.4. Compared to the solid dipole, the mesh dipole is slightly more efficient, and has a similar directivity as seen in Table 4.2.

4.4.3 Segmented Dipole

The third row in Figure 4.3 shows the current distribution of the segmented dipole shown in Figure 4.1 (b) at its peak resonance (1.8 GHz). The segmented dipole is similar to a shorter strip dipole with additional electromagnetically coupled arms. The weaker coupling between segments leads to lower current distributions in the outermost antenna segments than in the innermost and middle segments. The weak coupling results in a higher peak resonance with the inner segments controlling most of the radiation. It is also clear that most of the electromagnetic coupling between segments occurs below the dipole in the fat and muscle layers, as seen in the right column of Figure 4.3.

Compared to the solid and mesh dipoles, the segmented dipole has a higher peak resonance and weaker S_{11}. This is seen in Figure 4.4 and predicted by the current distribution in Figure 4.3. The mesh and segmented dipoles have a similarly small region of peak current distribution in the region between the antenna and the skin layer of the body model. As seen in Table 4.2, the segmented antenna is several dB more efficient than the

solid and mesh dipole, but more directive. The increased directivity is expected based on the region of high current shown in Figure 4.3.

4.5 Measurement of Antennas

This section confirms the feasibility of antennas in the fat layer by measuring antennas fabricated from PELCO conductive paste [28] and from a novel gold nanocomposite material [29]. Although the PELCO conductive ink is not specifically biocompatible, it is a good proxy for a material that could potentially be used for subdermal injection [19-21]. PELCO product #16062 is a conductive paint (10^5 S/m) from Ted Pella Co. that is easily spread [28]. The thickness (approximately 100 μm) is significantly greater than the skin depth (52 μm at 915 MHz), making it act very similar to PEC at this frequency [35-37]. The gold nanoparticle material is very thin (12.7 μm), close to its skin depth (19 μm at 915 MHz). Although it is very conductive (7.9 x 10^5 S/m), the skin depth effects reduce the antenna performance, making a conductivity above 10^5 S/m a good target for injectable antenna performance [37]. The properties of PELCO and the gold nanocomposite materials are summarized in Table 4.1.

The antennas were painted (PELCO) or placed (gold nanoparticle composite) on pork loin, as represented in Figure 4.2 (b). Excised rat skin (approximately 2.6 mm thick) with a 1.7 mm fat layer was placed over the top. A picture of the gold nanoparticle subdermal antenna is shown in Figure 4.1. The sub-fat antenna is in direct contact with the pork loin, so the muscle loss will be greater than in the simulations. The hair of the rat in this figure is bright yellow due to the preservation fluid. The dipole seen Figure 4.5 is the same gold nanoparticle antenna shown in Figure 4.1 (e).

To probe the antenna, metal pins (seen in Figure 4.5) are placed through the rat skin and fat and bent as represented in Figure 4.2 (b) so that they are in direct contact with the strip dipole. The metal pins are wrapped around a modified SMA probe that is connected to a network analyzer. The measured S_{11} for the PELCO and gold nanocomposite sub-fat dipoles are shown in Figure 4.6. The PELCO antenna (with thickness greater than skin depth) has a better S_{11} than the higher conductive gold nanocomposite, indicating that future designs will benefit from thicker conductive materials.

A pseudo-epidermal antenna was then created by flipping the rat skin over, so that the antenna is on top, as represented in Figure 4.2 (c). The measured S_{11} is shown in Figure 4.6. As compared to the sub-fat antenna, the fat layer in the pseudo-epidermal antenna reduces the shorting effect of the muscle, while also increasing the distance between the antenna and muscle. This increases the peak resonance and improves the S_{11}.

One concern with these measurements was that it was difficult to tell when a good contact with the antennas being measured. All of the materials are soft and flexible, the fat and pork are somewhat lumpy, and the probes are solid, hard wires that we are trying to connect to the antenna. Aligning the bent pins and antenna and making good contact between the pins and SMA connector all required care and can be expected to result in some variability in the measurements. To better understand this variability, the PELCO strip dipole was probed multiple times, slightly rearranging the location of the probe and antenna each time. The range of these measurements is shown as the shaded region in Figure 4.6. The solid lines show a single representative measurement. Despite the difficulty establishing probe to pin contact, probe contact with rat skin, and aligning the pins with the subdermal antenna, the well-controlled range of these results give confidence in the

repeatability of the measurements.

The measurements in this section support the idea that fat is capable of insulating an imbedded antenna, as seen from increased frequency and bandwidth of the pseudo-epidermal antenna in Figure 4.6. This is also supported by the current distributions in Figure 4.3.

4.6 Conclusion

This paper is an exploration of subdermal antennas near the Industrial Scientific Medical (ISM) 915 MHz band and how they may use the fat layer as electrical insulation. Fat is a relatively low-conductivity tissue compared to muscle and other higher water content tissues. This work examines the current distribution shared between the dipole and surrounding tissues, and its impact on antenna performance. Strip dipoles (30 mm x 6 mm) in three different configurations (solid, segmented, meshed) were simulated in a layer of fat with skin above and muscle below.

Several observations can be made from the current distributions and S_{11} for all of the antennas. The peak resonance is controlled by the effective length of the antenna, which is reduced by the conductive tissues shorting out the current and making it not fully reach the end of the antenna. The maximum current density occurs at the edges of the antenna, or in the case of the mesh, along each of the lines of the mesh. The width of the strip antenna creates multiple paths for the current and broadens its frequency response. The current distribution transmits further into the body below the antenna than outside the body above the antenna. This is because it is drawn or guided deeper into the body by the conductive muscle tissue.

Antennas with voids couple even more strongly to the tissues. The voids in the mesh antenna are less than λ/100, so it acts nearly like the solid dipole, except for the additional coupling of current into the body tissues. The slots in the segmented antenna make it act, effectively, like a set of shorter antennas (thus raising its peak resonance frequency).

Measurements were made to confirm the feasibility of antennas in a subdermal environment. The antennas were placed between the (rat) skin and fat and the (pork) muscle. PELCO conductive paint and a novel gold nanocomposite were tested. Both created effective antennas and confirmed the feasibility of the approach. The excised rat fat shows increased insulation in the pseudo-epidermal case compared to the sub-fat case, and this compares favorably with the insulating effects of the fat seen in the current distributions in Figure 4.3.

In future work, we will focus on the shape and design of the antenna. Simple strip dipoles were used here to create a simple model that could be used to evaluate the effect of current distribution on S11, but there are not meant to be the ideal final antenna configuration. This paper paves the way for future design work for subdermal antennas that use the fat layer as electrical insulation. This enables biomedical telemetry antennas that are much larger and more flexible in their designs.

Table 4.1: Properties of the materials at 915 MHz

	σ [S/m]	L [mm]	W [mm]	ε_r	Thickness	Skin Depth
Skin [113, 122, 123]	0.68	180	140	46.7	1.00 mm	20.2 mm
Fat [113, 122, 123]	0.081	180	140	11.6	8.00 mm	58.5 mm
Muscle [113, 122, 123]	0.82	180	140	57.9	30.0 mm	18.4 mm
Solid Dipole	PEC	30	6		100 µm	N/A
Segmented g=0.3mm	PEC	31	6		100 µm	N/A
Mesh opening 1.29mm	PEC	30.1	8.15		280 µm	N/A
Au Nanoparticle [109]	7.9×10^5	30	6		12.7 µm	19 µm
PELCO [82]	1×10^5	30	3		100 µm	52 µm

Table 4.2: Performance of the antennas shown in Figure 4.1(a-c)

1W Input Power	Solid	Mesh	Segmented
Peak Resonance Frequency (GHz)	0.7	0.69	1.8
Maximum Surface Current [A/m]	43.0	39.6	69.2
Radiation Efficiency [dB]	-15.3	-14.8	-11.4
Directivity [dBi]	2.7	2.8	3.2

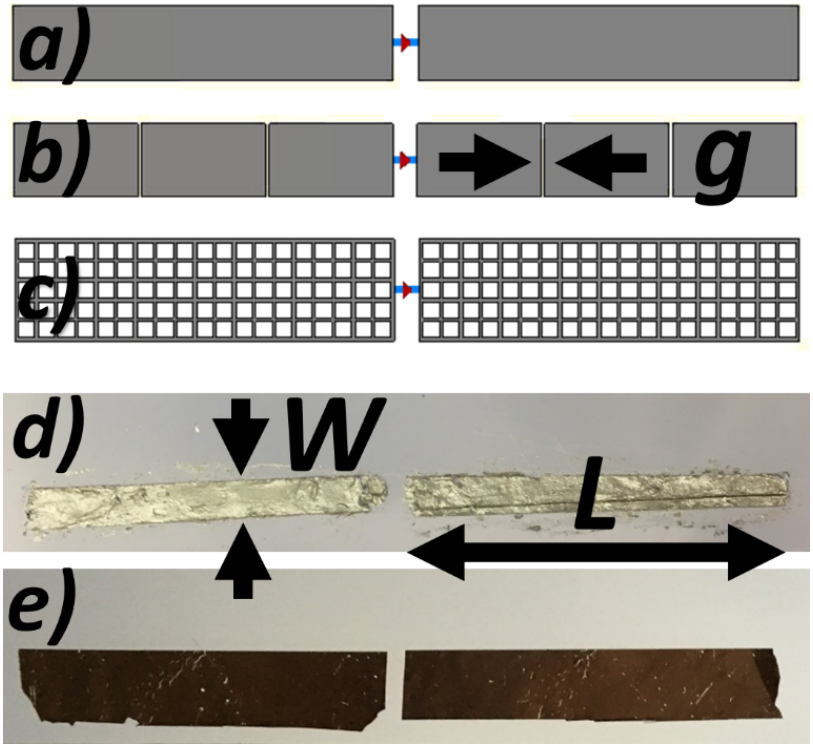

Figure 4.1 Simulated (a, b, c) and fabricated (d, e) strip dipole antennas used in this work. In b) Simulated PEC segmented strip dipole (gap size, *g*, is 0.3 mm). In c) Simulated PEC mesh strip dipole (mesh opening is 1.29 mm). d) Measured PELCO conductive ink strip dipole. e) Measured gold nanoparticle composite strip dipole. All other dimensions are found in Table 4.1.

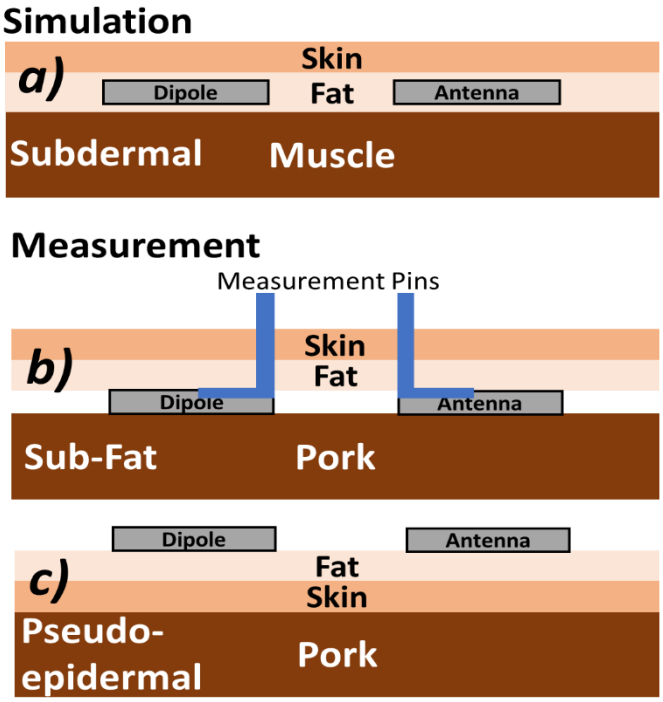

Figure 4.2 Depictions of the simulated (a) and measured (b, c) biological models. The simulated (a) subdermal biological model has a dipole antenna imbedded in the center of the fat layer, similar to a tattoo. The sub-fat model in (b) is fabricated with excised rat skin layered on top of pork so that the dipole antenna is between fat and pork. The pseudo-epidermal model in (c) has the dipole antenna on the excised rat fat layer, which has been flipped over to expose the antenna in (b) to the free space environment. A true epidermal antenna would best on the more conductive skin layer. This model is considered pseudo-epidermal, because the antenna is on a fat layer. The material properties and thicknesses are given in Table 4.1.

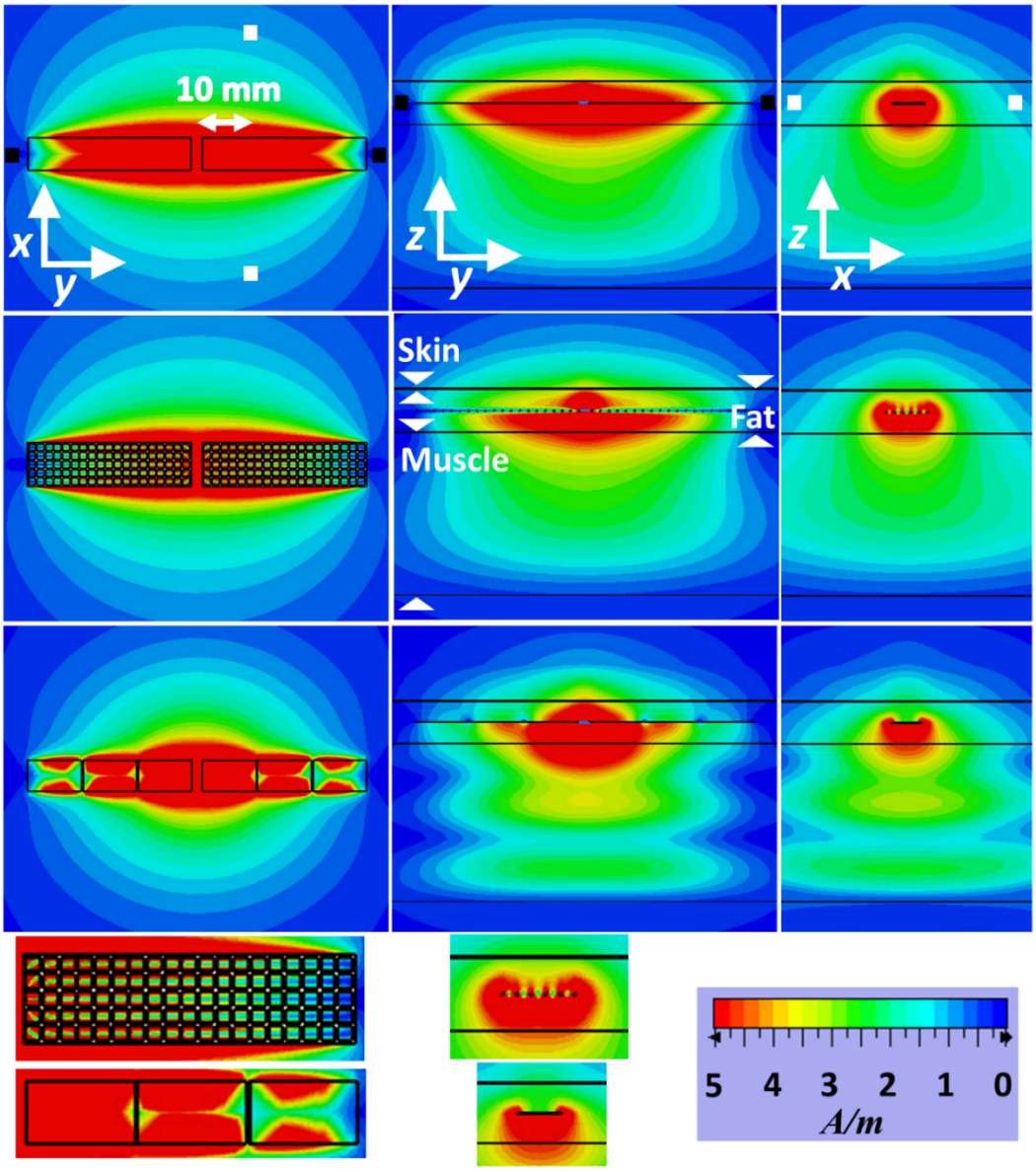

Figure 4.3 Current distribution of the strip dipole antennas shown in Figure 4.1 (a-c) imbedded in the center of the fat layer as shown in Figure 4.2 (a). The current distribution for each antenna type is taken at its peak resonance (see Figure 4.4), which is 0.70, 0.69, and 1.8 GHz for the strip, mesh and segmented antennas, respectively. The thicknesses of the skin (1 mm thick), the fat (8 mm thick), and the muscle (30 mm thick) are shown as black lines in the figures in the center column. Each column depicts the same cross section of a dipole antenna for easy comparison. The column on the right shows a cross section that is taken 10 mm from the center of the feeding gap between dipole arms. Black and white squares on the current distribution aid the reader in understanding the cross-section orientations. Figures at the bottom, by the color bar, zoom in on the mesh and segmented arms. The color bar legend is the same for all figures. The thickness of each layer is listed in Table 4.1. The length (parallel to the long antenna axis) is 180 mm and the width is 140 mm.

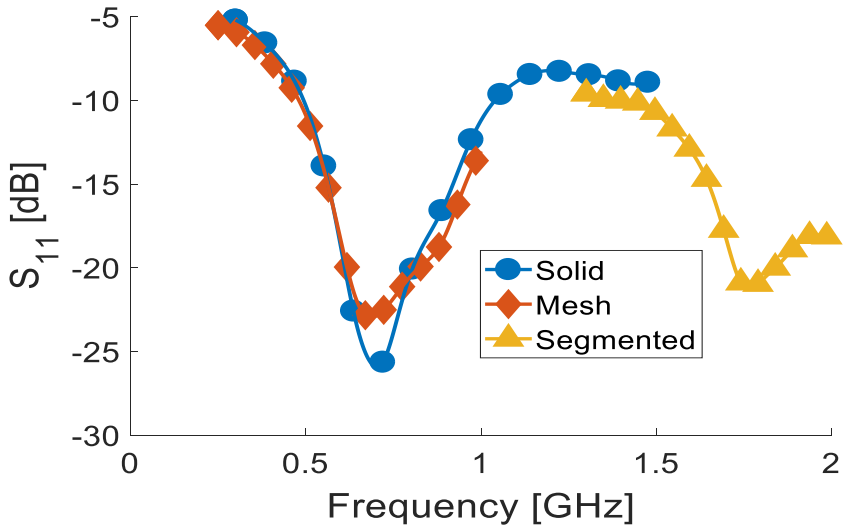

Figure 4.4 Comparison of simulated S_{11} for solid, mesh and segmented strip dipoles shown in Figure 4.1. The peak resonance (frequency with lowest S_{11}) is 0.70, 0.69, and 1.8 GHz for the strip, mesh, and segmented dipoles, respectively. The holes in the mesh are less than $\lambda/100$, making the mesh act like the solid antenna. Weak coupling between segments of the segmented antenna makes the antenna act shorter, leading to a higher peak resonance. The solid and mesh antennas have similar S_{11}, bandwidth, and frequency. The segmented antenna has a higher frequency and lower S_{11}.

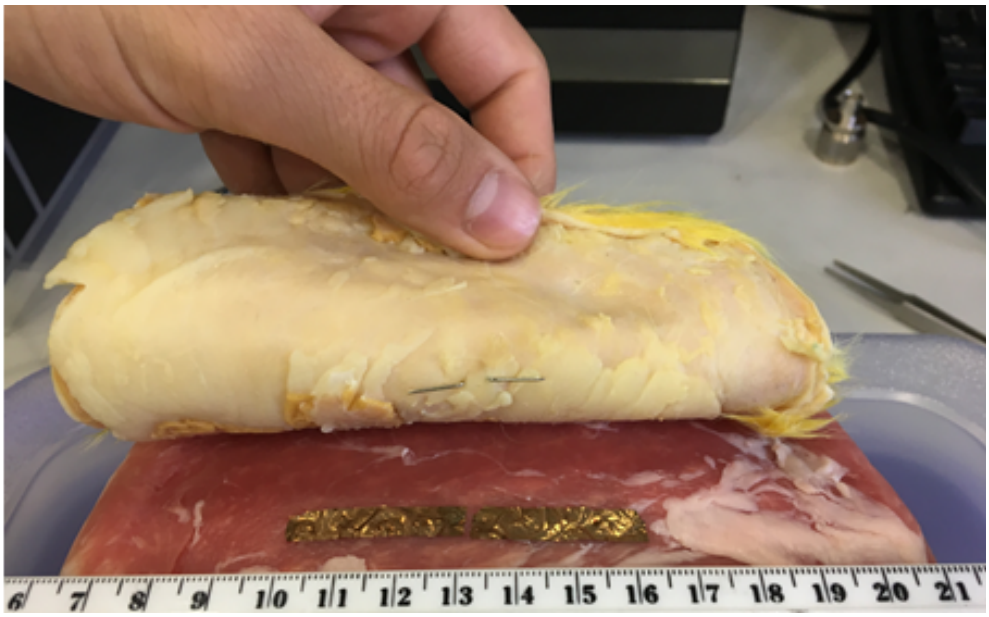

Figure 4.5 Sub-fat antenna made from gold nanoparticle material placed over pork, then covered with rat skin/fat. This is the same antenna shown in Figure 4.1 (e) in the sub-fat arrangement shown in Figure 4.2 (b). Similarly, the PELCO antenna was painted on the fatty side of the rat skin and then placed against the muscle. Pins were stuck through the skin/fat and bent to make contact with the antenna in order to connect the network analyzer and measure S_{11}. Note, the hair of the rat shown in this figure is bright yellow due to the preservation fluid.

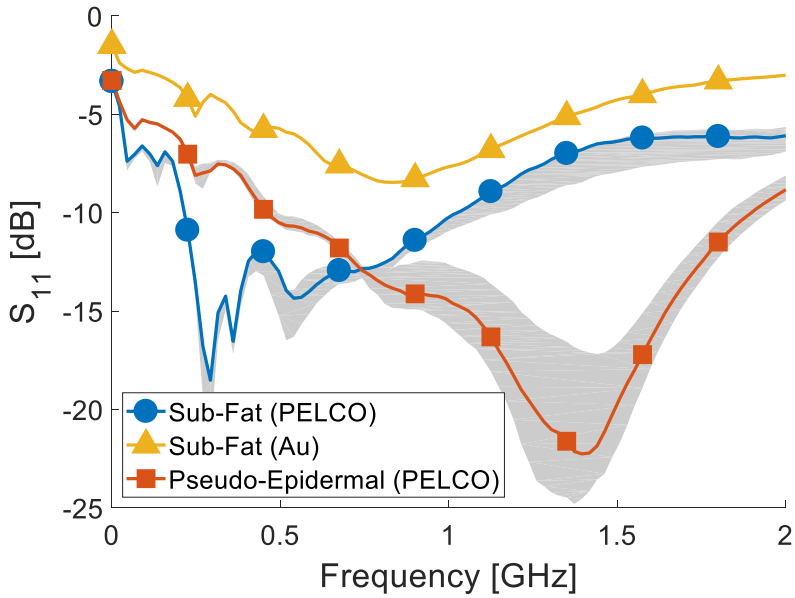

Figure 4.6 Measured S_{11} for the sub-fat gold and PELCO and pseudo-epidermal strip (PELCO) dipoles on excised rat skin and fat over pork. The shaded area represents the range of the measurements.

4.7 References

[1] G. Marrocco, "RFID antennas for the UHF remote monitoring of human subjects," *IEEE Transactions on Antennas and Propagation,* vol. 55, no. 6, pp. 1862-1870, 2007.

[2] M. A. Ziai and J. C. Batchelor, "Temporary on-skin passive UHF RFID transfer tag," *IEEE Transactions on Antennas and Propagation,* vol. 59, no. 10, pp. 3565-3571, 2011.

[3] A. Chrysler, C. Furse, and Y. Chung, "Biocompatible, implantable UHF RFID antenna made from conductive ink," in *2016 IEEE International Symposium on Antennas and Propagation (APSURSI)*, 2016, pp. 467-468.

[4] C. Furse, H. Lai, C. Estes, A. Mahadik, and A. Duncan, "An implantable antenna for communication with implantable medical devices," in *IEEE Antennas and Propagation/URSI International Symposium*, 1999.

[5] K. Gosalia, G. Lazzi, and M. Humayun, "Investigation of a microwave data telemetry link for a retinal prosthesis," *IEEE Transactions on Microwave Theory and Techniques,* vol. 52, no. 8, pp. 1925-1933, 2004.

[6] J. Kim and Y. Rahmat-Samii, "Implanted antennas inside a human body: Simulations, designs, and characterizations," *IEEE Transactions on Microwave Theory and Techniques,* vol. 52, no. 8, pp. 1934-1943, 2004.

[7] P. Soontornpipit, C. M. Furse, and Y. C. Chung, "Design of implantable microstrip antenna for communication with medical implants," *IEEE Transactions on Microwave Theory and Techniques,* vol. 52, no. 8, pp. 1944-1951, 2004.

[8] I. Bahl, P. Bhartia, and S. Stuchly, "Design of microstrip antennas covered with a dielectric layer," *IEEE Transactions on Antennas and Propagation,* vol. 30, no. 2, pp. 314-318, 1982.

[9] T. Karacolak, R. Cooper, and E. Topsakal, "Electrical properties of rat skin and design of implantable antennas for medical wireless telemetry," *IEEE Transactions on Antennas and Propagation,* vol. 57, no. 9, pp. 2806-2812, 2009.

[10] A. Moscicki, J. Felba, T. Sobierajski, J. Kudzia, A. Arp, and W. Meyer, "Electrically conductive formulations filled nano size silver filler for ink-jet technology," in *Polymers and Adhesives in Microelectronics and Photonics, Polytronic, 2005. Polytronic 2005. 5th International Conference on*, 2005, pp. 40-44: IEEE.

[11] J. Sidén, M. Fein, A. Koptyug, and H.-E. Nilsson, "Printed antennas with variable conductive ink layer thickness," *IET Microwaves, Antennas & Propagation,* vol. 1, no. 2, pp. 401-407, 2007.

[12] B. J. Willis, *Compact form fitting small antennas using three-dimensional rapid prototyping*. The University of Utah, 2012.

[13] K. Hall, A. Chrysler, and C. Furse, "A comparison of solid, mesh, and segmented broad dipoles in biological environments," in *2017 IEEE International Symposium on Antennas and Propagation (APSURSI)*, San Diego, CA, 2017.

[14] M. A. Gaynes, R. H. Lewis, R. F. Saraf, and J. M. Roldan, "Evaluation of contact resistance for isotropic electrically conductive adhesives," *IEEE Transactions on Components, Packaging, and Manufacturing Technology: Part B,* vol. 18, no. 2, pp. 299-304, 1995.

[15] K. Bock, "Polytronics-electronics and systems on flexible substrates," in *VLSI Technology, 2005.(VLSI-TSA-Tech). 2005 IEEE VLSI-TSA International Symposium on*, 2005, pp. 53-56: IEEE.

[16] A. R. Duggal and L. M. Levinson, "A novel high current density switching effect in electrically conductive polymer composite materials," *Journal of Applied Physics,* vol. 82, no. 11, pp. 5532-5539, 1997.

[17] NovaCentrix. *NovaCentrix Web Page*. [Online] Available: https://www.novacentrix.com/

[18] M. D. Dickey, "Emerging applications of liquid metals featuring surface oxides," *ACS Applied Materials & Interfaces,* vol. 6, no. 21, pp. 18369-18379, 2014.

[19] B. Yao *et al.*, "Ultrahigh- Conductivity Polymer Hydrogels with Arbitrary Structures," *Advanced Materials,* 2017.

[20] G. Chen, F. Svec, and D. R. Knapp, "Light-actuated high pressure-resisting microvalve for on-chip flow control based on thermo-responsive nanostructured polymer," *Lab on a Chip,* vol. 8, no. 7, pp. 1198-1204, 2008.

[21] N. S. Satarkar, W. Zhang, R. E. Eitel, and J. Z. Hilt, "Magnetic hydrogel nanocomposites as remote controlled microfluidic valves," *Lab on a Chip,* vol. 9, no. 12, pp. 1773-1779, 2009.

[22] F. C. Curry Jr., Andrew; Furse, Cynthia;Zhang, Huanan, "Gold Nanocomposite for Subdermal Antenna " presented at the AIChE Annual Meeting Minneapolis, MN, Oct 29-Nov 3, 2017.

[23] D. M. Pozar, *Microwave engineering*. John Wiley & Sons, 2009.

[24] A. Meguro, S. Harada, and M. Watanabe, "Key technologies for high-accuracy large mesh antenna reflectors," *Acta Astronautica,* vol. 53, no. 11, pp. 899-908, 2003.

[25] S. D. Keller, A. I. Zaghloul, V. Shanov, M. J. Schulz, and D. B. Mast, "Design considerations for a meshed carbon nanotube thread patch antenna," *IEEE Antennas and Wireless Propagation Letters,* vol. 12, pp. 1192-1195, 2013.

[26] T. W. Turpin and R. Baktur, "Meshed patch antennas integrated on solar cells," *IEEE Antennas and Wireless Propagation Letters,* vol. 8, pp. 693-696, 2009.

[27] J. R. Saberin, C. Furse, T. Yasin, and R. Baktur, "Passive feed methods for meshed antennas," in *Antennas and Propagation Society International Symposium (APSURSI), 2010 IEEE*, 2010, pp. 1-4: IEEE.

[28] Ted Pella Co. *PELCO 16062 Technical Notes*. [Online] Available: https://www.tedpella.com/technote_html/16062_TN.pdf

[29] Y. Kim *et al.*, "Stretchable nanoparticle conductors with self-organized conductive pathways," *Nature,* Letter vol. 500, no. 7460, pp. 59-63, 08/01/print 2013.

[30] K. Balmain and E. Jordan, *Electromagnetic waves and radiating systems*. Prentice Hall, New Jersey, 1968.

[31] LessEMF. *Copper Mesh*. [Online] Available: https://www.lessemf.com/1246.pdf

[32] C. Gabriel, S. Gabriel, and E. Corthout, "The dielectric properties of biological tissues: I. Literature survey," *Physics in Medicine and Biology,* vol. 41, no. 11, p. 2231, 1996.

[33] S. Gabriel, R. W. Lau, and C. Gabriel, "The dielectric properties of biological tissues: III. Parametric models for the dielectric spectrum of tissues," *Physics in Medicine and Biology,* vol. 41, no. 11, p. 2271, 1996.

[34] S. Gabriel, R. W. Lau, and C. Gabriel, "The dielectric properties of biological tissues: II. Measurements in the frequency range 10 Hz to 20 GHz," *Physics in Medicine and Biology,* vol. 41, no. 11, p. 2251, 1996.

[35] K. Hall, A. Chrysler, and C. Furse, "A comparison of solid, mesh, and segmented broad dipoles in biological environments," in *USNC-URSI Radio Science Meeting (Joint with AP-S Symposium), 2017*, 2017, pp. 53-54: IEEE.

[36] A. Chrysler, C. Furse, K. Hall, and Y. Chung, "Effect of material properties on a subdermal UHF RFID antenna," *IEEE Journal of RFID,* submitted, 2017.

[37] A. Chrysler, K. Hall, F. J. Curry, and H. Zhang, "Effect of conductivity on subdermal antennas," *Microwave and Optical Technology Letters,* submitted, 2017.

CHAPTER 5[2]

EFFECT OF MATERIAL PROPERTIES ON A SUBDERMAL UHF RFID ANTENNA

5.1 Abstract

This paper explores a subdermal RFID antenna at 918 MHz. The antenna, made from ink encapsulated in thin sheets of biocompatible PET, is designed to be implanted in the fat layer just below the skin, with the muscle acting as a lossy ground plane. The antenna is a patch that uses a T-slot for matching. Three materials are tested: 1) aluminum tape; 2) ELCOAT ink; and 3) inkjet printing. The effect of antenna conductivity and the properties of the fat/skin and muscle layers are explored. The ELCOAT ink performs very similar to the aluminum, but the inkjet printing creates a very thin layer that is subject to skin depth effects. This RFID antenna provides a good proxy for next generation work on subdermal antennas. It demonstrates that the fat layer can sufficiently insulate the antenna to enable subdermal applications, and that the muscle acts like a sufficient ground plane, but without the challenges of a PEC ground plane very near the antenna. The antenna could also be used on the skin surface if the impedance is properly tuned.

5.2 Introduction

As personalized healthcare and miniaturized sensors enable monitoring and data acquisition of biological signals at the skin surface, passive RFID technology provides a battery-free telemetry option that links healthcare to the internet of things [1]. Some high frequency (HF) RFID (13.56 MHz) work in this area includes glucose monitoring [2], orthopedic implant identification [3], and aortic pressure sensors [4]. Passive ultrahigh frequency (UHF) (865-956MHz) RFID has recently been considered for implantable communication applications due its longer read distances. It is also low-cost, convenient in size, battery free, and able to be seamlessly integrated into real-time healthcare monitoring applications [5].

Epidermal RFID tags placed on the skin surface are part of a trend of wearable electronics [6]. These are called tattoo tags [7], and are used as temperature sensors [8], strain sensors [9], and more. These and other RFID antennas have been manufactured at economies of scale using conductive ink, where the reduced conductivity of the ink produces mild reduction of antenna performance [7, 10-13]. When antennas are placed on the surface of the body, the body (particularly the highly conductive muscle) acts like a lossy ground plane and requires careful tuning of the antenna [14]. This is similar to the design of RFID antennas for placement on metal objects [15-17]. RFID tags have also been used extensively inside the body, particularly providing identification for pets and livestock, using very small coil antennas with limited range.

This paper describes a passive RFID antenna that is implanted just under the skin, injected or tattooed in the semi-insulating fat layer [18]. It builds on previous RFID experience in many ways while diverging in others. Unlike existing epidermal “tattooed”’

antennas that are printed on plastic stickers that adhere to the skin surface, the antenna in this paper is designed to be injectable below the skin, in the fat layer, more like a traditional tattoo. Subdermal antennas can be much larger, and have implantable RFID tags. The materials used for these antennas include inks and paints that could conceivably be injected under the skin. Current work in polymer engineering is underway to develop an injectable nanocomposite hydrogel that is initially a fluid but turns to a solid at body temperature [19-22]. The materials used in this paper are good proxies for this up-and-coming new material. Much existing RFID design experience with printed (imperfectly conducting) materials applies to the inherent imperfect conductivity of injectable materials. The design of RFID antennas over metal objects applies as well, as in our case, the muscle forms an imperfect, lossy ground plane for the antenna in the fat just above it.

This paper is an initial study of the effect of the various materials on the antenna performance--the imperfectly conducting injectable conductor making up the antenna, the imperfectly insulating fat that surrounds it, and the imperfectly conducting ground plane of the muscle below it. This work focuses on a fully implantable, subdermal UHF RFID antenna designed to cover the US (915MHz) and Korean (920MHz) RFID frequency bands. 918MHz is used for the simulations. This antenna uses an embedded T-match feed similar to [7, 23, 24]. Section 5.3 of this paper focuses on the effect of the material properties of the antenna by using two different inks that emulate injectable materials. The printed ink is very conductive (up to 2.22×10^7 S/m), but the skin depth exceeds the fabricated antenna thickness, leading to losses. The other ink (ELCOAT) is less conductive (10^5 S/m) and thick enough that skin depth losses are negligible. Both inks provide insight into constraints that injected tattoo antennas will face. Section 5.3 also examines the effect of the material

properties of the surrounding fat/skin (relatively low loss, acting as a sub and superstrate) and muscle (relatively high conductivity, acting as a lossy ground plane) [25-27]. Section 5.4 describes the fabrication and measurement of the antennas. Section 5.5 describes how impedance tuning the T-slot can improve the match between the antenna and RFID chip.

5.3 Effect of Material Properties – Antenna Design and Simulation

This RFID antenna shown in Figure 5.1 is similar to the T-slot antenna from [7, 24]. It is designed for conjugate match with an Higgs 2 RFID IC strap manufactured by Alien [28] which has a nominal complex impedance of 11.7 – 132jΩ at 918 MHz. To maximize read range [29], the antenna is tuned for maximum power transfer by adjusting the dimensions of the slot. The antenna is coated in a 0.1 mm PET envelope for biocompatibility and electrical insulation [30], has pointed ends to slightly improve the bandwidth, and is designed to operate in the fat layer under skin, as shown in Figure 5.2.

5.3.1 Effect of Antenna Conductivity

The conductive material the antenna is made of carries the surface current that produces the radiated fields, and is therefore critical to its performance and efficiency. Ideally, the highest conductivity material would be used. For an antenna that is injected or tattooed under the skin, there may be significant reduction in conductivity due to spreading out of the conductive material, incomplete connectivity due to surrounding biological material, etc. Reduction in conductivity alters the antenna performance, typically increasing its return loss, lowering the resonant frequency and increasing the bandwidth. Antennas with conductivities as low as 5×10^2 S/m have been proposed [31]. In this

research, two different conductive inks are used as proxies for injectable biocompatible materials with similar conductivities. The first ink is ELCOAT, a thick paste made with conductive silver flakes that is easily painted to create the antenna shape. It has a conductivity of 10^5 S/m and can be spread with a thickness of approximately 100 μm. The second is silver ink that is inkjet printed by NovaCentrix [32]. This printing has a nominal thickness between 0.75 and 1 μm, and sheet conductivity between 60 and 70 mΩ/square, giving it a conductivity between 2.04 x 10^5 and 2.22 x 10^7 S/m. Although the ink is highly conductive, it is so thin that at 918 MHz the skin depth is larger than the ink thickness [33].

This RFID antenna is designed to operate underneath the skin, in the fat layer with muscle below. In the body the skin and the muscle are rather conductive, while the fat is somewhat insulating. This creates an environment that is electromagnetically similar to a microstrip antenna above a lossy ground plane. Table 5.1 summarizes the properties of the materials used in this work.

The antenna in Figure 5.1(a) was simulated in the skin-fat-muscle environment shown in Figure 5.2 using full wave simulation from CST. The antenna was excited by a 50 Ω discrete port, but its connection to the Higgs IC was simulated by calculating the S_{11} using equation (5.1):

$$S_{11} = 20 \log_{10} \left| \frac{Z_A - Z_{IC}^*}{Z_A + Z_{IC}} \right| \tag{5.1}$$

where Z_A is the antenna impedance, Z_{IC} is the chip impedance (=11.7 – 132jΩ) and Z_{IC}^* is its complex conjugate. The S_{11} was calculated as the conductivity of the antenna was varied from 10^2 to 10^7S/m, as shown in Figure 5.3 and summarized in Table 5.2. When the

conductivity is above 10^5 S/m, the antenna performs very similar to if it is copper. Between 10^2 and 10^5 S/m the performance degrades significantly. As the conductivity decreases the resonant frequency decreases, the bandwidth increases (as expected from [34]), and the return loss increases.

5.3.2 Effect of Fat and Muscle

To examine the effect the biological tissues play in antenna performance, three simulations were performed and compared to the initial simulation environment shown in Figure 5.2. First, the PEC antenna (slot size 25 mm x 1 mm) was moved to the skin surface rather than being imbedded in the fat. The S_{11} for this case is similar to the initial simulation with the antenna imbedded in the fat, but the center frequency is shifted upwards from 918 MHz to 1.0 GHz. At 1.0 GHz the antenna impedance is 14.8 + j120.8 Ω. This detuning is caused by two things -- the additional separation between the antenna and muscle and the radiated fields being in air rather than partly in fat. The T-junction could be used to re-tune the antenna and bring the resonant frequency back to the desired band.

A second experiment was moving the antenna to the junction between the fat and muscle. In this case, the center frequency remains constant, but the S_{11} is reduced to -2.03 dB. This is caused by closer contact with the more lossy muscle. When the antenna is placed on the muscle, the impedance at 683 MHz resonance is 85.0 + j 87.3 Ω. Recall that this antenna does not directly short out against the muscle because of the plastic coating. A third experiment was to change the properties of the muscle to those of PEC with the PEC antenna imbedded in its original position in the fat layer. The center frequency is shifted slightly downwards from 918 MHz to 913 MHz, but the S_{11} is greatly improved to

-20.4 dB and the impedance is 9.83 + j133.2Ω. From these simulations, it becomes clear that the muscle is acting as a ground plane, albeit a lossy ground, for the antenna and that the deep implantation of the RFID tag can result in significant reduction in antenna performance. Placing the antenna directly on muscle greatly increases the real impedance, which detunes the antenna significantly. When the antenna is placed on skin or the muscle properties are changed to PEC the real impedance is close to 10 Ω which improves the return loss.

The RFID antenna is intended for implant under the skin, and farfield monitors in CST are used to calculate an efficiency of -15.77 dB and directivity of 2.99 dBi. These results are similar to those reported for other near-body applications.[7] Placing the antenna on the muscle reduces the efficiency by 7.9 dB to -23.66 dB. Placing the antenna on the skin increases the efficiency 0.71 dB to -15.06. These results are summarized in Table 5.3.

5.4 Fabrication and Measurement

To validate the simulations from Section 5.3, antennas shown in Figure 5.1(b-d) were fabricated and tested. The antenna in Figure 5.1(b) was fabricated using aluminum foil tape ($\sigma = 3.5 \times 10^7$ S/m, thickness of 0.07 mm) cut by hand and affixed to a PET lamination film 0.1 mm thick. The aluminum was used simply to have a comparison between the inks and a highly conductive, solid antenna. It was not considered as a viable biocompatible option. The antenna in Figure 5.1(c) was fabricated using ELCOAT conductive paste ($\sigma = 1 \times 10^5$ S/m, thickness approximately 0.1 mm [35]). Thickness was determined using a caliper accurate to 0.01 mm. The ELCOAT paste was applied using a template onto the PET lamination film. The antenna in Figure 5.1 (d) was inkjet printed by NovaCentrix (σ

approximately $2 \times 10^5 - 2 \times 10^7$, thickness approximately 0.75 – 1 μm [32]). Each antenna was designed for a center frequency of 918 MHz by simulating the material using the properties in Table 5.1 and adjusting the slot size (a and b seen in Figure 5.1) to give the best S_{11} at 918 MHz. These tuned slot dimensions given in the figure. The CST simulation results for S_{11} for the aluminum and ELCOAT antennas are shown in Figure 5.6. After each antenna was laid out onto the lamination film, a Higgs 2 RFID chip was placed across the terminal gap and affixed using ELCOAT paste. The functionality of the chip was verified using a handheld reader, and then the antenna assembly was passed through a laminating machine. The lamination process heats the PET film and affixes the antenna between the sheets creating a fully sealed, biocompatible envelope less than 0.3 mm thick.

The biological environment was approximated during measurement by placing the antenna on top of a block of pork loin meat (approximating muscle) at room temperature. The pork was approximately 60 x120 mm and 40 mm thick. A thin slice (approximately 2 mm thick) of deli meat (containing more fat than the pork) was placed on top of the antenna to simulate the effect of the fat and skin as seen in Figure 5.4.

The return loss of the antenna at 918 MHz was measured with an Agilent E5071B Vector Network Analyzer. To connect the antenna to the analyzer, a two-prong probe was built that could be held across the gap where the Higgs 2 strap would be placed during RFID operation. The probe was made from a piece of semi-rigid coax with the inner conductor protruding to act as one part of the probe, and a piece of wire soldered to the external rigid shield to act as the other probe. A comparison of the simulated and measured S_{11} of the antennas is shown in Figure 5.6. The ELCOAT and aluminum antennas are very similar, indicating that ELCOAT is sufficiently conductive to be used for this type of antenna

development. A simulated PEC antenna is shown for comparison, although it should be noted that the properties used for the biological materials (Table 5.1) may not be exactly the same as those used for measurement. The NovaCentrix inkjet printed antenna is thinner than the skin depth, so we adjusted the conductivity of the simulated antenna until it performed approximately the same as the NovaCentrix antenna. This gives an approximate effective conductivity of 10^3 S/m for the inkjet printed antenna.

As discussed in Section 5.3, the antenna is designed to have a large inductance and small resistance at 918 MHz in order to create a complex conjugate impedance match to a Higgs 2 IC (Z=11.7 – 132jΩ). The impedance of each antenna and its resonant frequency is given in Table 5.4. The NovaCentrix and the low conductivity metal have different slot sizes, but both have very large resistance at the design frequency. The other high impedance antennas have lower resistance, and the PEC antenna has the lowest resistance. All antennas have a large inductive component. As seen in Table 5.4, the slot dimensions can be readily adjusted to match the imaginary part of the impedance quite well, regardless of the material used. The real part of the impedance is more difficult to control. The lower loss materials (e.g., PEC) have lower real part of the impedance, which better matches the RFID chip. Thus, methods that improve the real part of the match would be beneficial for higher loss materials. Also, the frequency for each antenna can be adjusted by changing the overall size of the antenna, which was not done in this paper, because we wanted to compare antennas of exactly the same size.

The read range of the RFID tags was measured in a hallway in the engineering building at Daegu University to approximate a rich multipath environment as seen in Figure 5.5. An Alien 9800 reader at 1 W was connected to two 6 dBi antennas to read the RFID

antenna. The antenna was placed in the pork/deli meat proxy for the body and slowly moved toward the reader antennas until a positive read was verified. Maximum average read range was 109 cm for the aluminum antenna and 101 cm for the ELCOAT antenna. The NovaCentrix inkjet printed antenna was not tested for read range.

The measured read range in this work was calculated using RFID antennas fabricated with a Higgs 2 IC, which is an older, inexpensive IC chip with an activation power of 40 μW [28]. A newer IC, such as the Higgs 4 has an activation power of 8.9 μW [36]. Assuming the efficiency and impedance match stay the same, the increase in read range for this antenna can be calculated as a gain:

$$R_{Higgs4} = R_{Higgs2}\sqrt{\frac{P_{Tr_{Higgs2}}}{P_{Tr_{Higgs4}}}} = R_{Higgs2}\sqrt{\frac{8.9\ \mu W}{40\ \mu W}} = 2.12R_{Higgs2} \qquad (5.2)$$

where R represents the read range (cm), and P_{Tr} represents the activation power. Thus, by fabricating this RFID antenna with a newer IC chip such as the Higgs 4, the read range could be more than doubled to 214 cm and 231 cm for ELCOAT and aluminum antennas, respectively.

5.5 T-slot matching

The dimensions of the slot are important to the operation of this antenna and may be tuned to improve performance. The NovaCentrix inkjet printed antenna was used for this experiment, because it has the best ability to precisely control slot size. Figures 5.7-5.10 show the real and imaginary impedance variance and S_{11} for several slot dimensions.

First, the antenna impedance is tuned by keeping slot length, a, constant at 25 mm while the width, b, is varied from 0.5 – 2.5 mm. As seen in Figures 5.7 and 5.8, as the slot width, b, increases the measured impedance and reactance of the antenna increases greatly. Decreasing slot width, b, increases the center frequency of the S_{11}. This effect is expected based on [7]. Next, the antenna impedance is tuned by keeping slot width, b, constant at 0.5 mm and the length, a, is varied from 20-30 mm. As seen in Figures 5.9 and 5.10, the real impedance is not affected as strongly as the reactance. Decreasing the slot length, a, increases the S_{11} center frequency. At the 918 MHz design frequency the slot length, a, appears to have less effect on the antenna tuning than the slot width, b. Again, this effect is also expected based on [7].

As the slot dimensions are closely related to antenna performance it is expected that there should be a considerable current distribution around the slot. Figure 5.11 shows the high current density around the slot during several phases of the wave. Both the pointed edges and the bottom of the antenna have low current distributions indicating that these portions of the antenna could be removed or reduced if desired. When considering injectable antennas, these current distributions indicate that larger conductivity is needed near the feed/slot, and lower conductivity could be used further from the slot.

5.6 Conclusions and Future Work

A subdermal RFID antenna made from conductive ink is presented here. The materials used here are proxies for biocompatible inks that could be injected in the fat layer below the skin, with muscle below. The fat acts like a semi-insulator for the antenna and the muscle as a lossy ground plane, creating an environment that is electromagnetically

similar to a microstrip antenna above a lossy ground plane.

The effect of the conductivity of the antenna is considered using aluminum tape and two different types of conductive ink. The first ink, ELCOAT, has a conductivity of 10^5 S/m and performs nearly as well as an antenna made from aluminum tape. Both have a read distance using an Alien 1W RFID reader at 918 MHz of greater than 100 cm. The second antenna is made by NovaCentrix and is very conductive (up to 10^7 S/m) but suffers from skin effect losses. The skin effect losses cause the antenna to behave similar to an antenna with a conductivity in the range of 10^3 S/m. Simulations show that antennas with conductivity as low as 10^2 may be useful in some applications. The slot dimensions can be used to tune the impedance of the antenna, as demonstrated using the NovaCentrix inkjet printed antennas.

This RFID antenna provides a good proxy for next generation work on subdermal antennas. It demonstrates that the fat layer can sufficiently insulate the antenna to enable subdermal applications, and that the muscle acts like a sufficient ground plane. An antenna injected in the fat this way acts very similar to an antenna on the skin surface, thus making it possible to utilize the experience with epidermal RFID tags to design subdermal tags as well, with some retuning via the slot.

Table 5.1 Properties of materials at 918 MHz

Material	ε_r	σ [S/m]	Thickness	Skin Depth
Aluminum Tape		3.5×10^7	70 μm	2.8 μm
NovaCentrix [79]		2.04×10^5 --2.22×10^7	0.75 – 1 μm	3.52 - 36.7 μm
ELCOAT [81]		1×10^5	100 μm	52.5 μm
Muscle [113, 122, 123]	57.9	0.82	Simulation, 200 mm Measurement > 25 mm	18.3 mm
Skin [113, 122, 123]	46.7	0.68	0.062 mm	20.1 mm
Fat [113, 122, 123]	11.6	0.081	8.00 mm	58.4 mm

Table 5.2: Simulated effect of antenna conductivity on S_{11}, resonant frequency and bandwidth. The slot size is a = 25 mm and b = 1 mm, and S11 is calculated assuming it is connected to a Higgs 2 chip with $Z = 11.7 - 132j\Omega$.

Conductivity [S/m]	Resonant Frequency [MHz]	S_{11} [dB]	3 dB Bandwidth [%]
10^2	563	-2.51	--
10^3	768	-3.11	7.3
10^4	868	-5.02	16.0
10^5	902	-7.53	15.2
5.8×10^7 (Copper)	917	-10.45	13.7

Table 5.3. Calculated efficiency and directivity of the PEC RFID antenna with slot size 25 mm x 1 mm using CST for three locations.

Location	Gain (IEEE) [dB]	Directivity [dBi]	Radiation Efficiency, η_{rad} [dB]	Radiation Efficiency, η_{rad} [%]
On Skin	-11.98	3.09	-15.06	3.11
In Fat	-12.78	2.99	-15.77	2.65
On Muscle	-21.52	2.14	-23.66	0.43

Table 5.4. Impedance of simulated and RFID antennas shown in Figure 5.1. These antennas were designed to conjugate match to a Higgs 2 RFID IC (Z=11.7 – 132jΩ). Antennas were measured on pork as described above.

Antenna	Slot Size (a x b) [mm]	Impedance [Ω]	Resonant Frequency [MHz]
PEC Simulation	25 x 1.0	21.2 + j130	918
Low Conductivity (10^3 S/m) Simulation	21 x 0.5	68.4 + j126	889
Aluminum Tape Measured	25 x 0.5	32.6 + j126.2	905
ELCOAT Ink Measured	25 x 0.5	35.5 + j124.0	915
NovaCentrix Measured	26 x 2.0	62.8 + j100.7	900

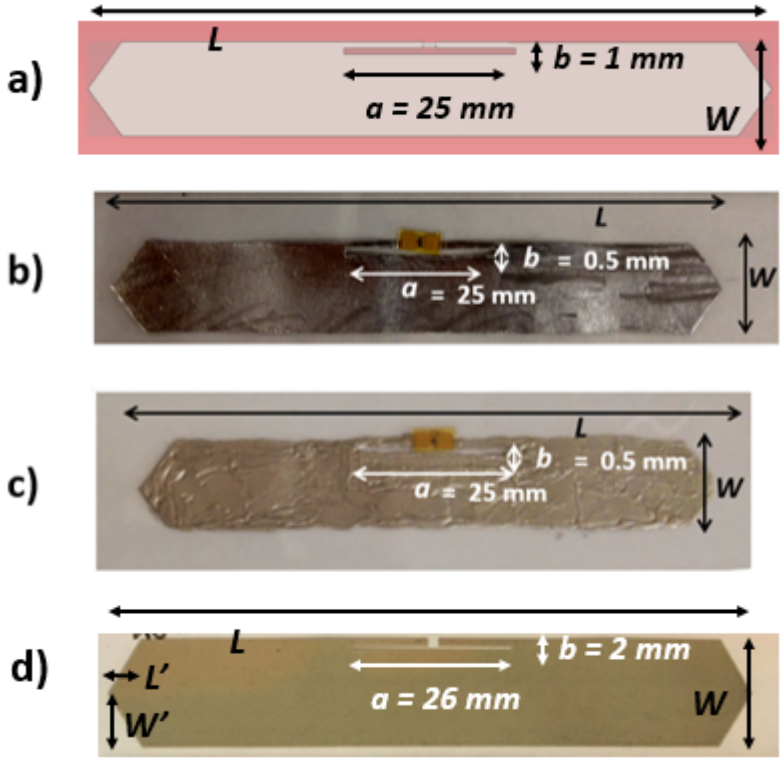

Figure 5.1 Simulated and fabricated RFID antennas. The antennas are symmetric with L = 100 mm, L' = 5 mm, W = 15 mm, and W' = 7.5 mm. a) Simulated antenna b) Aluminum tape (for comparison) c) ELCOAT conductive ink (painted) d) NovaCentrix inkjet printed

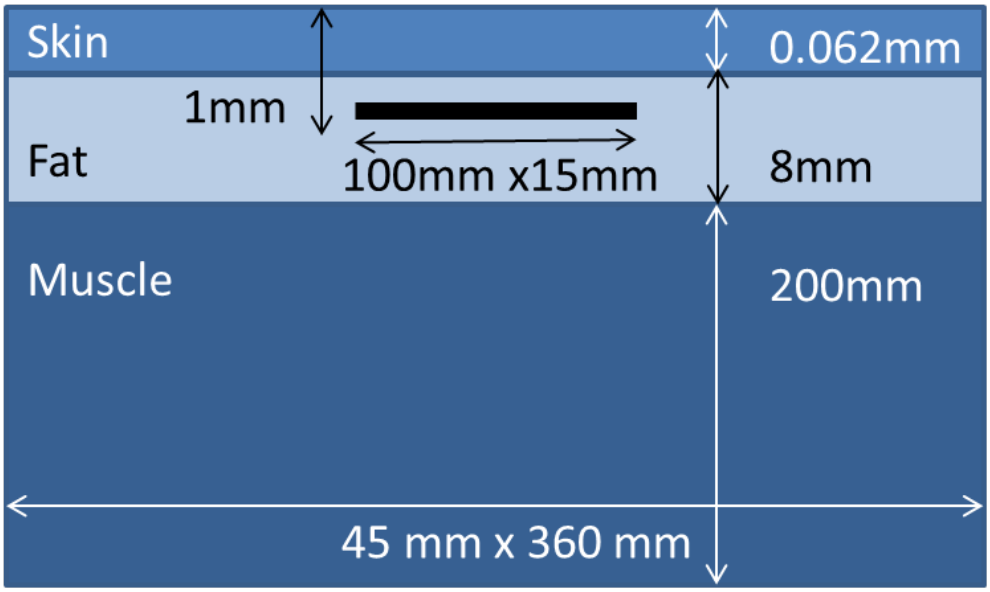

Figure 5.2 Simulation model of the RFID antenna shown in Figure 5.1, embedded in the fat layer. The antenna (0.07 mm thick) is coated with 0.1 mm of insulating PET. The bottom of the coated antenna is 1 mm below the surface of the skin.

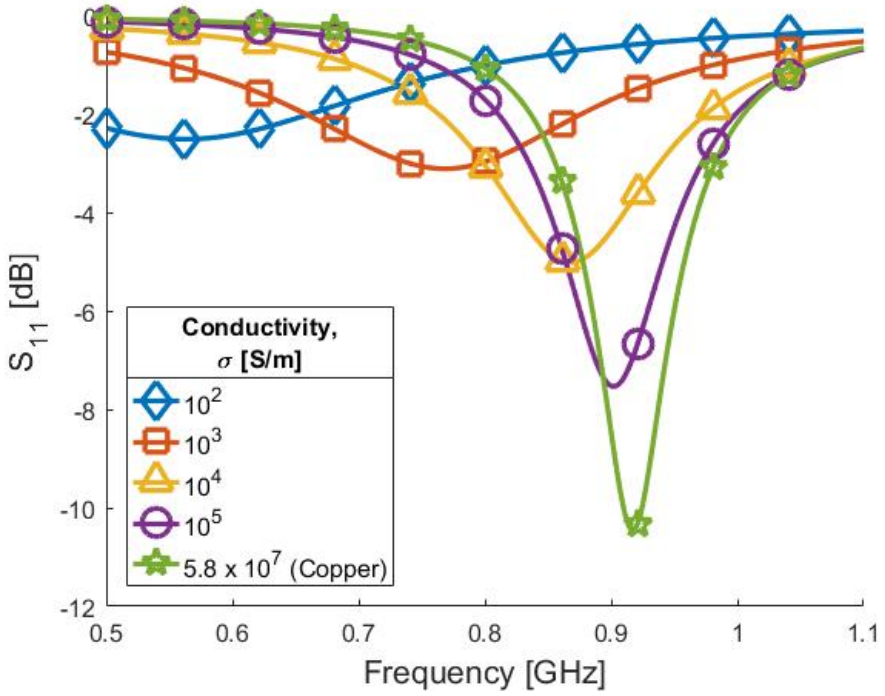

Figure 5.3. Simulated S_{11} of antenna in Figure 5.1(a) in the environment shown in Figure 5.2 as the conductivity of the antenna is varied. The simulated antenna is assumed to be excited by a Higgs 2 IC. As the conductivity decreases, the S_{11} deteriorates, the resonant frequency decreases, and the bandwidth increases. Antennas with conductivity as low as 10^2 S/m may be useful in some applications.

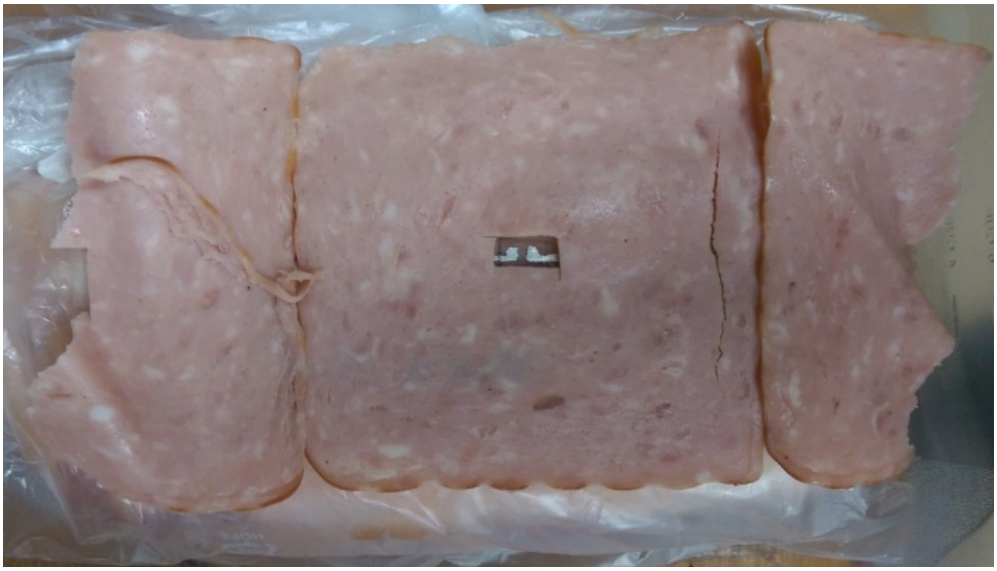

Figure 5.4. RFID antenna S_{11} measurement set up. The ELCOAT RFID is on block of pork meat and covered by deli meat approximately 2 mm thick. There is a small window for measurement using a two-prong probe.

Figure 5.5. RFID read distance measurement setup in a multipath environment of a hallway in the engineering building at Daegu University.

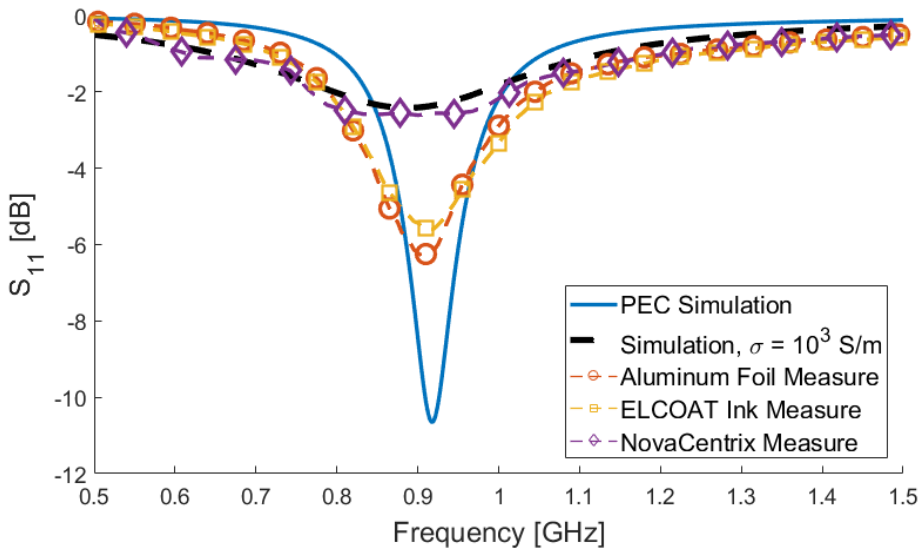

Figure 5.6 Comparison of S_{11} for the RFID antennas shown in Figure 5.1 when matched to a Higgs 2 chip. The ELCOAT and aluminum antenna behave very similarly. The NovaCentrix antenna behaved similar to a simulated antenna with $\sigma=10^3$ S/m.

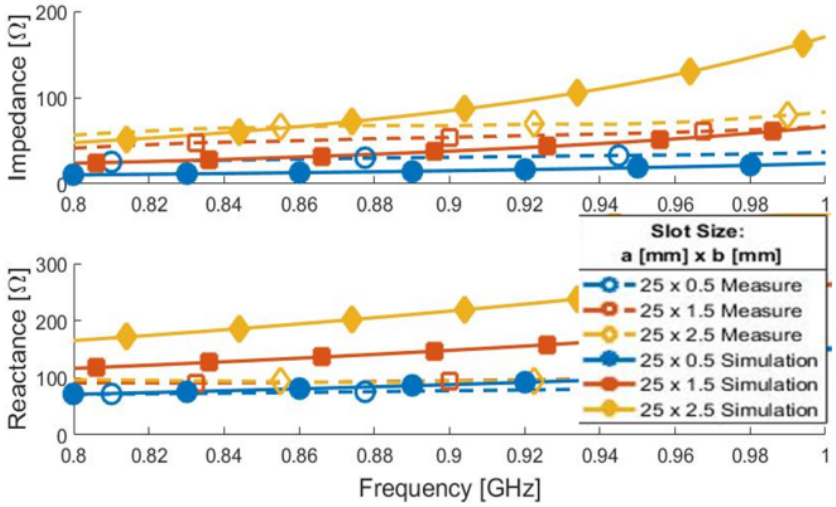

Figure 5.7. Impedance of the NovaCentrix RFID antenna as slot length, a, is kept constant at 25 mm and the width, b, is varied from 0.5 – 1.5 mm

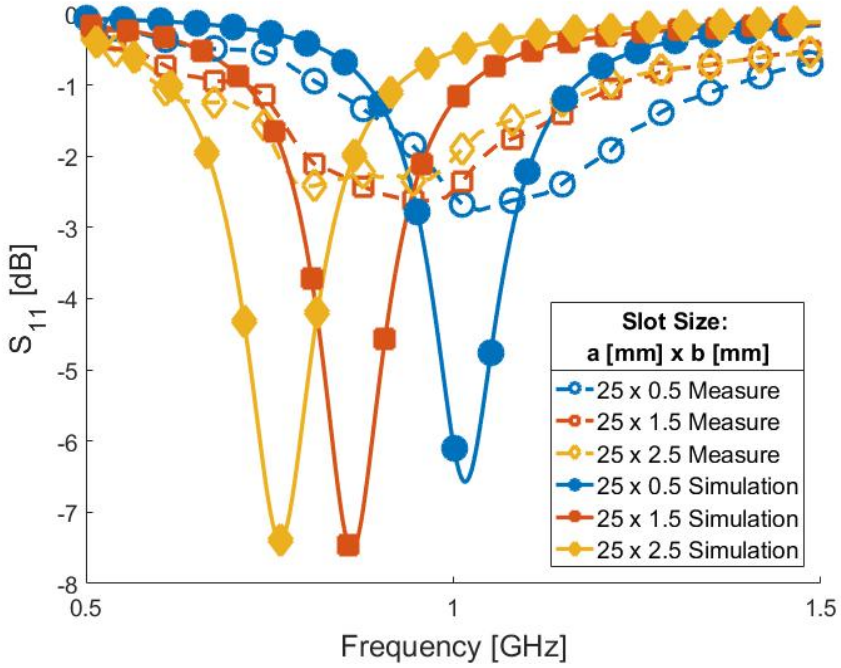

Figure 5.8. S_{11} of the NovaCentrix inkjet printed antenna as slot length, a, is kept constant at 25 mm and the width, b, is varied from 0.5 – 1.5 mm

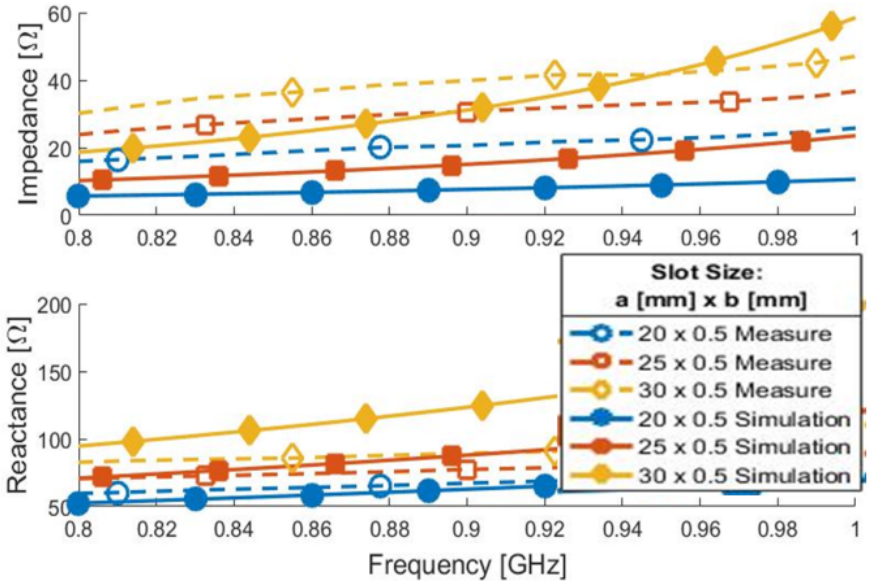

Figure 5.9. Impedance of the NovaCentrix RFID antenna as slot width, b, is kept constant at 0.5 mm and the length, a, is varied from 20-30 mm.

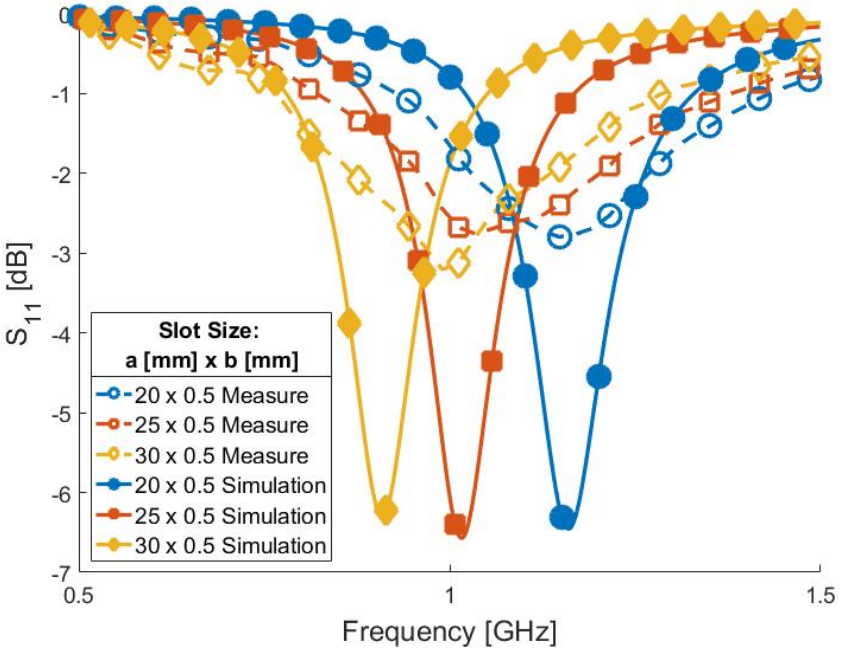

Figure 5.10. S_{11} of the NovaCentrix inkjet printed RFID antenna as slot width, b, is kept constant at 0.5 mm and the length, a, is varied from 20-30 mm.

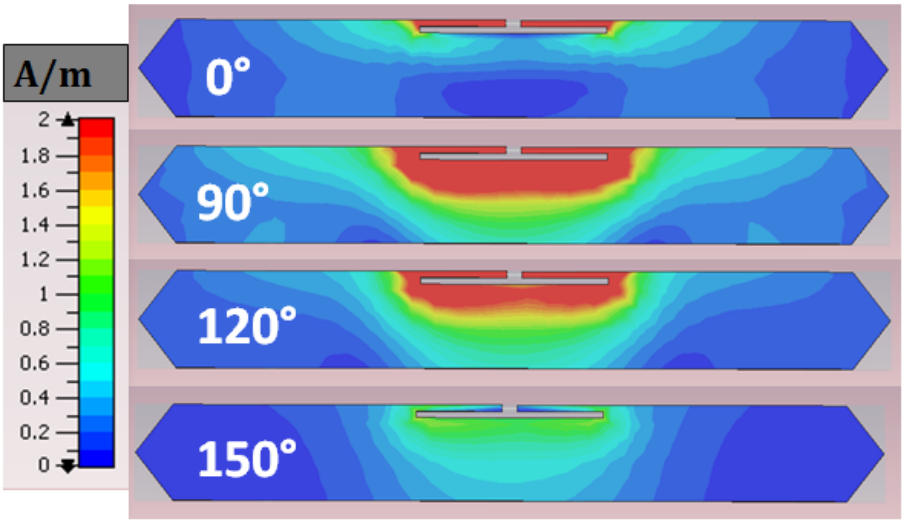

Figure 5.11. Simulated current distribution in the PEC RFID antenna at 918 MHz. The current is strongest near the slot and weaker away from it.

5.7 References

[1] S. Amendola, R. Lodato, S. Manzari, C. Occhiuzzi, and G. Marrocco, "RFID technology for IoT-based personal healthcare in smart spaces," *IEEE Internet of Things Journal,* vol. 1, no. 2, pp. 144-152, 2014.

[2] Z. Xiao *et al.*, "An implantable RFID sensor tag toward continuous glucose monitoring," *IEEE Journal of Biomedical and Health Informatics,* vol. 19, no. 3, pp. 910-919, 2015.

[3] X. Liu, J. L. Berger, A. Ogirala, and M. H. Mickle, "A touch probe method of operating an implantable RFID tag for orthopedic implant identification," *IEEE Transactions on Biomedical Circuits and Systems,* vol. 7, no. 3, pp. 236-242, 2013.

[4] O. Romain *et al.*, "RFID implantable pressure sensor for the follow-up of abdominal aortic aneurysm stented," in *2011 6th International Conference on Design & Technology of Integrated Systems in Nanoscale Era (DTIS)*, 2011, pp. 1-6.

[5] G. Marrocco, "Body-matched RFID antennas for wireless biometry," in *2006 First European Conference on Antennas and Propagation*, 2006, pp. 1-5.

[6] D.-H. Kim *et al.*, "Epidermal electronics," *Science,* vol. 333, no. 6044, pp. 838-843, 2011.

[7] M. A. Ziai and J. C. Batchelor, "Temporary on-skin passive UHF RFID transfer tag," *IEEE Transactions on Antennas and Propagation,* vol. 59, no. 10, pp. 3565-3571, 2011.

[8] S. Milici, S. Amendola, A. Bianco, and G. Marrocco, "Epidermal RFID passive sensor for body temperature measurements," in *2014 IEEE RFID Technology and Applications Conference (RFID-TA)*, 2014, pp. 140-144.

[9] O. O. Rakibet, C. V. Rumens, J. C. Batchelor, and S. J. Holder, "Epidermal passive RFID strain sensor for assisted technologies," *IEEE Antennas and Wireless Propagation Letters,* vol. 13, pp. 814-817, 2014.

[10] G. A. Casula, G. Montisci, and G. Mazzarella, "A wideband PET inkjet-printed antenna for UHF RFID," *IEEE Antennas and Wireless Propagation Letters,* vol. 12, pp. 1400-1403, 2013.

[11] A. Chrysler, C. Furse, and Y. Chung, "Biocompatible, implantable UHF RFID antenna made from conductive ink," in *2016 IEEE International Symposium on Antennas and Propagation (APSURSI)*, 2016, pp. 467-468.

[12] D. Bechevet, V. Tan-Phu, and S. Tedjini, "Design and measurements of antennas for RFID, made by conductive ink on plastics," in *2005 IEEE Antennas and Propagation Society International Symposium*, 2005, vol. 2B, pp. 345-348 vol. 2B.

[13] J. Siden and H. E. Nilsson, "Line width limitations of flexographic-screen- and inkjet printed RFID antennas," in *2007 IEEE Antennas and Propagation Society International Symposium*, 2007, pp. 1745-1748.

[14] S. Amendola, S. Milici, and G. Marrocco, "Performance of epidermal RFID dual-loop tag and on-skin retuning," *IEEE Transactions on Antennas and Propagation,* vol. 63, no. 8, pp. 3672-3680, 2015.

[15] S. Genovesi and A. Monorchio, "Low-profile three-arm folded dipole antenna for UHF band RFID tags mountable on metallic objects," *IEEE Antennas and Wireless Propagation Letters,* vol. 9, pp. 1225-1228, 2010.

[16] H. Kwon and B. Lee, "Compact slotted planar inverted-F RFID tag mountable on metallic objects," *Electronics Letters,* vol. 41, no. 24, pp. 1308-1310, 2005.

[17] L. Ukkonen, L. Sydanheimo, and M. Kivikoski, "Patch antenna with EBG ground plane and two-layer substrate for passive RFID of metallic objects," in *IEEE Antennas and Propagation Society Symposium, 2004.*, 2004, vol. 1, pp. 93-96 Vol.1.

[18] A. Chrysler, C. Furse, and Y. Chung, "Biocompatible, implantable UHF RFID antenna made from conductive ink," in *Antennas and Propagation (APSURSI), 2016 IEEE International Symposium on*, 2016, pp. 467-468: IEEE.

[19] B. Yao *et al.*, "Ultrahigh-conductivity polymer hydrogels with arbitrary structures," *Advanced Materials,* 2017.

[20] G. Chen, F. Svec, and D. R. Knapp, "Light-actuated high pressure-resisting microvalve for on-chip flow control based on thermo-responsive nanostructured polymer," *Lab on a Chip,* vol. 8, no. 7, pp. 1198-1204, 2008.

[21] N. S. Satarkar, W. Zhang, R. E. Eitel, and J. Z. Hilt, "Magnetic hydrogel nanocomposites as remote controlled microfluidic valves," *Lab on a Chip,* vol. 9, no. 12, pp. 1773-1779, 2009.

[22] F. C. Curry Jr., Andrew; Furse, Cynthia;Zhang, Huanan, "Gold nanocomposite for subdermal antenna " presented at the AIChE Annual Meeting Minneapolis, MN, Oct 29-Nov 3, 2017.

[23] G. Marrocco, "RFID antennas for the UHF remote monitoring of human subjects," *IEEE Transactions on Antennas and Propagation,* vol. 55, no. 6, pp. 1862-1870, 2007.

[24] G. Marrocco, "The art of UHF RFID antenna design: Impedance-matching and size-reduction techniques," *IEEE Antennas and Propagation Magazine,* vol. 50, no. 1, pp. 66-79, 2008.

[25] C. Gabriel, S. Gabriel, and E. Corthout, "The dielectric properties of biological tissues: I. Literature survey," *Physics in Medicine and Biology,* vol. 41, no. 11, p. 2231, 1996.

[26] S. Gabriel, R. W. Lau, and C. Gabriel, "The dielectric properties of biological tissues: III. Parametric models for the dielectric spectrum of tissues," *Physics in Medicine and Biology,* vol. 41, no. 11, p. 2271, 1996.

[27] S. Gabriel, R. W. Lau, and C. Gabriel, "The dielectric properties of biological tissues: II. Measurements in the frequency range 10 Hz to 20 GHz," *Physics in Medicine and Biology,* vol. 41, no. 11, p. 2251, 1996.

[28] Alien. *Higgs 2 Data Sheet*. [Online] Available: http://www.rfidusa.com/Pdf/Specials/Alien-DS_Higgs-2_EPC_Class_1.pdf

[29] K. V. S. Rao, P. V. Nikitin, and S. F. Lam, "Antenna design for UHF RFID tags: A review and a practical application," *IEEE Transactions on Antennas and Propagation,* vol. 53, no. 12, pp. 3870-3876, 2005.

[30] H. Seitz, S. Marlovits, I. Schwendenwein, E. Müller, and V. Vécsei, "Biocompatibility of polyethylene terephthalate (Trevira® hochfest) augmentation device in repair of the anterior cruciate ligament," *Biomaterials,* vol. 19, no. 1-3, pp. 189-196, 1998.

[31] C. D. Rouse, M. R. Kurz, B. R. Petersen, and B. G. Colpitts, "Performance evaluation of conductive-paper dipole antennas," *IEEE Transactions on Antennas and Propagation,* vol. 61, no. 3, pp. 1427-1430, 2013.

[32] NovaCentrix. *NovaCentrix Web Page*. [Online] Available: https://www.novacentrix.com/

[33] J. R. Saberin and C. Furse, "Challenges with optically transparent patch antennas," *IEEE Antennas and Propagation Magazine,* vol. 54, no. 3, pp. 10-16, 2012.

[34] M. Shahpari and D. V. Thiel, "The impact of reduced conductivity on the performance of wire antennas," *IEEE Transactions on Antennas and Propagation,* vol. 63, no. 11, pp. 4686-4692, 2015.

[35] Hana Tech Co. *ELCOAT Ink Purchase Site*. [Online] Available: http://www.hanatechno.com/front/php/product.php?product_no=377&main_cate_no=86&display_group=1

[36] Alien Technology. *Higgs 4 Datasheet.* [Online] Available: http://www.alientechnology.com/wp-content/uploads/Alien-Technology-Higgs-4-EPC-Class-1-Gen-2-RFID-Tag-IC.pdf.

CHAPTER 6

A KA-BAND (26 GHZ) SINGLE PATCH ELEMENT WITH TRUNCATED CORNERS FOR CIRCULAR POLARIZATION

6.1 Abstract

Corners truncated, 50 Ω edge-fed, LHCP patch antennas are designed for use at 26 GHz in the Ka-band on RT/duroid 5880 (ε_r = 2.2, ½ oz. copper cladding). Microstrip feed width, AR bandwidth, and best AR at 26 GHz are optimized by the use of 10 mil substrate. Patch length is 3.75 mm, truncation amount is 0.49 mm, and feed width is 0.74 mm. AR is 0.748 dB, and its bandwidth is 1.19%. The effects of corner truncation are further investigated, showing that increasing corner truncation increases AR bandwidth, increases percent offset between best S_{11} and AR frequencies, and worsens the best AR. A truncation of 0.57 mm is a good compromise between these effects with AR bandwidth of 6.17 % (measured) and 1.37 % (simulated). Increasing ratio of substrate thickness to design frequency, $t / \lambda d$, improves AR bandwidth. For $t / \lambda d$ below 0.01 (10 mil RT/duroid 5580), 0.02 (62 mil RT/duroid 5880), 0.05 (10 mil RT/duroid 6006) a corners truncated patch antenna will not produce CP. A new nearly-square, corners truncated patch antenna is measured and simulated as a method of increasing CPBW.

6.2 Introduction

A reliable satellite communication link requires antennas with high efficiency and high gain, which are small in size, light weight, and capable of operating with circular polarization (CP) over extended periods of time under the extreme conditions of space without maintenance. Circular polarization is important, because it eliminates the need for precise alignment between the transmitting and receiving apertures, compensates for electromagnetic effects of the ionosphere, and is more resistant to signal degradation due to atmospheric conditions [1].

Because of the larger available bandwidth for satellite communications at millimeter-wave frequencies, the commercial SATCOM industry and the U.S. Government organizations have expressed tremendous interest in Ka-band links. Consequently, the design of high-efficiency antenna arrays for such applications have been reported by several investigators. As examples, these include horn arrays [2-4], reflectarrays [5-8], slotted waveguide arrays [9, 10], and microstrip arrays [11-15]. Among these designs, the microstrip arrays are attractive due to their inherent simplicity and ease of manufacture, despite their narrow bandwidth. The primary objective of this work is focused on the design of a Ka-band (26 GHz) microstrip patch antenna with corners truncated for CP. The patch is excited by an in-plane single microstrip line coupled to any one of the radiating edges as illustrated in Figure 6.1. Such a feeding arrangement enables the realization of a simple power divider network for a four element sub-array, which forms the basic building block of a larger $N \times N$ planar array.

Although patch antennas were first introduced in the early 1950s [16], their popularity increased dramatically in the 1970s [17], and by the early 1980s, many CP

designs had been demonstrated [18-20]. Of the early CP designs, the corners truncated patch antenna first reported in [21, 22] has achieved lasting popularity due to simple design equations and easy fabrication.

Truncated corner CP theory was validated by experiments performed at S-band (3.175 GHz) and X-band (9.57 GHz). In [21], the S-band CP patch antenna was fabricated on a 1/8" polystyrene ($\varepsilon_r = 2.52$) substrate and excited by a probe feed. In [22], the X-band CP antenna was designed using perturbation theory for best AR, and it was demonstrated that the AR bandwidth increases with thickness of the dielectric substrate. The corners truncated patch antenna operates by generating two orthogonal linearly polarized modes (at slightly different frequencies due to the truncated and untruncated corners) that resolve as CP [17, 21].

The AR bandwidth (where AR < 3 dB) and the return loss bandwidth (S_{11} < -10dB) determine the usable frequency range for a CP antenna. The usable region where the AR and return loss bandwidths overlap is considered to be the CP bandwidth (CPBW). Patch antennas tend to have narrow return loss bandwidth [23]. Truncated corners CP patch antennas tend to have narrow CPBW, since the best AR frequency is offset from the return loss bandwidth due to resonant frequencies of the diagonal orthogonal modes.

In most single patch works, such as [21] and [22], the narrow CPBW effect is noted but not further investigated. Other higher frequency works on array design in the Ka-band tend to disregard the narrow CPBW of a single patch in favor of optimizing the CP performance of the complete patch array [11, 14, 15]. Other works that consider the narrow CPBW are low frequency (4 GHz), use air dielectric ($\varepsilon_r = 1$), and favor increasing CPBW through broadbanding techniques such as adding U-slots or L-probe feeds [24, 25].

Increasing CPBW using the U-slot and L-probe methods introduces manufacturing complexity and may be difficult, costly, or both at millimeter wave frequencies where patch dimensions are much smaller. Additionally, the probe method of feeding a patch from the back is more difficult to manufacture and becomes even more difficult to realize at millimeter-wave frequencies.

The CPBW is a good metric for describing antennas with good impedance match to the input feed, but for the edge-fed patch antenna with a standard 50 Ω feed, the CPBW is small or nonexistent. For this reason, the frequency offset between the best S_{11} and best AR frequency is considered as a more applicable metric in this work. In later design stages, a corners truncated patch antenna can be impedance matched using methods such as the quarter-wave transformer to increase CPBW with minimal effect on the frequency with the best S_{11}.

Since an edge-fed, 26 GHz CP patch with simple construction and good CPBW is desired for a future NxN array, this work presents three previously unconsidered design effects of single patch elements: (1) the CPBW of single edge-fed corners truncated patch antennas at millimeter wave frequencies, (2) CPBW as a function of higher dielectrics (such as those commonly available from Rogers Corporation), (3) increasing CPBW through a combination of corner truncation and broadband effects of nearly-square patch antennas. This work investigates these effects using measurement and commercially available software simulation tools (CST).

Section 6.3 presents the design guidelines for a patch with corners truncated for CP at Ka-band and also develops a relationship between truncation amount, AR, and S_{11}. Section 6.4 discusses the relationship between the design frequency, substrate thickness,

and substrate dielectric constant. Section 6.5 presents a method for improving AR performance of a patch with corners truncated. Section 6.6 presents the conclusion and directions for future work.

6.3 Truncated Corner Patch Antenna Design

6.3.1 Design Equations for the Truncation Amount, a

A truncated corner patch antenna used to create left-hand CP (LHCP) radiation is shown in Figure 6.1. If the feed location is unchanged, truncating the opposite corners produces a right-hand CP (RHCP) radiation. The perturbation created by the truncated corners propagates two orthogonal degenerate modes with slightly different frequencies that are resolved as CP [17, 21]. In this paper, the length, *L* of the patch antenna for a 26 GHz design frequency is given by:

$$L = \frac{c}{2f\sqrt{\varepsilon_r}} - 2\,\Delta L\ . \tag{6.1}$$

The length, *L*, is compensated for excess capacitance caused by fringing fields by subtracting *ΔL,* which is expressed as [19]:

$$\Delta L = h\left[0.412\frac{\varepsilon_{eff}+0.3}{\varepsilon_{eff}-0.258}\frac{{}^{W}/_{h}+0.262}{{}^{W}/_{h}+0.813}\right]. \tag{6.2}$$

Values for the effective permittivity, $\varepsilon_{eff,}$ and the patch width to height ratio, *W/h*, are calculated using the microstrip equations in [26]. The truncation amount, *a*, is given by [22]:

$$a = \sqrt{\frac{L^2}{Q}} \tag{6.3}$$

The quality factor of the patch, Q, is related to the bandwidth, BW, and VSWR as follows:

$$Q = \frac{VSWR-1}{BW\sqrt{VSWR}}. \tag{6.4}$$

The VSWR is selected based on design constraints. Selecting VSWR = 2 is equivalent to S_{11} = -10 dB and is the constraint used throughout this work. The bandwidth, *BW*, is calculated using

$$BW = \frac{16}{3\sqrt{2}}\frac{p}{\epsilon_r}\frac{1}{\varepsilon_r}\frac{h}{\lambda_o}\frac{W}{L}q \tag{6.5}$$

where ϵ_r is the substrate permittivity, and p and q are defined by the following equations:

$$p = 1 - \frac{0.16605}{20}(k_oW)^2 + \frac{0.02283}{560}(k_oW)^4 - 0.009142(k_oL)^2 \tag{6.6}$$

$$q = 1 - \frac{1}{\varepsilon_r} + \frac{2}{5\varepsilon_r} \tag{6.7}$$

The wavelength, λ, is taken at the 26 GHz design frequency, and the wavenumber, k_o, is given by

$$k_o = \frac{2\pi}{\lambda} \tag{6.8}$$

Combining equations (6.1) – (6.8) gives S_{11} as a function of truncation amount, *a*. This is shown in Figure 6.2 for a 26 GHz design frequency on RT/duroid 5880 with 5, 10, and 20 mil thicknesses. This assumes that the input feed impedance is perfectly matched to the patch edge impedance. From these equations, the truncation amount, *a*, to produce an S_{11} of -10 dB is 0.34 mm, 0.49 mm, and 0.68 mm for the 5, 10, and 20 mil substrates, respectively. For any given truncation amount in Figure 6.2, a thinner substrate produces a smaller S_{11}. This trend is consistent with results observed in [21].

6.3.2 Fabrication

Three corners truncated LHCP patch antennas (as in Figure 6.1) were designed for operation at 26 GHz and prototyped on RT/ duroid 5880 substrate ($\varepsilon_r = 2.2$, ½ oz. copper cladding) with standard thicknesses of 5, 10, and 20 mils. The microstrip feed line thickness, w_o, is designed to be 50 Ω at 26 GHz for each substrate thickness. The patch side length, *L*, is calculated from (6.1), and the truncation amount, *a*, is calculated using (6.3). The truncation amount is designed for S_{11} = -10 dB at 26 GHz as shown in Figure 6.2. Design values of w_o, *L*, and *a* are listed in Table 6.1 for the three antennas.

6.3.3 Measurement

Three patch antennas (dimensions indicated in Table 6.1) are characterized by measurement of S_{11} and AR. To measure S_{11}, the antenna is mounted to an aluminum test fixture allowing simple connection between a 2.4 mm coaxial connector and a 50 Ω patch antenna microstrip feedline. The S_{11} measurement is taken using a vector network analyzer.

The AR is calculated from two orthogonal insertion loss (S_{21}) measurements

between the CP patch antenna and a linearly polarized standard gain horn on a coaxial rotary joint aligned boresight to the patch antenna. The distance between the CP patch antenna and the horn antenna is 30 cm. The maximum dimension of the horn is 2.8 cm (measured across the diagonal of the rectangular aperture), so the horn antenna is in the far field. The measurement set up is surrounded by microwave absorber to minimize reflections.

To measure insertion loss, the linear horn is first horizontally aligned, and an S_{21} measurement is recorded on a two-port network analyzer. Then the horn is rotated 90° to a vertical position about the coaxial rotary joint, and a second S_{21} measurement is taken. The only movement or change in the measurement system occurs as the horn is rotated. The difference (in dB) between the two insertion loss measurements is the AR. The measured and simulated S_{11} and AR are presented as a function of frequency in Figure 6.3.

6.3.4 S11 and AR Frequency Offset

For CP antennas that are well matched to the feed, the CPBW describes the usable frequency range of an antenna as the range where the S_{11} is below -10 dB, and the AR is below 3 dB. In this work, the patches are fed with 50 Ω lines, and the corner truncation of the patch is designed for S_{11} = -10dB using Figure 6.2. As seen from measurements in Figure 6.3, there is an offset in frequency at which the best S_{11} occurs, f'_{S11}, and the frequency at which the best AR occurs, f'_{AR}. Additionally, due to the patch truncation and 50 Ω feed, the -10dB patch bandwidth is narrow or nonexistent for the 5,10, and 20 mil antennas. For this reason, the CPBW does not accurately describe the antennas in this work. Instead the S_{11} and AR frequency percent offset is defined and used:

$$\%\, offset = \frac{abs(f'_{S11} - f'_{AR})}{f'_{S11}} \times 100\% \quad (6.9)$$

Compared to CPBW, percent offset is a better comparison metric for corners truncated patch antennas, because the f'_{S11} is minimally affected by impedance matching. Since previous works [21, 22] focused on the design of one or two CP patches at low frequencies (< 10 GHz) with well-matched back-feeds, the percent offset was safely ignored. However, for the edge-fed patch at high frequency, this effect becomes significant as will be demonstrated in this work.

6.3.5 Effect of Thickness at 26 GHz

The offset between f'_{S11} and f'_{AR} for three substrate thicknesses (5, 10, and 20 mil) on RT/duroid 5880 can be seen in Figure 6.3. The offset creates a design tradeoff between the S_{11} and AR, as both cannot be simultaneously optimized for a square patch. This offset increases as the substrate thickness increases. The offset found from simulation of the antennas on RT/duroid 5880 with 5,10 and 20 mil substrates is 50, 160, and 160 MHz, respectively. The best S_{11} for antennas with 5, 10, and 20 mil substrates is -5.68 dB (at 25.55 GHz), -6.38 dB (at 25.68 GHz), and -18.97 dB (at 26.04 GHz), respectively. The best AR for the antennas with the 5, 10, and 20 mil substrates is 1.961 dB (at 25.5 GHz), 0.748 dB (at 25.52 GHz), and 1.292 (at 25.88 GHz), respectively.

The AR bandwidth for the antenna in Figure 6.3 increases as the substrate thickness increases, which is predicted by [21, 22]. AR bandwidth for the 5, 10, and 20 mil substrate thicknesses is found from simulation to be 0.47%, 1.19%, and 2.47%, respectively. Although the antenna on 20 mil substrate has a larger AR bandwidth, the antenna on 10

mil substrate has a better AR. The AR of the antenna on 10 mil substrate is 0.748 dB, which is 0.544 dB lower than the antenna on 20 mil substrate.

Since the patch design is intended for use in an $N \times N$ array, the patch feed width, w_o, must be considered due to limited footprint available for array design. It is well known that for a given impedance, the width of a microstrip increases with substrate thickness [27]. For 20 mil RT/duroid 5580, a 50 Ω microstrip feed line has a large width, w_o = 1.46 mm, that makes array feed network design difficult. For a favorable compromise between AR, S_{11} and 50Ω feed width (w_o), the 10 mil RT/duroid 5880 substrate is used for further study on the relationship between S_{11} and AR.

6.3.6 Effect of Corner Truncation at 26 GHz

A square patch antenna can produce either LHCP or RHCP, depending on which pair of corners are truncated. The surface current for both senses of polarization is shown in Figure 6.4 for antennas on 10 mil RT/duroid 5880 substrate with parameters listed in Table 6.1.

The truncation amount, a, shown in Figure 6.1 affects both S_{11} and AR. This section evaluates the impact of truncation amount for an LHCP antenna with 26 GHz design frequency on 10 mil RT/duroid 5880 substrate. In this study, truncation amount, a, is varied, while the other parameters are held constant at values listed in Table 6.1. A larger truncation amount, a, results in a lower S_{11} at f'_{S11}. However, increasing truncation amount has minimal change in f'_{S11}. This effect is shown for both simulated and measured results in Figure 6.5.

Figure 6.6 shows that corner truncation amount has a more complicated effect on

AR than S_{11}. Three effects are seen in AR as the truncation amount, a, increases: (1) The AR bandwidth increases; (2) The best AR worsens (antenna becomes more linearly polarized); (3) The f'_{AR} shifts down in frequency for simulated results, and up in frequency for measured results. Table 6.2 summarizes the effect of truncation amount on AR for measured and simulated results.

The truncation amount, a, has little effect on f'_{S11} (Figure 6.5), but does change f'_{AR} (Figure 6.6). Thus, for a corners truncated patch antenna, increasing a increases the percent offset described in (8). From Figure 6.5 and Figure 6.6, the offset is considerable in the measurement data and also appears in the simulation data.

For example, in the S band (3.175 GHz) for a well-matched, back-fed antenna, this offset was reported as less than 10 MHz (0.31 % offset) of f'_{S11} [21]. In the 26 GHz Ka-band the measured offset between Figure 6.5 and 6.6 is more than 400 MHz (1%) of f'_{S11} for all measured truncation amounts. The simulated results show offsets of 30 MHz (0.12%) or more. S_{11} and AR center frequency, their offset, and AR bandwidth for the antennas in Figures 6.5 and 6.6 are summarized in Table 6.2.

Measured results in Figure 6.6 indicate that $a = 0.57\ mm$ or $a = 0.60\ mm$ will result in S_{11} less than -10 dB with minimal shift in f'_{AR} and AR bandwidth greater than 2%. Measured results from the antenna boresight indicate that antennas with truncation amount of a =0.50 mm, 0.57 mm or 0.60 mm will be circularly polarized with a best AR that will approach 0 dB. The simulated results also indicate that antennas with a =0.57 mm and 0.60 mm truncation amounts have the largest AR bandwidth and best AR below 3 dB. The simulated results show that $a = 0.50\ mm$ creates the best AR, but suffers from narrow AR bandwidth and S11 above -10 dB.

Although the $a = 0.50\ mm$ truncation amount offers the best AR (in simulation and measurement) and $a = 0.60\ mm$ offers the widest AR bandwidth, $a = 0.57\ mm$ is the best compromise between $a = 0.50\ mm$ and $a = 0.60\ mm$. The 50 Ω edge-fed, corners truncated patch antenna with $a = 0.57\ mm$ is the design choice for future $N \times N$ arrays based on the compromise between minimal percent offset, large AR bandwidth, best AR, and low S_{11}. A summary of the data supporting this design decision is found in Table 6.2.

6.4 Effect of Design Frequency and Substrate on AR and S_{11} Performance

6.4.1 Effect of Design Frequency

This section investigates the effect of design frequency on 50 Ω edge-fed LHCP corners truncated patch antennas on 10 mil RT/duroid 5880. Five design frequency bands are simulated: S (2 – 4 GHz), C (4 – 8 GHz), X (8-12 GHz), Ku (12 – 18 GHz), and Ka (26.5 – 40 GHz). The S band and Ka-band antennas are designed at 2.5 GHz and 26 GHz, respectively. The other three antenna design frequencies are 6 GHz, 10 GHz, and 15 GHz, which is the center of the C, X, and Ku bands. The truncation amount, a, for each antenna is chosen using (3) to produce S_{11} = -10 dB (when the feed is perfectly matched to the patch edge). Table 6.3 lists the dimensions and performance (S_{11}, AR) of the five antenna designs.

Figure 6.7 shows simulated S_{11} and the best AR for the antennas with dimensions listed in Table 6.3. The AR bandwidths for the X, Ku, and Ka-band antennas are 0.05%, 0.66%, and 1.19%, respectively. The S and C band antennas are linearly polarized (AR > 3 dB) and have no AR bandwidth. The best AR improves as frequency increases, as does

AR bandwidth. The AR bandwidth is known to increase with substrate thickness [21, 22], but Figure 6.7 shows that AR bandwidth also increases with substrate thickness relative to design frequency.

6.4.2 Effect of Substrate Thickness

The previous section indicates that for a corners truncated patch antenna with a truncation amount producing S_{11}< -10 dB on 10 mil RT/duroid 5880, the simulated AR approaches 0 dB as the patch design frequency increases. Previously, the AR bandwidth of an antenna at a given design frequency is known to increase as substrate thickness increases [21, 22]. This work expands on previous knowledge by investigating the changes in both AR bandwidth and best AR for edge-fed, corners truncated patch antennas over a range of design frequencies using two substrates. This section considers the five design frequencies used in the previous section on RT/duroid 5880 with thicknesses of 10 mil and 62 mil ($1/16''$). The dimensions of the antennas designed on 10 mil and 62 mil substrates are listed in Table 6.3 and Table 6.4, respectively. Table 6.3 and Table 6.4 also list the ratio of substrate thickness, t, to design frequency wavelength in substrate, λ_d. For a constant substrate thickness, the λ_d increases as frequency increases.

Five edge-fed, corners truncated antennas with design frequency listed in Table 6.3 are designed on 10 mil RT/duroid 5880. The truncation amount is designed for S_{11} = -10 dB using (6.3). The antennas are simulated, and S_{11} (blue lines) and best AR (single red squares) are plotted in Figure 6.7. The S_{11} for all antennas remains relatively constant, but as frequency and t / λ_d, increases, the best AR approaches perfect CP (AR = 0 dB). Previously, it was known that increasing substrate thickness at a given design frequency

increases AR bandwidth, but Table 6.4 shows that increasing t / λ_d for a given substrate dielectric and substrate thickness also increases AR bandwidth. In addition, Figure 6.7 also shows that below about $t / \lambda_d = 0.01$, a corners truncated patch antenna will not produce CP (AR < 3 dB). For 10 mil RT/duroid 5880, the percent offset between f'_{S11} and f'_{AR} is below 0.5 % for the four antennas in the C band and above.

When the thickness of the RT/duroid 5880 substrate is increased to 62 mil ($1/16''$) (truncation amount designed for S_{11} = -10 dB) the AR performance of the S, C and X band antennas significantly improves. The best AR for C and X band frequencies is below 3 dB, and the AR bandwidth is greater than 1 % for these antennas. However, the percent offset between f'_{S11} and f'_{AR} increases, and the offset increases with frequency, as seen in Figure 6.8 and listed in Table 6.4. For the 62 mil substrate thickness t / λ_d needs to be larger than 0.02 to create an edge-fed, corners truncated patch antenna with CP. Due to the 50 Ω edge fed requirement, design frequencies above the X band cannot be realized due to the feed width, w_o, being greater than the patch side length, L.

Figure 6.7 and Figure 6.8 indicate that for each substrate thickness studied, there is some critical value of t / λ_d above which the corners truncated patch antenna will generate CP. For the 10 mil substrate this value is near 0.01, and for the 62 mil substrate this value is near 0.02. Below this value of t / λ_d, it is possible to design patch antennas with good S_{11}, but the antenna will be linearly polarized, despite the corner truncation. In addition to the well-known effect of AR bandwidth increasing with substrate thickness, it is clear that the best AR also improves as thickness increases.

6.4.3 Effect of Substrate Dielectric Constant

This section uses commercially available 10 mil RT/duroid 6006 (ε_r = 6.15) to investigate the effect of higher dielectric constant substrates on edge-fed, corners truncated patch antenna design. The 10 mil, high dielectric substrate lends to design of millimeter-wave patch antennas in the Ka-band and above, so in addition to the five previously studied design frequencies, a sixth design frequency of 40 GHz is studied. All six design frequencies are listed in Table 6.5, and 40 GHz is listed as the bottom of the V band (40 – 75 GHz). The six antennas are designed using the methods in Section 6.3 with 50 Ω edge feeds and S_{11} = -10 dB truncation amounts. Simulated S_{11} and best AR are plotted in Figure 6.9 for the six antennas.

The best AR occurs for the Ka-band antenna, and is slightly worse for the V band antenna as shown in Table 6.5. The antennas below the Ka-band did not produce suitable CP (AR > 3 dB). The mismatch between best AR and S_{11} increases with frequency, as shown in Figure 6.9 and Table 6.5. Increasing the dielectric constant increases t / λ_d, similar to increasing substrate thickness.

Similar to Figure 6.8, in Figure 6.9 as the frequency increases, percent offset between f'_{S11} and f'_{AR} increases. This effect occurs for both the RT/duroid 5880 (Figure 6.8) and 6006 (Figure 6.9). Thus, both substrate thickness and dielectric have an effect on the AR that is captured by t / λ_d. For the RT/duroid 6006, design frequencies above $t / \lambda_d = 0.05$ are CP. Again, antennas below $t / \lambda_d = 0.05$ have acceptable S_{11} for many applications, but the radiation is linearly polarized despite the corner truncation. Among all studied variations of substrate thickness and dielectric constant, a t / λ_d value between 0.01 – 0.05 is needed to create CP for the corners truncated patch antenna.

6.5 Technique for Alignment of S_{11} and AR

For an edge-fed, corners truncated patch antenna to be suitable for use in satellite communication, the percent offset between f'_{S11} and f'_{AR} must be minimal and the patch edge impedance should be matched to the feed impedance to create the largest possible CPBW. As seen in Figures 6.8 and 6.9, the edge-fed, corners truncated, square patch antenna has a large percent offset between f'_{S11} and f'_{AR} for certain frequencies and substrates.

First, a strategy for independently adjusting f'_{S11} and f'_{AR} is needed in order to reduce the percent offset between f'_{S11} and f'_{AR}. Increasing truncation amount as demonstrated in Section 6.3 will improve S_{11}, but it also increases linear polarization, so a different method is needed. Here we propose to create a corners truncated, nearly-square patch in which the length, L, and width, W, are slightly different as shown on the inset in Figure 6.10. In Figure 6.10, the patch width has a much larger effect on f'_{S11} and f'_{AR} than the patch length. Using the nearly-square technique, L and W can be varied to reduce the percent offset.

Second, although the proposed nearly-square patch can be used to reduce percent offset, the CPBW may still be narrow or nonexistent due to poor impedance matching between the edge-feed and the patch antenna. For future applications such as a millimeter-wave $N \times N$ array, there may be limited footprint for the array feed to use impedance matching tuning stubs. However, the real edge impedance can be matched with a small footprint near the design frequency using quarter-wave transformers.

This matching technique is effective as seen in Figure 6.11 for a corners truncated patch antenna on 10 mil RT/duroid 5880. The dimensions of the nearly square patch are: L = 3.75 mm, W = 3.67 mm, a = 0.50 mm, w_q = 0.19 mm, w_o = 0.74, and the length of the quarter-wave transformer is 2.19 mm. The impedance of the quarter wave transformer

($Z_1 = 108\ \Omega$) is chosen to match the $Z_0 = 50\ \Omega$ edge-feed to the strictly real antenna impedance ($R_L = 234\ \Omega$) at 25.3 GHz where the imaginary impedance is zero using well-known equation (6.10) [27].

$$Z_1 = \sqrt{Z_0 R_L} \tag{6.10}$$

Although the antenna design frequency is 26 GHz, a 25.3 GHz quarter-wave transformer creates an exact impedance match at that frequency, which increases the impedance bandwidth and the CPBW at design frequency. Because feed line length effects phase, Figure 6.11 shows two different feed lengths (6 mm and 11 mm) to show that using only a quarter-wave transformer creates a similar bandwidth.

6.6 Conclusions and Future Work

In this paper, a 50 Ω edge-fed, corners truncated, CP patch antenna is evaluated for use in the Ka-band with a 26 GHz design frequency. RT/duroid 5880 ($\varepsilon_r = 2.2$, ½ oz. copper cladding) with substrate thicknesses of 5, 10, and 20 mil are initially considered for the design. After comparison between the designs, the 10 mil substrate design is chosen, as it offers wide bandwidth and the best AR, closest to zero. Increasing substrate thickness increases AR bandwidth, but also increases the microstrip feed width, w_o. Increasing microstrip feed width will make future $N \times N$ array design difficult, so a narrower feed is desired. Initial patch design is edge-fed with a 50 Ω (w_o = 0.74 mm) microstrip line, and the patch length is L = 3.75 mm. For a perfectly impedance matched, edge-fed, corners truncated patch antenna on 10 mil RT/duroid 5880, truncation amount is calculated as a =

0.49 mm to produces an S_{11} of -10 dB at 26 GHz. At this corner truncation, the AR is 0.748 dB, and its bandwidth is 1.19%. Corner truncation may be used to produce LHCP or RHCP, but the LHCP polarization is considered throughout the work.

In previous works on single-feed, corners truncated patch antennas, the patch antennas are back-fed and perfectly matched. This works seeks to use the edge-fed patch for its inherent manufacturing simplicity. The previous back-fed patch antennas have a large CPBW, meaning that the frequency region where AR < 3 dB and S_{11} < -10 dB is large. When the CPBW is large, the percent offset between the frequency of best S_{11}, f'_{S11}, and best AR, f'_{AR}, is small. However, in this work four truncation amounts are considered, and the percent offset is seen to change with truncation amount. Truncation amount has little effect on f'_{S11} but has a larger effect on f'_{AR}. Increasing truncation amount increases AR bandwidth, increases percent offset between f'_{S11} and best f'_{AR}, and worsens the best AR. Thus, selecting truncation amount becomes a complex optimization process. Measured and simulated data indicates that a truncation amount of 0.57 mm is a good compromise providing large AR bandwidth, minimal percent offset between f'_{S11} and best f'_{AR}, a best AR close to 0 dB, and a minimum S_{11}.

Further investigation of the edge-fed, corners truncated patch antenna is performed by varying design frequency, substrate thickness, and substrate dielectric constant. Increasing the design frequency of an antenna while maintaining substrate thickness results in an increasing AR bandwidth, a corollary to the well-known result of maintaining design frequency and increasing substrate thickness. Increasing substrate thickness increases AR bandwidth, and below a certain t / λ_d threshold, the antenna will not produce CP, although it may have an S_{11} sufficient for many applications. For 10 mil RT/duroid 5880, the percent

offset between f'_{S11} and f'_{AR} is below 0.5 % for the four antennas in the C band and above. AR performance of S, C, and X band antennas on 62 mil RT/duroid 5880 is much better than on 10 mil RT/duroid 5880. Antennas on 62 mil RT/duroid with t / λ_d below 0.02 will not produce CP. Each substrate studied has some t / λ_d threshold below which CP is not produced by corners truncated patch antennas. For high dielectric RT/duroid 6006, the t / λ_d threshold is 0.05. Antennas designed on the high dielectric RT/duroid 6006 experience large percent offset between f'_{S11} and f'_{AR} as frequency increases. The best AR is seen to increase with frequency for RT/duroid 6006, but only to a certain frequency. Of the antenna designs studied, the best AR begins to deteriorate above the 26 GHz Ka-band design.

One way of decreasing percent offset between f'_{S11} and f'_{AR} is to use a nearly-square, corners truncated patch. The patch width shifts both f'_{S11} and f'_{AR} and can be tuned to reduce the percent offset. The magnitude of the AR is minimally impacted, but the nearly-square design damages impedance match, so the S_{11} is not as good as with a square patch. Due to this effect, a quarter-wave matching network is designed to improve S_{11} by matching on the real impedance of the patch at a frequency near the design frequency. This method eliminates the large tuning stub, which is important for compact $N \times N$ array feed design.

This paper extends what is known about truncated corner CP patch antennas from low frequencies on low dielectric substrates where percent offset between f'_{S11} and best f'_{AR} is minimal, to 26 GHz, where it must be considered. Additionally, high dielectric effects on patch design are also considered. Changing the patch width to make a nearly-square patch reduces percent offset between f'_{S11} and best f'_{AR} and adding a quarter-wave matching network improves the impedance match. The single element patch designs

described in this work will be used in a larger 2×2 sub-array that could eventually be incorporated into a $N \times N$ feed for an offset reflector.

Table 6.1: Design parameters for corners truncated CP patch antennas as illustrated in Figure 6.1. The design frequency is 26 GHz, and the substrate is RT/ duroid 5880 (ε_r = 2.2, ½ oz. copper cladding)

Substrate Thickness (mils)	w_o (50 Ω) [mm]	L [mm]	a [mm]	Frequency for best S_{11} (GHz)	Frequency for best AR (GHz)	AR BW (%)
5	0.367	3.83	0.34	25.55	25.5	0.47
10	0.741	3.75	0.49	25.68	25.52	1.19
20	1.461	3.56	0.68	26.04	25.88	2.47

Table 6.2 Changing the truncation amount (a shown in Figure 6.1) changes the frequencies at which S_{11} and AR are lowest, and their frequency offset. Results are shown here for LHCP truncated corner patch antennas on 10 mil Rogers duroid/5880. The % offset is calculated from (8).

	Meas	Sim	Meas	Sim	Meas	Sim	Meas	Sim
Truncation Amount (a , see Fig.6.1)	S_{11} Center [GHz]	S_{11} Center [GHz]	AR Center Freq [GHz]	AR Center Freq [GHz]	Offset [MHz/ %]	Offset [MHz/ %]	3 dB AR BW [%]	3 dB AR BW [%]
0.49	--	--	--	25.52	--	--	--	1.19
0.50	26.85	25.58	26.05	25.55	800/ 2.98	30/ 0.12	4.22	1.37
0.57	26.10	25.60	25.66	25.65	440/ 1.69	50/ 0.20	6.73	1.37
0.60	26.10	25.62	25.60	25.65	500/ 1.92	30/ 0.12	2.07	0.78
0.74	26.20	25.61	25.30	--	900/ 3.44	--	1.78	--

Table 6.3: Antenna dimensions and simulated performance for antennas designed on 10 mil RT/duroid 5880. In each case, the antennas were designed for S_{11} = -10 dB, and are edge-fed with a 50 Ω line.

Band	L [mm]	a [mm]	λ_d [mm]	t/λ_d	AR 3dB Bandwidth [%]	AR Best [dB]	AR Center [GHz]	S_{11} Center [GHz]	Offset [GHz/ %]
S	40.4	1.563	80.9	0.0031	--	--	--	2.48	--
C	16.7	1.011	33.7	0.0075	--	4.45	5.90	5.92	0.02/ 0.34
X	10.0	0.784	20.2	0.0126	0.05%	2.92	9.83	9.82	0.01/ 0.10
Ku	6.6	0.641	13.5	0.0188	0.66%	1.19	14.70	14.73	0.03/ 0.20
Ka	3.7	0.487	7.8	0.0330	1.19%	0.75	25.52	25.55	0.03/ 0.12

Table 6.4: Antenna dimensions and simulated performance for antennas designed on 62 mil Rogers duroid/5880. In each case, the antennas were designed for S_{11} = -10 dB, and are fed with a 50 Ω line.

Band	L [mm]	a [mm]	λ_d [mm]	t/λ_d	AR 3dB Bandwidth [%]	AR Best [dB]	AR Center [GHz]	S_{11} Center [GHz]	Offset [MHz/ %]
S	39.7	3.91	80.9	0.020	--	5.51	2.45	2.45	0/ 0
C	15.9	2.52	33.7	0.047	1.08	1.92	5.90	6.36	460/ 7.23
X	9.1	1.92	20.2	0.078	2.58	1.59	9.90	10.88	980/ 9.01

Table 6.5: Antenna dimensions and simulated performance for antennas designed on 10 mil Rogers duroid/6006. In each case, the antennas were designed for S_{11} = -10 dB, and are fed with a 50 Ω line.

Band	L [mm]	a [mm]	λ_d [mm]	t/λ_d	AR 3dB Bandwidth [%]	AR Best [dB]	AR Center [GHz]	S_{11} Center [GHz]	Offset [GHz/ %]
S	24.2	0.67	48.4	0.0052	--	--	--		
C	10.1	0.44	20.2	0.013	--	--	--		
X	6.0	0.34	12.1	0.021	--	--	--		
Ku	4.0	0.29	8.1	0.032	--	3.84	14.65	14.71	0.06/ 0.41
Ka	2.3	0.22	4.7	0.055	0.69	1.69	25.1	26.39	1.29/ 4.89
V	1.4	0.18	3.0	0.084	1.00	1.89	38.3	41.36	3.06/ 7.40

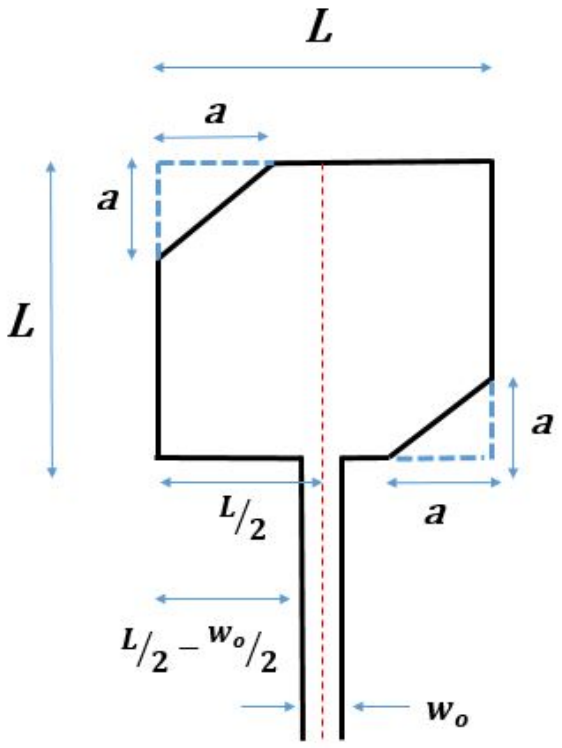

Figure 6.1. An edge-fed patch antenna with corners truncated for LHCP. The patch is a square patch with a side length of L. The truncation amount is a. The width of the feed line is w_o, which in this work is adjusted to 50 Ω for each antenna. The dotted red line indicates the center of the patch. Dimensions of this patch for three substrate thicknesses at a design frequency of 26 GHz are given in Table 6.1.

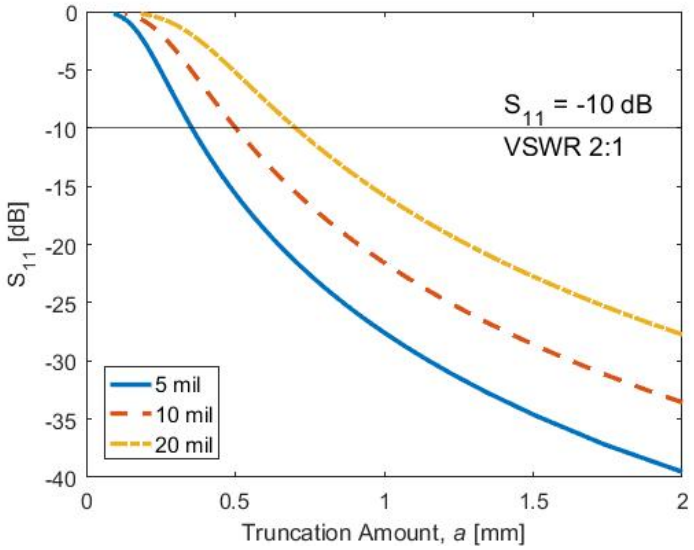

Figure 6.2. Increasing truncation or reducing substrate thickness results in better matching as seen from the simulated S11 for the three patch antennas with truncated corners at 26 GHz. The dimensions for side length, L, and feed line width, wo, are given in Table 6.1. The S11 in Figure 6.2 assumes that the patch is perfectly matched to the input feed line.

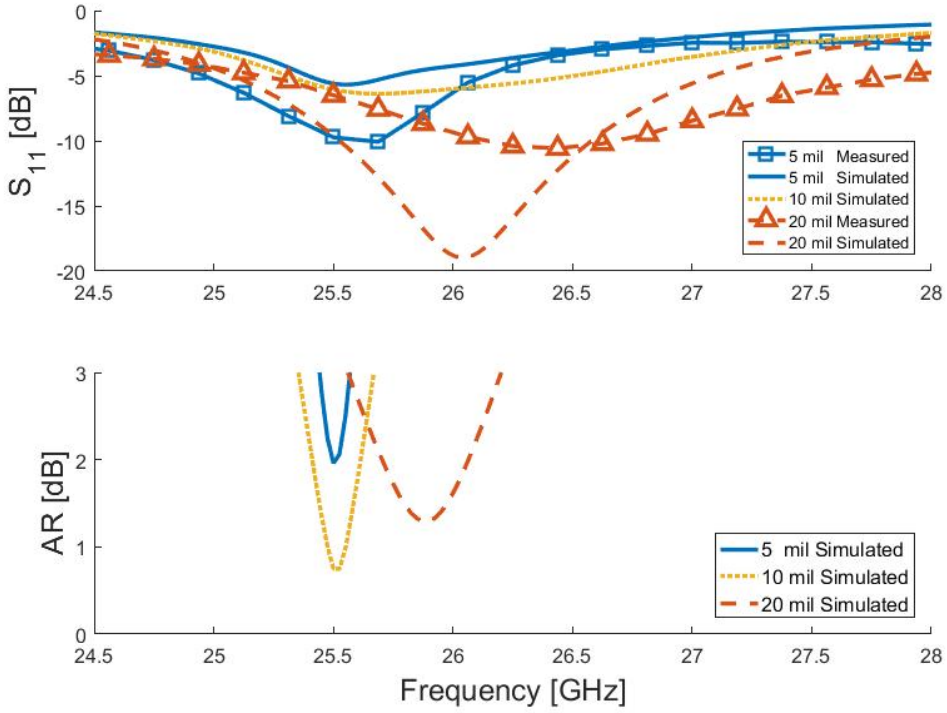

Figure 6.3. S_{11} and AR as a function of frequency for 50 Ω edge-fed, corners truncated patch antennas on 5, 10, 20 mil RT/duroid 5880 with 26 GHz design frequency. Increasing substrate thickness increases AR bandwidth, but results in a greater percent offset between $\boldsymbol{f'_{S11}}$ and $\boldsymbol{f'_{AR}}$. These effects can be seen from the measured and simulated S_{11} and simulated AR for the three patch antennas with dimensions listed in Table 6.1.

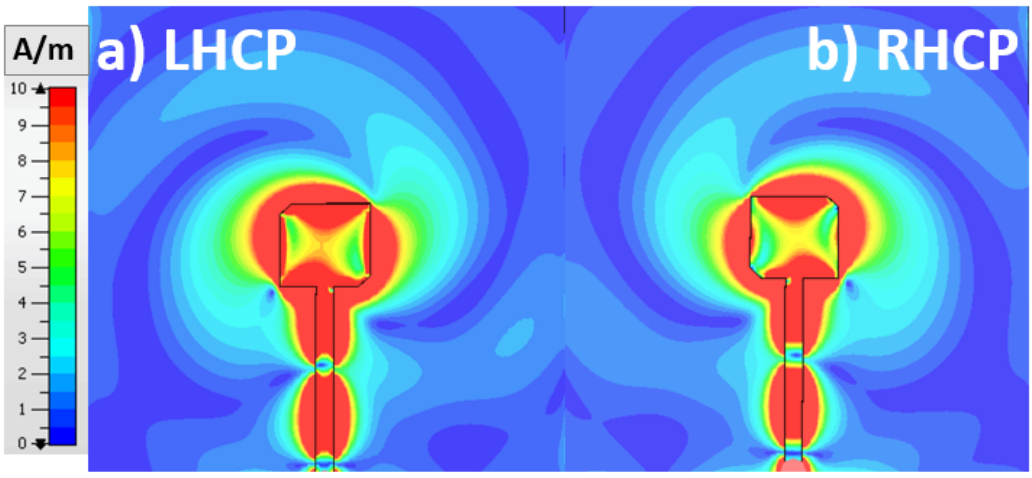

Figure 6.4 The left and right-hand rotation of surface currents are seen from these distributions on the truncated corner CP patch antennas on 10 mil RT/duroid 5880 described in Table 6.1. (a) Upper left and lower right corners are truncated, giving the left-hand polarization (LHCP) (b) Upper right and lower left corners are truncated, giving the right-hand polarization (RHCP).

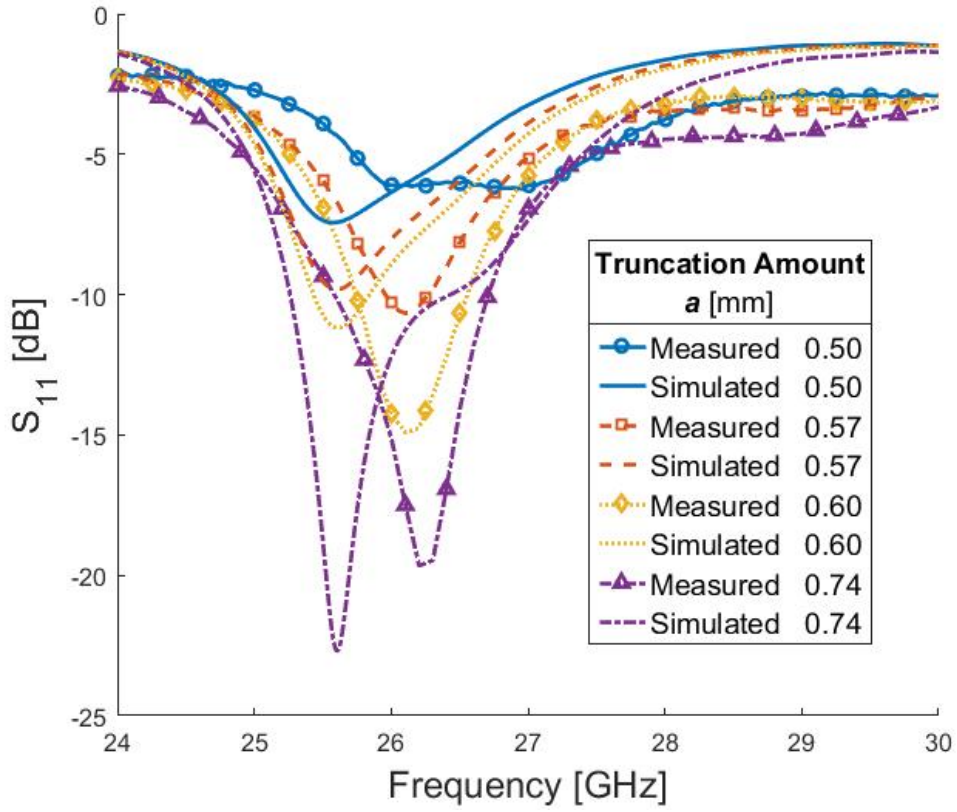

Figure 6.5. Measured and simulated S_{11} for patch antennas with various truncation amounts. Increasing truncation amount, a, reduces the S_{11} with minimal change to $\boldsymbol{f'_{S11}}$. Truncation amounts, a, is described by Figure 6.1 and values for the antennas in this figure are listed in Table 6.1. All antennas in this figure are designed as 50 Ω edge-fed, LHCP with 26 GHz design frequency on 10 mil RT/duroid 5880 with dimensions and some characteristic properties given in Table 6.1.

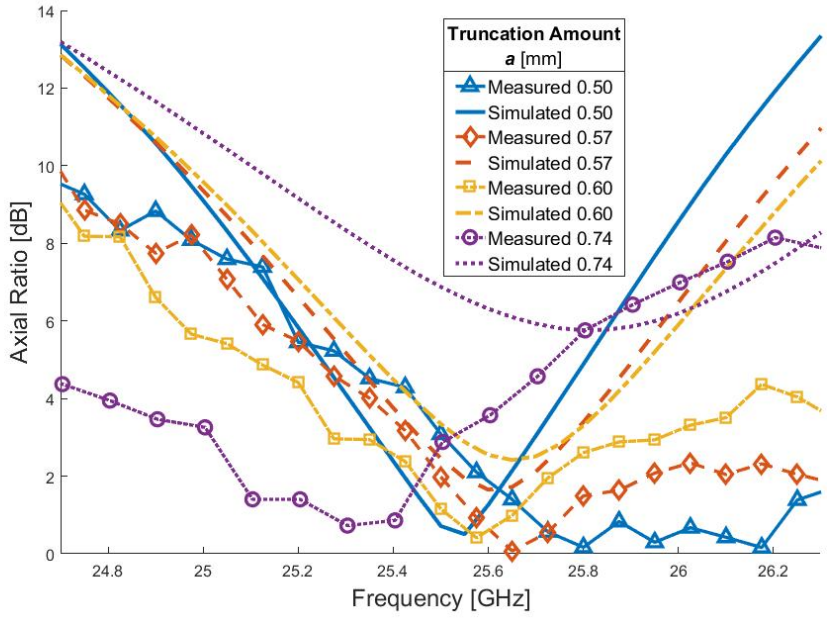

Figure 6.6. Measured and simulated AR for patch antennas with various truncation amounts. Simulation and measurement show that as the truncation amount, $\boldsymbol{a}$ increases: (1) The AR bandwidth increases; (2) The antenna become more linearly polarized (AR increases); (3) The percent offset increases due to $\boldsymbol{f'_{AR}}$ shifting (downward for simulated results, and upwards for measured). Truncation amount, $\boldsymbol{a}$ is described by Figure 6.1, and values for the antennas in this figure are listed in Table 6.1. All antennas in this figure are designed as 50 Ω edge-fed, LHCP with 26 GHz design frequency on 10 mil RT/duroid 5880 with complete dimensions and some characteristic properties given in Table 6.1.

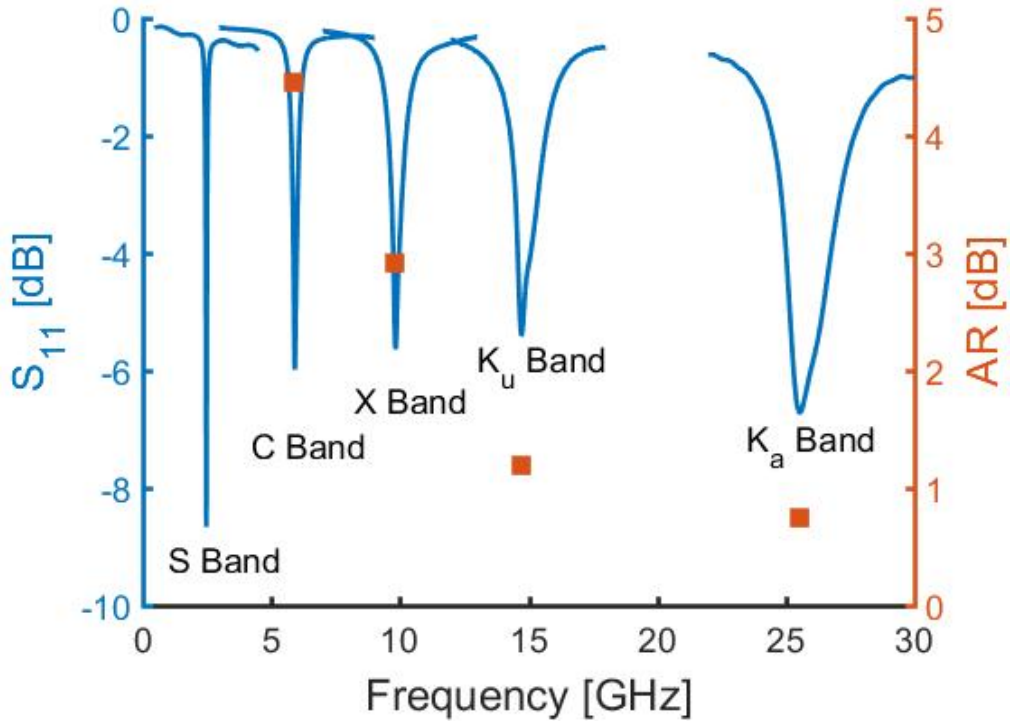

Figure 6.7. Simulated S_{11} for five corners truncated patch antenna on 10 mil RT/duroid 5880 (ε_r = 2.2) with different design frequencies. Each antenna is 50 Ω edge-fed, and truncation amount is designed for S_{11}= -10 dB. Simulated S_{11} remains near -10 dB for all antennas as design frequency increases, while the best AR approaches 0 dB as frequency increases. The 3 dB AR bandwidth for both increases with frequency. Percent offset between f'_{S11} and f'_{AR} is below 0.5 % for the four antennas in the C band and above. For 10 mil RT duroid 5880 t / λ_d should be larger than 0.01, or the antenna will not produce CP (AR < 3 dB). Square markers indicate AR and correspond to the right y-axis; lines indicate S_{11} and correspond to the left y-axis. For this relatively thin board, there is minimal percent offset between f'_{S11} and f'_{AR}. Corners truncated patch antennas on below the X-band on this substrate create sufficient S_{11} for many applications, but are linearly polarized with AR above 3 dB. Table 6.3 lists antenna dimensions and performance parameters.

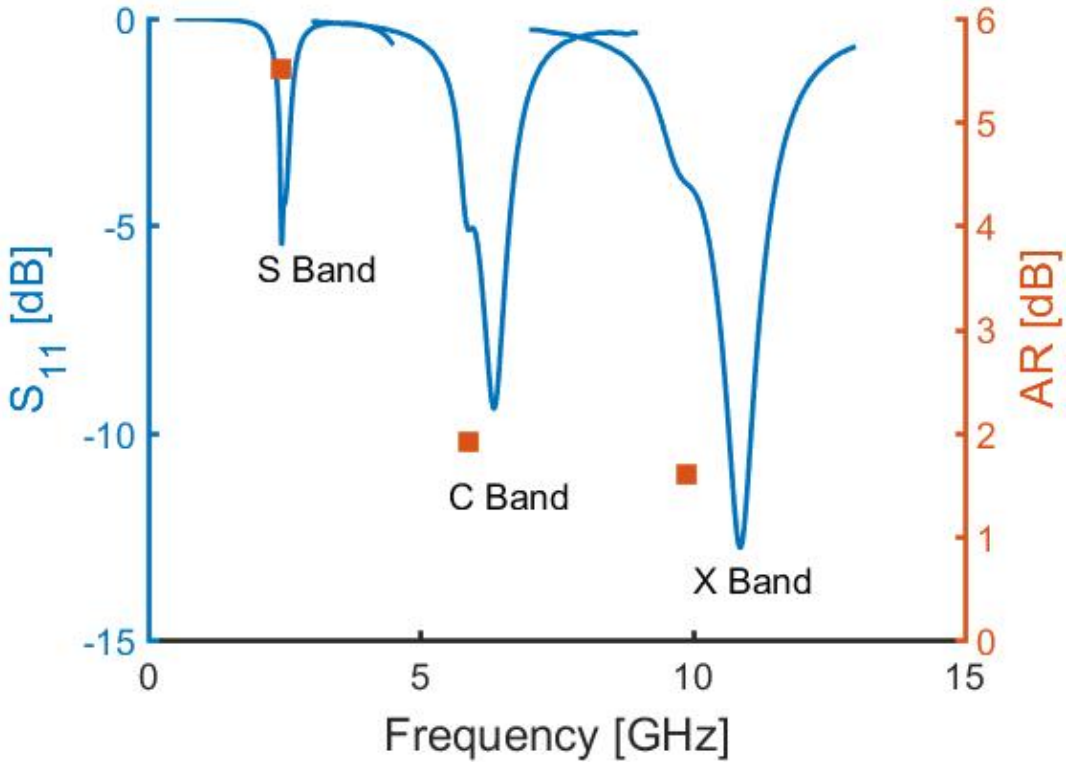

Figure 6.8. Simulated S_{11} for three different corners truncated patch antennas on 62 mil (1/16") RT/duroid 5880 ($\varepsilon_r = 2.2$) with different design frequencies. Each antenna is 50 Ω edge-fed and truncation amount is designed for S_{11}= -10 dB. Percent offset between f'_{S11} and f'_{AR} is large for this substrate for all design frequencies compared to those in Figure 6.7 on 10 mil RT/duroid 5880. AR performance of the S, C and X band antennas significantly improves on 62 mil compared to the 10 mil board (seen in Figure 6.7). For the 62 mil substrate thickness t / λ_d *needs* to be larger than 0.02 to create an edge-fed, corners truncated patch antenna with CP. Again, the best AR approaches 0 dB as frequency increases. Square markers indicate AR and correspond to the right y-axis; lines indicate S_{11} and correspond to the left y-axis. Table 6.4 lists antenna dimensions and performance parameters.

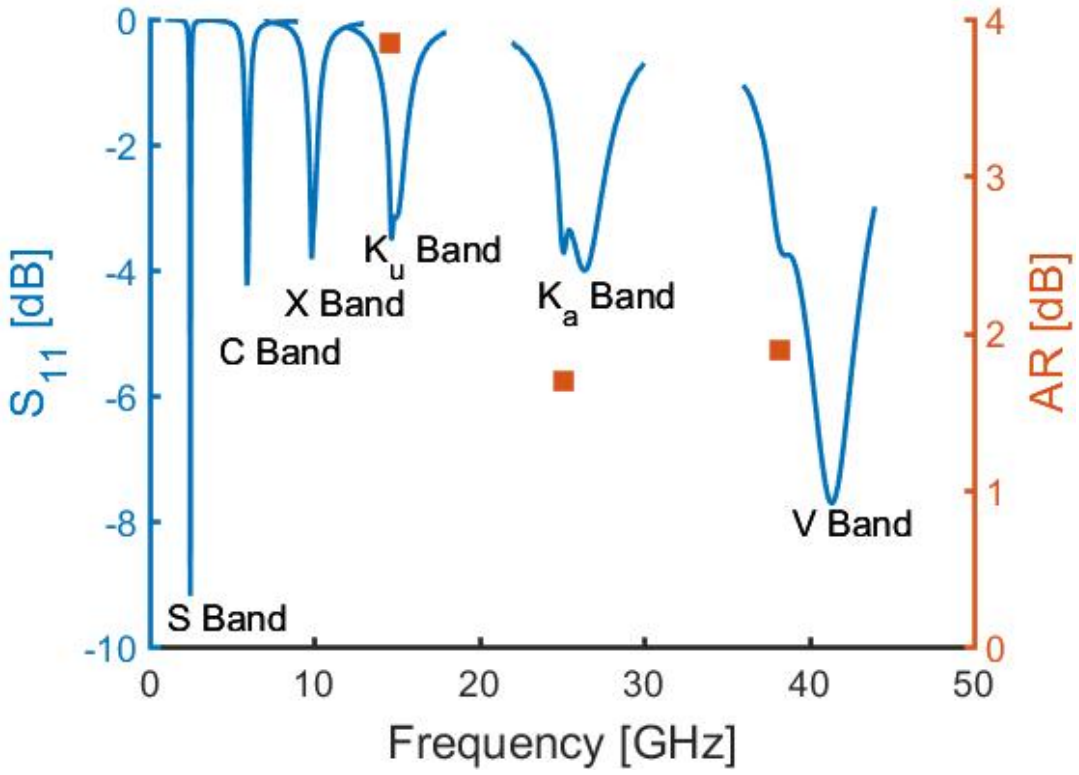

Figure 6.9. Simulated S_{11} for three different corners truncated patch antennas on 10 mil RT/duroid 6006 ($\varepsilon r = 6.15$) with different design frequencies. Each antenna is 50 Ω edge-fed and truncation amount is designed for S_{11}= -10 dB. When the substrate thickness is increased the percent offset between f'_{S11} and f'_{AR} is increased. For the 10 mil RT/duroid 6006, substrate thickness t / λ_d needs to be larger than 0.02 to create CP. The best AR again increases with frequency, but only to a certain point. Above the Ka-band, the best AR begins to become more linearly polarized. As with other substrate thicknesses and dielectric constants, the AR bandwidth increases with frequency. Square markers indicate AR and correspond to the right y-axis; lines indicate S_{11} and correspond to the left y-axis. Table 6.5 lists antenna dimensions and performance parameters.

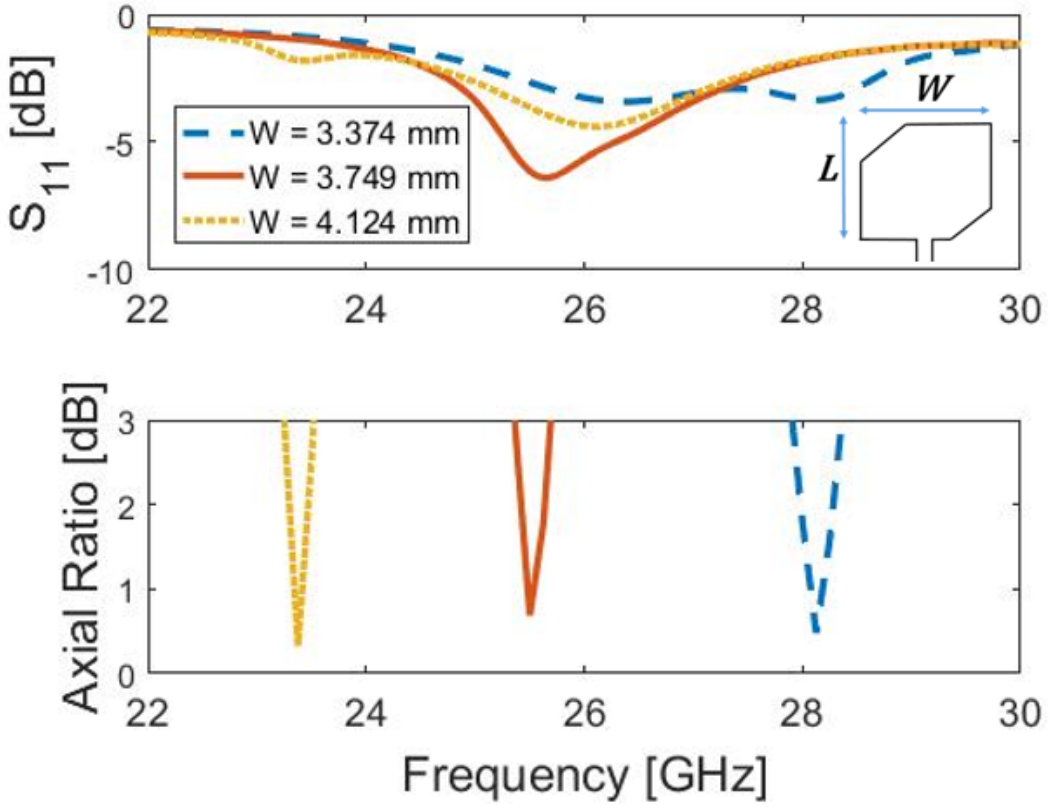

Figure 6.10. Simulated S_{11} for three different nearly-square corners truncated patch antennas on 10 mil RT/duroid 5880. A nearly-square patch antenna may be used to align the frequencies of best S_{11} and AR at millimeter wave frequencies as seen from simulation of S_{11} and AR as a function of patch width, W. Patch length, L, remains constant at 3.75 mm.

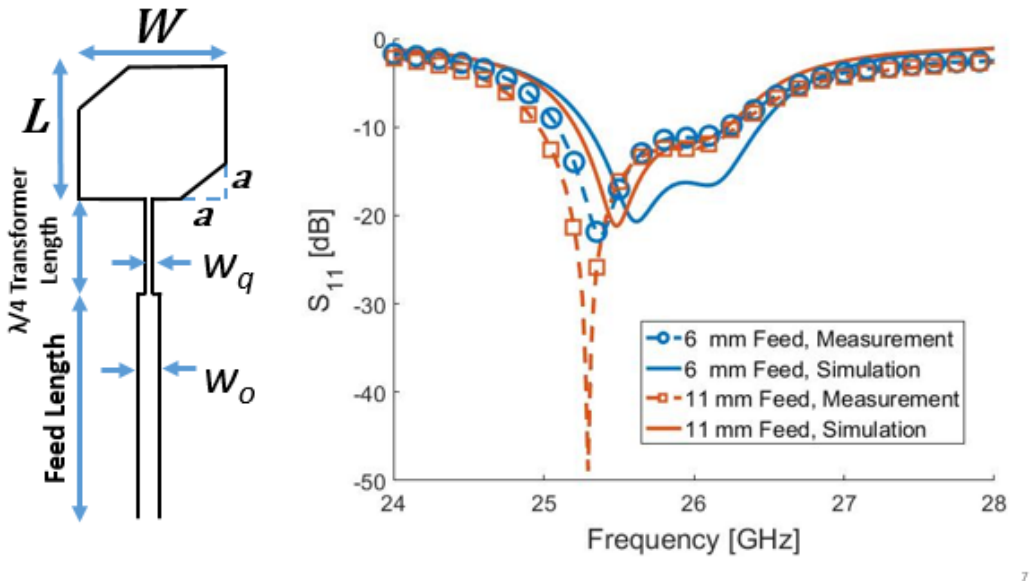

Figure 6.11. Simulated and measured S_{11} for three different quarter-wave transformer impedance matched, *nearly-square* corners truncated patch antennas on 10 mil RT/duroid *5880.* The feed length for the two patches are 6 mm and 11 mm. The other dimensions are identical. L = 3.75 mm, W = 3.67 mm, a = 0.50 mm, w_q = 0.19 mm, w_o = 0.74. The λ/4 transformer length is 2.19 mm for matching the patch's real impedance at 25.3 GHz.

6.6 References

[1] B. Y. Toh, R. Cahill, and V. F. Fusco, "Understanding and measuring circular polarization," *IEEE Transactions on Education,* vol. 46, no. 3, pp. 313-318, 2003.

[2] F. Bongard, M. Gimersky, S. Doherty, X. Aubry, and M. Krummen, "3D-printed Ka-band waveguide array antenna for mobile SATCOM applications," in *2017 11th European Conference on Antennas and Propagation (EUCAP)*, 2017, pp. 579-583.

[3] A. I. Dimitriadis, M. Favre, M. Billod, J. P. Ansermet, and E. d. Rijk, "Design and fabrication of a lightweight additive-manufactured Ka-band horn antenna array," in *2016 10th European Conference on Antennas and Propagation (EuCAP)*, 2016, pp. 1-4.

[4] Y. B. Jung and S. O. Park, "Ka-band shaped reflector hybrid antenna illuminated by microstrip-fed horn array," *IEEE Transactions on Antennas and Propagation,* vol. 56, no. 12, pp. 3863-3867, 2008.

[5] J. Huang and R. J. Pogorzelski, "A Ka-band microstrip reflectarray with elements having variable rotation angles," *IEEE Transactions on Antennas and Propagation,* vol. 46, no. 5, pp. 650-656, 1998.

[6] M. M. Tahseen and A. A. Kishk, "Broadband performance of novel closely spaced elements in designing Ka-band circularly polarized reflectarray antennas," *IEEE Antennas and Wireless Propagation Letters,* vol. 16, pp. 1184-1187, 2017.

[7] A. Yu, F. Yang, A. Z. Elsherbeni, and J. Huang, "Design and measurement of a circularly polarized Ka-band reflectarray antenna," in *2009 3rd European Conference on Antennas and Propagation*, 2009, pp. 2769-2773.

[8] R. Deng, F. Yang, S. Xu, and M. Li, "An FSS-backed 20/30-GHz dual-band circularly polarized reflectarray with suppressed mutual coupling and enhanced performance," *IEEE Transactions on Antennas and Propagation,* vol. 65, no. 2, pp. 926-931, 2017.

[9] S. Chatterjee and A. Majumder, "Design of circularly polarized waveguide crossed slotted array antenna at Ka-band," in *2015 International Conference on Microwave and Photonics (ICMAP)*, 2015, pp. 1-2.

[10] T. Li, H. Meng, and W. Dou, "Design and implementation of dual-frequency dual-polarization slotted waveguide antenna array for Ka-band application," *IEEE Antennas and Wireless Propagation Letters,* vol. 13, pp. 1317-1320, 2014.

[11] J. Huang, "A Ka-band circularly polarized high-gain microstrip array antenna," *IEEE Transactions on Antennas and Propagation,* vol. 43, no. 1, pp. 113-116, 1995.

[12] A. S. Hussam, F. Mohmmad, W. M. Abdel-Wahab, G. Rafi, and S. Safavi-Naeini, "A 4x4 circularly polarized aperture coupled antenna array for Ka-band satellite communication," in *2015 IEEE International Symposium on Antennas and Propagation & USNC/URSI National Radio Science Meeting*, 2015, pp. 1896-1897.

[13] Nasimuddin, Q. Xianming, and C. Zhi Ning, "A wideband circularly polarized microstrip array antenna at Ka-band," in *2016 10th European Conference on Antennas and Propagation (EuCAP)*, 2016, pp. 1-4.

[14] A. Chen, Y. Zhang, Z. Chen, and S. Cao, "A Ka-band high-gain circularly polarized microstrip antenna array," *IEEE Antennas and Wireless Propagation Letters,* vol. 9, pp. 1115-1118, 2010.

[15] A. Chen, Y. Zhang, Z. Chen, and C. Yang, "Development of a Ka-band wideband circularly polarized 64-element microstrip antenna array with double application of the sequential rotation feeding technique," *IEEE Antennas and Wireless Propagation Letters,* vol. 10, pp. 1270-1273, 2011.

[16] G. A. Deschamps and W. Sichak, "Microstrip microwave antennas," pp. 103-105.

[17] K. F. Lee and K. F. Tong, "Microstrip patch antennas—basic characteristics and some recent advances," *Proceedings of the IEEE,* vol. 100, no. 7, pp. 2169-2180, 2012.

[18] S. Long, S. Liang, D. Schaubert, and F. Farrar, "An experimental study of the circular-polarized elliptical printed-circuit antenna," *IEEE Transactions on Antennas and Propagation,* vol. 29, no. 1, pp. 95-99, 1981.

[19] S. Liang, "The elliptical microstrip antenna with circular polarization," *IEEE Transactions on Antennas and Propagation,* vol. 29, no. 1, pp. 90-94, 1981.

[20] H. Weinschel, "A cylindrical array of a circularly polarized microstrip antenna," in *1975 Antennas and Propagation Society International Symposium*, 1975, vol. 13, pp. 177-180.

[21] P. Sharma and K. Gupta, "Analysis and optimized design of single feed circularly polarized microstrip antennas," *IEEE Transactions on Antennas and Propagation,* vol. 31, no. 6, pp. 949-955, 1983.

[22] M. Haneishi and S. Yoshida, "A design method of circularly polarized microstrip antenna by one-point feed," *Electronics and Communications in Japan,* vol. 64-B, no. 4, pp. 46-54, 1981.

[23] A. A. Oliner, D. R. Jackson, and J. L. Volakis, "Antenna engineering handbook," *McGrawHill, New York,* 2007.

[24] S. S. Yang, K.-F. Lee, A. A. Kishk, and K.-M. Luk, "Design and study of wideband single feed circularly polarized microstrip antennas," *Progress in Electromagnetics Research,* vol. 80, pp. 45-61, 2008.

[25] K. F. Tong and T. P. Wong, "Circularly polarized U-slot antenna," *IEEE Transactions on Antennas and Propagation,* vol. 55, no. 8, pp. 2382-2385, 2007.

[26] E. O. Hammerstad, "Equations for microstrip circuit design," in *1975 5th European Microwave Conference*, 1975, pp. 268-272.

[27] D. M. Pozar, *Microwave engineering*. John Wiley & Sons, 2009.

CHAPTER 7

CONCLUSION AND FUTURE WORKS

The purpose of this work is the study of losses in implantable and spacecraft antennas. Implantable antennas are important to the advancement of healthcare, internet of things technology, and future implantable medical devices. Spacecraft antennas are important for national security, space exploration, and worldwide communications networks. Both applications require antennas capable of operating in extreme environments where power supply is limited. Losses in these antenna systems are of great importance, and this work offers contributions to understanding the losses that will aid future research.

7.1 Contributions

7.1.1 Contribution 1 (Chapters 3, 4, and 5): Fat as an Insulator, Muscle as a Ground Plane

Although implantable antennas have typically used thin films of plastic or silicone for insulation from the short-circuiting effects of the human body, this work demonstrates that fat in the body can also provide insulating effects. This contribution supports future development in tattoo antennas and implantable RFID antennas. Chapter 3 and 5 support this contribution with accepted publications [1, 2] and Chapter 4, which has been submitted

[3]. Additionally, this information has been presented professionally [4, 5].

Subdermal strip antennas made from various low-conductivity material are examined in Chapter 3. The antennas were studied in free space and in a biological environment, and the fat is shown to provide a similar level of insulation as a thin layer of plastic wrap. Additionally, increasing the thickness of the fat is shown to increase the level of insulation.

The work in Chapter 4 extends from Chapter 3 by offering simulation and measurement of dipole antennas in biological environments. Simulations show dipole antennas with voids such as mesh holes and segment gaps couple strongly to the biological environment, creating current distributions similar to a solid strip dipole. Measurement with excised rat fat and pork loin confirm the feasibility of an uninsulated dipole operating the biological environment, and support the effects seen in simulation.

Lastly, Chapter 5 also supports the contribution of muscle acting as a lossy ground plane by simulating implantable RFID antennas and varying material properties. When muscle is changed to a perfect electric conductor (PEC), the S_{11} is improved and there is a resonant frequency shift. Simulations show that the muscle is acting as a weaker, lossier version of a PEC ground plane and that the fat is insulating the RFID antenna from the ground plane (muscle or PEC). This concept can be extended in the future with injectable RFID antennas or novel RFID designs.

Although the biological environment introduces a significant amount of loss into implanted antenna systems, the body's fat is demonstrated to be a good insulator and muscle a good, albeit lossy, ground plane. This provides a new set of concepts that enable subdermal antennas, and these three chapters demonstrate the feasibility of subdermal

tattoo antenna systems utilizing the natural electrical properties of the human body.

7.1.2 Contribution 2 (Chapters 4 and 5): Current Distribution of Antennas in Biological Environments

This study of the current distribution supports future tattoo antenna work that will use tattoo antennas in the fat layer. The body tissues play a strong role in adapting the current distributions of the antenna. This contribution is supported by Chapter 4, which has been submitted for publication [3] and Chapter 5, which has been accepted for publication [2]. The information contained within has been presented at a professional conference as well [5].

An examination of the current distribution shared between the dipole and surrounding tissues, and its impact on antenna performance is provided in Chapter 4. The peak resonant frequency is controlled by the effective length of the antenna, which is reduced by the conductive tissues shorting out the current and making it not fully reach the end of the antenna. The maximum current density occurs at the edges of the antenna, or in the case of the mesh, along each of the lines of the mesh. The width of the strip antenna creates multiple paths for the current and broadens its frequency response. The current distribution transmits further into the body below the antenna than outside the body above the antenna. This is because it is drawn or guided deeper into the body by the conductive muscle tissue. Antennas with voids couple even more strongly to the tissues, sharing current with their conductive surroundings.

Current distribution of an implantable RFID antenna is considered in Chapter 5 to show the interaction of an impedance matching T-slot with the surrounding biological

environment. The antenna's current distribution and resulting input impedance is partially controlled by the surrounding tissue, as seen when the muscle conductivity is increased to PEC in simulation.

The work in Chapters 4 and 5 demonstrate that the body tissues play a strong role in adapting the current distributions of the antenna. This contribution of the current distribution of antennas in biological environments supports future tattoo antenna work that will use tattoo antennas in the fat layer.

7.1.3 Contribution 3 (Chapters 3 and 5): Applications and Use of Low-Conductivity Material in Biological Antennas

Initial studies of conductive tattoo inks showed that these were actually insufficient for the conductive tattoos needed to create antennas. However, there are a variety of other conductive inks available, and Chapter 3 and Chapter 5 demonstrate their potential. Chapter 3 offers an initial study of a novel gold nanoparticle material, and Chapter 5 offers a comparison of antenna performance between several materials. Chapter 3 and Chapter 5 have been accepted for publication [1, 2], and the information contained within has been presented professionally [4, 5].

A novel gold nanoparticle material as a dipole antenna in a biological environment and a minimum conductivity for this antenna is identified in Chapter 3. Also, whether the antennas were in air or in contact with muscle, as the conductivity or skin depth of the antenna material is reduced, the resonant frequency is lowered, the S_{11} degrades, and the bandwidth is increased, similar to results previously reported for other types of antennas in air in [6, 7].

Implantable RFID antennas made from several materials, including two with conductivity lower than traditional metals (copper), are considered in Chapter 5. These low-conductivity antennas perform nearly as well as metal antennas in both S_{11} and read range. Antennas that suffer from skin-depth losses are also shown to operate similar to a low-conductivity antenna.

The loss of the antenna as the conductivity is varied is studied and compared to several other materials. The low-conductivity materials are demonstrated to be sufficient for antenna design in a variety of biological applications.

7.1.4 Contribution 4 (Chapter 6): Effect of Corner Truncation, Board Thickness, Board Dielectric, Design Frequency on Edge-Fed, Circularly Polarized (CP) Antenna

Spacecraft antennas require both good matching and circular polarization to be effective. The popular corners truncated patch antenna is studied at millimeter-wave frequency and the effect of corner truncation, board thickness, board dielectric, and design frequency on the edge-fed, CP antenna is shown. This is supported by Chapter 6, which is being prepared for submission [8], and has been presented professionally [9].

A design for a 26 GHz 50 Ω edge-fed corners truncated patch antenna with good AR and AR bandwidth is demonstrated in Chapter 6. Increasing the design frequency of an antenna while maintaining board thickness results in an increasing AR bandwidth. The effect of corner truncation amount on antenna performance is investigated, and a design compromise is suggested. Also, a minimum ratio of board thickness to design frequency is suggested in order to produce patch antennas with CP. These contributions will aid future

antenna designers seeking to create low-cost millimeter-wave CP antennas.

7.2 Future Work

Both implantable antennas and spacecraft antennas will continue to have importance in the future. This work will aid future antenna designers and also offers many opportunities for future research. Some potential future research areas are described below.

7.2.1 Implantable Antennas

As discussed throughout this work, there is much potential for applying this knowledge as a tattoo antenna in the future. The insulating fat layer throughout much of the body offers a good location to implant antenna structures through injection or surgical methods. The muscle layer can provide a lossy ground plane for the tattoo antenna. Based on the current distribution of antennas in the body, new antenna architectures can be implemented that take advantage of the ways that body tissue shape current distribution. In particular, RFID antennas without any electrical insulation could be designed for implant in the body using a T-slot for impedance matching. Also, future work includes creating tattoo antennas that are coupled to other implanted antennas that can be used as re-radiating structures.

7.2.2 Spacecraft Antennas

Future work on millimeter-wave antennas for spacecraft application involves creating NxN arrays using the patch in Chapter 6 as the individual array elements. Future work includes optimizing the array design and also exploring the power divider in the array

network. The array can be designed in a traditional manner, or using a new compact design such as the one presented here [9]. The power divider network can be optimized to further reduce losses by investigating T-junction compensation and phase matching at each port of the divider network.

7.3 References

[1] A. Chrysler, K. Hall, F. Curry, C. Furse, and H. Zhang, "Effect of conductivity on subdermal antennas ", ed. *Microwave and Optical Technology Letters - Accepted*.

[2] A. Chrysler, C. Furse, K. Hall, and Y. Chung, "Effect of material properties on a subdermal UHF RFID antenna," ed. *IEEE Journal of RFID - Accepted*.

[3] A. Chrysler, K. Hall, and C. Furse, "A comparison of solid, mesh, and segmented strip dipoles in a subdermal environment," ed. *IEEE Journal of Electromagnetics, RF and Microwaves in Medicine and Biology - Submitted*.

[4] A. Chrysler, C. Furse, and Y. Chung, "Biocompatible, implantable UHF RFID antenna made from conductive ink," in *2016 IEEE International Symposium on Antennas and Propagation (APSURSI)*, 2016, pp. 467-468.

[5] K. Hall, A. Chrysler, and C. Furse, "A comparison of solid, mesh, and segmented broad dipoles in biological environments," in *2017 IEEE International Symposium on Antennas and Propagation (APSURSI)*, San Diego, CA, 2017.

[6] M. Shahpari and D. V. Thiel, "The impact of reduced conductivity on the performance of wire antennas," *IEEE Transactions on Antennas and Propagation,* vol. 63, no. 11, pp. 4686-4692, 2015.

[7] C. D. Rouse, M. R. Kurz, B. R. Petersen, and B. G. Colpitts, "Performance evaluation of conductive-paper dipole antennas," *IEEE Transactions on Antennas and Propagation,* vol. 61, no. 3, pp. 1427-1430, 2013.

[8] A. Chrysler, R. Simons, C. Furse, and F. Miranda, "A Ka-band (26 GHz) single patch element with truncated corners for circular polarization," ed. *IEEE Transaction Antennas and Propagation - In Preparation*.

[9] A. Chrysler, C. Furse, R. N. Simons, and F. A. Miranda, "A Ka-band (26 GHz) circularly polarized 2x2 microstrip patch sub-array with compact feed," 2017.